arXiv:hep-th/0405275v1 29 May 2004

DCPT-02/81
SPhT-T04/048
hep-th/0405275
May 2004

Mass scales and crossover phenomena in the Homogeneous Sine-Gordon Models

Patrick Dorey[1,2] and J. Luis Miramontes[3,2]

[1] *Department of Mathematical Sciences*
University of Durham
Durham DH1 3LE, UK

[2] *Service de Physique Théorique*
CEA-Saclay
F-91191 Gif-sur-Yvette Cedex, France

[3] *Departamento de Física de Partículas,*
Facultad de Física
Universidad de Santiago de Compostela
15782 Santiago de Compostela, Spain

e-mails: p.e.dorey@durham.ac.uk, miramont@usc.es

Abstract

The finite-size behaviours of the homogeneous sine-Gordon models are analysed in detail, using the thermodynamic Bethe ansatz. Crossovers are observed which allow scales associated with both stable and unstable quantum particles to be picked up. By introducing the concept of shielding, we show that these match precisely with the mass scales found classically, supporting the idea that the full set of unstable particle states persists even far from the semiclassical regime. General rules for the effective TBA systems governing individual crossovers are given, and we also comment on the Lagrangian treatment of the theories, novel issues which arise in the form-factor approach for theories with unstable particles, and the role of heterotic cosets in the staircase flows exhibited by the HSG models.

1 Introduction

The homogeneous sine-Gordon (HSG) models [1] are two-dimensional quantum field theories with a number of remarkable properties. They are integrable perturbations of level-k G-parafermions [2], that is of coset conformal field theories of the form $G_k/U(1)^{r_g}$, where G is a simple compact Lie group with Lie algebra g, $k > 1$ is an integer, and r_g is the rank of g. In the limit $k \to \infty$ they can be analysed using semiclassical techniques, and the resulting data used to make conjectures for the mass spectra and exact S-matrices at arbitrary values of k [3][1]. Checks of the S-matrices using both thermodynamic Bethe ansatz (TBA) [5] and form-factor [6, 7, 8] approaches leave little doubt that they describe the perturbed parafermionic theories correctly, even for small values of k far from the semiclassical regime.

An interesting feature to emerge from the semiclassical studies was the presence of unstable particles [9]. If h_g is the Coxeter number of g, a total of $(k-1)\, r_g h_g/2$ particle-like states (in the simply-laced cases) were identified, $k-1$ for each positive root of g. Those corresponding to the simple roots are stable; all the rest are semiclassically unstable. On the other hand, in the S-matrix treatment of the full quantum theory, only stable particles are seen directly. Evidence for the unstable particles must come by more indirect routes, such as the appearance of resonance poles at complex rapidities in the scattering amplitudes of pairs of stable asymptotic particle states. However, for the HSG models only the r_g-1 sets of unstable particles associated with the roots of height two can be picked up in this way[2]. And at small values of k, far from the semiclassical regime, the resonance peaks for the height-two particles are very broad, and their interpretation becomes delicate. This raises an immediate question – how should we verify the existence of the remaining particles in the quantum theory, and what influence do they have on the physical properties of the models? Are the extra unstable particles even present in the models with k small, or do they merely emerge when the limit $k \to \infty$ is taken?

In this paper we shall address these and related issues by returning to the study of finite-size effects using the TBA technique. At mass scales where new stable or unstable particle states become important, we predict analytically (and confirm numerically) a change in the behaviour of the finite-size scaling function, even for those unstable particles which are not seen directly in the two-particle S-matrices.

The influence of the extra unstable particles gives the HSG models a much richer structure of renormalisation group flows than was initially thought, unifying and generalising the simplest flows between conformal field theories within a common structure. Moreover, as a result of parity breaking, some of these flows turn out to involve heterotic coset models.

Our main observations were first presented in [10, 11], and [11] can be consulted for further background material. The rest of the present paper is organised as follows. In section 2 some key features of the HSG models and their resonances are recalled, and our strategy for detecting the unstable resonances is described. This requires us to be able to separate the relevant mass scales suitably, and section 3 is devoted to an analysis of this problem in the classical theory. The idea of 'shielding' is introduced, and it is shown

[1] We restrict ourselves to simply-laced G in this paper, but we note that S-matrices for the non simply-laced cases have also been proposed, in [4].

[2] Recall that if $\boldsymbol{\beta} = \sum_1^{r_g} c_i \boldsymbol{\alpha}_i$ is a root of g, with $\{\boldsymbol{\alpha}_i\} \equiv \Delta$ a set of simple roots, then the *height* of $\boldsymbol{\beta}$ with respect to Δ is $\mathrm{ht}(\boldsymbol{\beta}) = \sum_1^{r_g} c_i$.

how certain mass scales one might naïvely expect to find in a classical HSG model may be missing. Then in section 4 we show, through a detailed analysis of the TBA equations which we illustrate with a number of examples, that these classical effects are precisely matched in the finite-size behaviour of the quantum theory. The maximal number of separated steps that a general HSG model can exhibit, a question rendered non-trivial by shielding, is discussed in section 5. We then move on to other ways to understand the crossovers, first discussing predictions from the Lagrangian approach in section 6 before making some comments on form factor calculations in section 7. Finally, section 8 contains our conclusions and there are two appendices.

2 The HSG models and their resonances

Throughout this paper, we shall be considering the HSG models corresponding to perturbations of the level-k parafermionic coset conformal field theories $G_k/U(1)^{r_g}$, where G is a simple compact Lie group, with Lie algebra g of rank r_g, Coxeter number h_g, and dual Coxeter number $h_g^\vee$. Since we will only discuss the cases where g is simply-laced, $h_g^\vee = h_g$, but we shall preserve the distinction in formulae of more general applicability.

Unlike the cases first studied by Zamolodchikov [12] and others, the HSG models are multiparameter deformations of conformal field theories[3]. The basic operators of the unperturbed theory lie in multiplets $\Phi^{\boldsymbol{\Lambda},\overline{\boldsymbol{\Lambda}}}_{\boldsymbol{\omega},\overline{\boldsymbol{\omega}}}$ labelled by two representations of G with highest weights $(\boldsymbol{\Lambda},\overline{\boldsymbol{\Lambda}})$, and two weights $(\boldsymbol{\omega},\overline{\boldsymbol{\omega}})$ in those representations [16], and the HSG perturbing operators are certain spinless primary fields $\phi \in \Phi^{\mathrm{adj},\,\mathrm{adj}}_{\mathbf{0},\,\mathbf{0}}$, with conformal dimensions $\Delta_\Phi = \bar{\Delta}_\Phi = h_g^\vee/(k+h_g^\vee)$. Since the multiplicity of the weight $\mathbf{0}$ in the adjoint representation is r_g , $\Phi^{\mathrm{adj},\,\mathrm{adj}}_{\mathbf{0},\,\mathbf{0}}$ is ${r_g}^2$-dimensional, and has a basis $\{\phi^{\mathrm{adj},\,\mathrm{adj}}_{p\,,\,q} \mid p,q = 1\ldots r_g\}$. The perturbations within this multiplet which lead to HSG models are conveniently parametrised by a pair of r_g-dimensional vectors $\boldsymbol{\lambda}$ and $\overline{\boldsymbol{\lambda}}$ as

$$\phi_{\boldsymbol{\lambda},\overline{\boldsymbol{\lambda}}} = \sum_{p,q=1}^{r_g} \lambda_p\, \overline{\lambda}_q\, \phi^{\mathrm{adj},\,\mathrm{adj}}_{p\,,\,q}\,, \tag{2.1}$$

where $\lambda_1 \ldots \lambda_{r_g}$ and $\overline{\lambda}_1 \ldots \overline{\lambda}_{r_g}$ are the components of the vectors $\boldsymbol{\lambda}$ and $\overline{\boldsymbol{\lambda}}$. From this perspective the HSG actions have the form

$$S_{HSG} = S_{CFT} + \mu \int d^2x\, \phi_{\boldsymbol{\lambda},\overline{\boldsymbol{\lambda}}}\,, \tag{2.2}$$

where S_{CFT} denotes an action for the conformal field theory of level-k G-parafermions, and μ is a dimensionful coupling which can be related to the overall mass scale, once the combined normalisation of $\boldsymbol{\lambda}$ and $\overline{\boldsymbol{\lambda}}$ has been fixed by demanding the standard short-distance behaviour of two-point functions involving $\phi_{\boldsymbol{\lambda},\overline{\boldsymbol{\lambda}}}$. Note that $\phi_{\boldsymbol{\lambda},\overline{\boldsymbol{\lambda}}}$ is trivially invariant under a joint rescaling

$$\boldsymbol{\lambda} \to \alpha\boldsymbol{\lambda}\,, \quad \overline{\boldsymbol{\lambda}} \to \alpha^{-1}\overline{\boldsymbol{\lambda}}\,, \tag{2.3}$$

[3]Other possibilities for constructing multiparameter integrable perturbations of conformal field theories are discussed in, for example, [13, 14, 15].

which together with the normalisation condition leaves $2r_g - 2$ dimensionless parameters in $\boldsymbol{\lambda}$ and $\overline{\boldsymbol{\lambda}}$. Thus the theory is determined by a total of $2r_g - 1$ parameters, one of which can be mapped onto the overall scale.

A more explicit construction of the HSG actions (2.2) is provided by the identification of S_{CFT} with the gauged Wess-Zumino-Novikov-Witten (WZW) action associated with a coset of the form G/H at level k, where $H \subset G$ is a maximal abelian torus (see [1, 2] and section 6 for details). Then, $\phi^{\mathrm{adj},\,\mathrm{adj}}_{p\,,\,q}$ are the Cartan matrix elements of the spinless primary field corresponding to the WZW field in the adjoint representation [17]. One of the nicest features of this formulation is that it simplifies the analysis of these models in the large-k limit, which corresponds to both the weak-coupling (perturbative) and semiclassical regimes of the perturbed gauged WZW action.

The HSG models can also be characterised by their long-distance, infrared, behaviour. The exact S-matrices proposed in [3] describe the scattering of a set of stable solitonic particles labelled by two quantum numbers, (i, a), where $i = 1 \ldots r_g$ labels a simple root of g, and $a = 1 \ldots k-1$. The mass of the particle (i, a) is

$$M^i_a = M m_i \, \mu_a \, , \tag{2.4}$$

where M is a dimensionful overall mass scale, $m_1, \ldots, m_{r_g}$ are r_g arbitrary (non-vanishing) relative masses, one for each simple root of g, and the numbers $\mu_a = \sin(\pi a/k)/\sin(\pi/k)$ are the components of the Perron-Frobenius eigenvector of the a_{k-1} Cartan matrix. The S-matrix elements of these particles depend on a further $r_g - 1$ real 'resonance parameters' $\sigma_{ij} = -\sigma_{ji}$, defined for each pair $\{i, j\}$ of neighbouring nodes on the Dynkin diagram of g. The resonance parameters are most conveniently specified by assigning a variable σ_i to each node of g and setting $\sigma_{ij} = \sigma_i - \sigma_j$. The resulting set of infrared parameters M, $\{m_i\}$, and $\{\sigma_i\}$ is redundant, but the obvious symmetries $M \to \alpha M$, $\{m_i\} \to \{\alpha^{-1} m_i\}$, and $\{\sigma_i\} \to \{\sigma_i + \beta\}$, ensure that there are only $2r_g - 1$ independent parameters, just as for the ultraviolet description of the models.

Classically, the theory exhibits further solitonic particle-like solutions associated with all of the other positive roots $\boldsymbol{\beta} \in \Phi^+_g$ [9]. Their masses can be specified in a concise way via

$$\boldsymbol{\lambda}_\pm = \sum_1^{r_g} m_i \, e^{\pm\sigma_i} \, \boldsymbol{\lambda}_i \tag{2.5}$$

where the $\boldsymbol{\lambda}_i$, $i = 1 \ldots r_g$, are the fundamental weights of g and satisfy $\boldsymbol{\lambda}_i \cdot \boldsymbol{\alpha}_j = \delta_{ij}$. The relative mass scale for the solitonic particles associated with the positive root $\boldsymbol{\beta}$ is then

$$m^2_{\boldsymbol{\beta}} = (\boldsymbol{\lambda}_+ \cdot \boldsymbol{\beta}) \, (\boldsymbol{\lambda}_- \cdot \boldsymbol{\beta}) \, , \tag{2.6}$$

which reduces to m_i^2 for $\boldsymbol{\beta} = \boldsymbol{\alpha}_i$. The semiclassical analysis performed using the gauged WZW formulation in [3] shows that the classical particles associated with non-simple roots decay, and so do not appear directly in the spectrum of asymptotic quantum states[4]. In particular, if $\boldsymbol{\alpha}_i + \boldsymbol{\alpha}_j$ is a root of g or, equivalently, $\{i, j\}$ is a pair of neighbouring nodes on the Dynkin diagram of g, the relative mass scale and decay width of the soliton particles associated with that root are $m^2_{\boldsymbol{\alpha}_i + \boldsymbol{\alpha}_j} = m_i^2 + m_j^2 + 2 m_i m_j \cosh(\sigma_i - \sigma_j)$ and $\Gamma_{\boldsymbol{\alpha}_i, \boldsymbol{\alpha}_j} = \frac{\pi}{k} \frac{2 m_i m_j}{m_{\boldsymbol{\alpha}_i + \boldsymbol{\alpha}_j}} \sinh |\sigma_i - \sigma_j|$.

[4] As recalled in section 6 below, this formulation also shows that $\boldsymbol{\lambda}_+$ and $\boldsymbol{\lambda}_-$ correspond in the semi-classical limit to the two vectors $\boldsymbol{\lambda}$ and $\overline{\boldsymbol{\lambda}}$ specifying the action (2.2).

In the full quantum theory, such long-lived unstable particles should correspond to *resonances* in interactions among the stable particles [18]. For example, if two stable particles scatter at a center-of-mass energy $\sqrt{s}$ close to the mass of an unstable state with appropriate quantum numbers, then they can form that state and remain in it for a time roughly equal to its lifetime, before decaying. Consequently, the transition amplitude shows a bump at the appropriate energy, which normally corresponds to a complex simple pole in the S-matrix amplitude. This pole is located on the second Riemann sheet of the complex (Mandelstam) s-plane, and its position can be conveniently written as $s_{\rm R} = (M_{\rm R} - i\Gamma_{\rm R}/2)^2$. In this way, $\tau = \hbar/\Gamma_{\rm R}$ measures the lifetime of the unstable particle, and the form of the resonance pole is given by the Breit-Wigner formula

$$S \approx 1 - i\,\frac{2M_{\rm R}\Gamma_{\rm R}}{(s - s_R)} \quad , \qquad s_R \equiv (M_{\rm R} - i\Gamma_{\rm R}/2)^2 \,. \tag{2.7}$$

Notice that the bump in the scattering probability $|1-S|^2$ occurs around $s = {\rm Re}(s_{\rm R})$, justifying the usual identification of $M_\rho \equiv \sqrt{{\rm Re}(s_{\rm R})}$ with the physical mass of the unstable particle (see for example the discussions in [19], especially [20]). Another definition sometimes used for this mass is $M_{\rm R} = {\rm Re}(\sqrt{s_{\rm R}})$. If the lifetime is large, which translates into the condition[5] $\Gamma_{\rm R} \ll M_{\rm R}$ and corresponds to the situation when the pole is close to the real (physical) axis of the complex s-plane, then $M_{\rm R} \simeq M_\rho$. Otherwise, when $\Gamma_{\rm R}$ is larger, the lifetime is short and the unstable particle does not have a definite physical mass, as a consequence of the uncertainty principle. This has made the proper definition of the masses of unstable particles a subject of debate, which becomes of phenomenological relevance when the experimental data is accurate enough, as is exemplified by the cases of the Z^0 boson [21] or the baryon resonances [22] (see also [23]). In particular, there is no general consensus as to how to choose between M_ρ and $M_{\rm R}$ to characterise the mass of the unstable state, even though they differ significantly when $\Gamma_{\rm R}/M_{\rm R}$ is large.

In the HSG models this question can be studied in a context where the S-matrix and related observables are known exactly. Even though it was the correspondence between unstable particles and resonance poles in the semiclassical limit that provided the starting-point for the S-matrix elements conjectured in [3], the fact that they are thought to be exact even away from this limit allows non-trivial predictions to be made and tested. For the scattering between particles $(i,1)$ and $(j,1)$, with i and j neighbouring nodes on the Dynkin diagram of g and with $(i,1)$ initially to the left of $(j,1)$, the relevant amplitude $S_{11}^{i\,j}(\theta)$ has a resonance pole at the complex rapidity value $\theta_{{\rm R}_{ij}} = \sigma_{ji} - i\pi/k$. This corresponds to a pole on the second sheet of the complex s-plane at $s = s_{{\rm R}_{ij}}$, where

$$s_{{\rm R}_{ij}} = M^2(m_i^2 + m_j^2 + 2m_i m_j \cosh\theta_{{\rm R}_{ij}}) \,. \tag{2.8}$$

This pole can only be associated with a physical unstable particle if ${\rm Im}(s_{{\rm R}_{ij}}) < 0$ [18], which requires $\sigma_{ji} > 0$. (If $\sigma_{ji} < 0$, the pole is a 'shadow pole' whose existence is required by the Hermitian anlyticity condition satisfied by the S-matrix amplitudes [3].) In the semiclassical limit, k is large and the parameters $\Gamma_{{\rm R}_{ij}}$ and $M_{{\rm R}_{ij}}$ corresponding to $s_{{\rm R}_{ij}}$ satisfy the bound $\Gamma_{{\rm R}_{ij}}/M_{{\rm R}_{ij}} < \pi/k$. The consequent smallness of this ratio means that the pole at $s_{{\rm R}_{ij}}$ can be immediately interpreted as a trace of a long-lived unstable particle

[5] For real physical unstable particles, the ratio $\Gamma_{\rm R}/M_{\rm R}$ runs from $\sim 10^{-2}$–10^{-1} for hadron resonances and the Z^0 and $W^\pm$ bosons, to much smaller values for other electroweakly decaying particles, like $\sim 10^{-7}$ or $\sim 10^{-15}$ for the pions π^0 and $\pi^\pm$, respectively [19].

associated with the height-two root $\boldsymbol{\alpha}_i + \boldsymbol{\alpha}_j$. In this regime the mass scale of the unstable particle is unambiguously defined by $M_{\rho_{ij}} \simeq M_{\mathrm{R}_{ij}} \simeq M m_{\boldsymbol{\alpha}_i+\boldsymbol{\alpha}_j}$, where $m_{\boldsymbol{\alpha}_i+\boldsymbol{\alpha}_j}$ is given by (2.6).

For small k, beyond the semiclassical limit, the interpretation of this pole is not so clear. It is so far from the physical real axis that the approximation provided by the Breit-Wigner formula is less useful, as illustrated by figure 1. This is particularly clear for $k = 2$, when the pole is located at $s_{\mathrm{R}_{ij}} = M^2(m_i^2 + m_j^2 - i m_i m_j \mathrm{e}^{\,\sigma_{ji}})$. Then, for large enough values of the resonance parameter, namely $\sigma_{ji} \gg \ln\,(m_i^2 + m_j^2)/m_i m_j$, the ratio $\Gamma_{\mathrm{R}_{ij}}/M_{\mathrm{R}_{ij}} \approx 2$ and, not surprisingly, the two standard ways to characterise the mass scale of the would-be unstable state lead to very different values:

$$M_{\rho_{ij}} = M\sqrt{m_i^2 + m_j^2} \quad \text{and} \quad M_{\mathrm{R}_{ij}} \approx M\sqrt{\frac{m_i m_j}{2}}\,\mathrm{e}^{\,\sigma_{ji}/2}\,. \tag{2.9}$$

Letting σ_{ji} tend to infinity, these two scales can be made arbitrarily far apart.

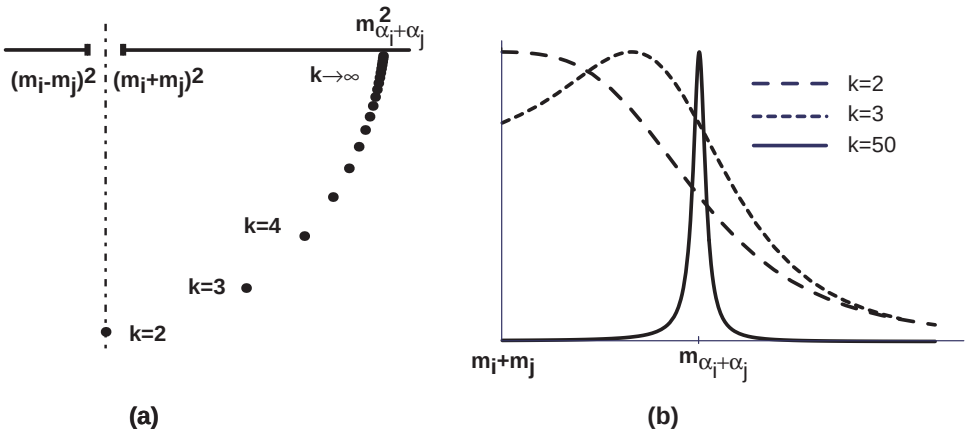

Figure 1: (a) The resonance pole of $S_{11}^{i\,j}$ in the second Riemann sheet of the complex s-plane for various values of k. (b) The scattering probability $|\eta_{ij}\mathrm{e}^{\,-i\pi/k} - S_{11}^{i\,j}|^2$ as a function of the center-of-mass energy $\sqrt{s}/M$ for $\sigma_{ji} = 5$, where $\eta_{ij}\mathrm{e}^{\,-i\pi/k} = \lim_{\,\theta\to+\infty} S_{11}^{i\,j}(\theta)$.

Thus, even the unstable particles whose resonance poles can in principle be seen in the elementary amplitudes $S_{11}^{i\,j}(\theta)$ are hard to identify unambiguously once the semiclassical domain has been left. The more general amplitudes $S_{ab}^{i\,j}(\theta)$ have a plethora of resonance poles for generic values of k – either $\min(a,b)$ or $k-\max(a,b)$, depending on whether $a+b \leq k$ or $a+b \geq k$ – and the classification of the resonances in multiparticle scattering, necessary to see the unstable particles of height greater than 2, becomes more and more involved as the number of particles increases.

Fortunately, there are other physical observables, such as correlation functions and finite-size effects, where all types of particles play similar roles, setting the scales of crossover phenomena. This is because the effective behaviour of the system at a given scale depends on the number of particle states which are effectively light at that scale, irrespective of their stability. Examining the system at different scales thus provides a well-defined method to detect the existence of physical mass scales associated with both stable and unstable particles. There is just one limitation: the nature of crossover phenomena means that their study cannot provide the values of mass scales with arbitrary

precision. In fact, this is not surprising: while the masses of the *stable* particles can alternatively be extracted, with in principle arbitrary accuracy, from the far-infrared asymptotics of correlation functions and finite-size data, no such option can exist for the unstable particles, given the uncertainty principle.

In the next sections we shall study the finite-size behaviour of generic HSG models using the thermodynamic Bethe ansatz, or TBA. Mass scales can only be picked up approximately, and some may be impossible to split apart, but within these limitations we find complete agreement with the idea that there is a scale in the quantum theory associated with each positive root of g, given by eqs. (2.5) and (2.6) as a function of the S-matrix parameters $\{m_i, \sigma_i\}$. This is consistent with the idea that all of the semiclassical soliton particles survive in the quantum theory as stable or unstable particles, for any value of k. Moreover, taking (2.9) into account, our results indicate that, at least for $k = 2$, the commonly-used formula $M_\rho = \sqrt{\mathrm{Re}(s_\mathrm{R})}$ *fails* to characterise the mass scales of the unstable particles, and favour the use of M_R instead.

3 Separating the classical mass scales

The classical theories depend on $2r_g-1$ independent parameters, but have a set of solitonic particle states for each of the $r_g\, h_g/2$ positive roots. For generic values of the parameters, the masses assigned to these roots by the formula (2.6) will all be different, and if mass scales could be discerned with arbitrary precision, one might hope to distinguish $r_g\, h_g/2$ different values. However, this is too much to expect in the quantum theory: as just discussed, unstable particles only show up in resonance poles or crossover phenomena, and these do not yield sharply-defined mass scales. The most that can be asked is to pick up *well-separated* scales, and this raises the question of how many of these can be manufactured by varying the $2r_g-1$ parameters at our disposal. Even at the classical level this is a non-trivial problem, the investigation of which forms the topic of the present section. With this out of the way we shall return to the quantum theory in section 4.

Before we begin, we should explain what we mean by 'well-separated'. The theory has $2r_g - 1$ parameters; for two scales to be well-separated, we mean that their ratio can be made arbitrarily large by varying those parameters, while leaving the overall ordering of all scales in the model unchanged. There may of course be many ways to do this, but one general prescription will be given in eq. (4.37) below. At some stages we shall also consider the logarithms of well-separated quantities, whose *differences* can be made large; to distinguish between the two concepts, we set up the following notation:

$$a \gg b \quad \Leftrightarrow \quad a - b > \kappa \tag{3.1}$$

$$A \ggg B \quad \Leftrightarrow \quad A/B > K \tag{3.2}$$

where the constants κ and K can be made arbitrarily large by varying the available parameters, uniformly for all quantities under discussion. In particular, $a \gg b \Leftrightarrow e^a \ggg e^b$.

The classical discussion starts with the mass formula (2.6), which we repeat here:

$$m_{\boldsymbol{\beta}}^2 = (\boldsymbol{\lambda}_+ \cdot \boldsymbol{\beta})\, (\boldsymbol{\lambda}_- \cdot \boldsymbol{\beta}) \ , \tag{3.3}$$

where

$$\boldsymbol{\lambda}_\pm = \sum_{i=1}^{r_g} m_i\, e^{\pm\sigma_i}\, \boldsymbol{\lambda}_i \ , \quad \boldsymbol{\lambda}_i \cdot \boldsymbol{\alpha}_j = \delta_{ij} \ . \tag{3.4}$$

Our task is to characterise, for given values of the parameters m_i and σ_j, how many separated scales appear in the set of numbers $\{m^2_{\boldsymbol{\beta}}\,,\,\boldsymbol{\beta}\in\Phi^+_g\}$.

Expanding $\boldsymbol{\beta}$ in the basis of simple roots $\{\boldsymbol{\alpha}_i\}$,

$$\boldsymbol{\beta}=\sum_{i=1}^{r_g} c_i(\boldsymbol{\beta})\,\boldsymbol{\alpha}_i \tag{3.5}$$

where the non-negative integers $c_i(\boldsymbol{\beta})=\boldsymbol{\lambda}_i\cdot\boldsymbol{\beta}$ are all of order one (the largest possible value, found for the highest root of the e_8 theories, is 6). Substituting into (3.3),

$$m^2_{\boldsymbol{\beta}}=\sum_{i,j=1}^{r_g} c_i(\boldsymbol{\beta})c_j(\boldsymbol{\beta})\,m_im_j\,e^{\sigma_i-\sigma_j}, \tag{3.6}$$

and thus all squared masses are linear combinations of the $r_g(r_g{+}1)/2$ quantities

$$m_im_j\cosh(\sigma_i{-}\sigma_j)\;,\quad i,j=1\ldots r_g\,, \tag{3.7}$$

with coefficients $2c_i(\boldsymbol{\beta})c_j(\boldsymbol{\beta})$ that are fixed, and so independent of the parameters $\{m_i,\sigma_j\}$, and are the squares of numbers of order one. Therefore, we can be sure that the model has no more than $r_g(r_g{+}1)/2$ separable scales, given by the numbers

$$m_{ij}=\sqrt{m_im_j}\,e^{|\sigma_i-\sigma_j|/2}\;,\quad i,j=1\ldots r_g\,. \tag{3.8}$$

Only in the a_n theories, for which $h_g=n{+}1=r_g{+}1$, is $r_g(r_g{+}1)/2$ equal to the number of positive roots – in all other cases it is smaller. An immediate consequence is that the maximal number of separated mass scales that a classical HSG model can exhibit is generally less than the number of positive roots. However, two more issues remain. First, we should check that the m_{ij} really can be separated. Second, since these scales only ever appear in the linear combinations (3.6), for a given configuration of the parameters, it could be that some numbers from the set (3.7) never occur as the largest term in these sums, but rather are always swamped, or shielded, by other terms. This would mean that the number of scales actually present was less than a naive analysis of (3.8) would suggest.

The first issue is easily resolved by means of a specific example. Take the particular choice $m_j=\mathrm{e}^{\,ja}$ and $\sigma_j=jb$, for two real numbers $a,b\gg 0$. Then

$$m_im_j\cosh(\sigma_i{-}\sigma_j)\approx\tfrac{1}{2}\,\mathrm{e}^{\,(i+j)\,a}\,\mathrm{e}^{\,|i-j|\,b}\,. \tag{3.9}$$

For generic a and b with a/b irrational this provides $r_g(r_g+1)/2$ different scales, which can be made of arbitrarily different magnitude by choosing a and b large enough.

The second question is more subtle, and requires some more detailed properties of root systems. Consider a particular number from the set (3.7), say $m_km_l\cosh(\sigma_k{-}\sigma_l)$. If $k=l$ then this can always be realised as the squared mass of a classical particle simply by taking $\boldsymbol{\beta}=\boldsymbol{\alpha}_k$ in (3.6), and so we can take $k\neq l$. For $m_km_l\cosh(\sigma_k{-}\sigma_l)$ to appear in the sum (3.6) for a specific root $\boldsymbol{\beta}$, it must be true that $c_k(\boldsymbol{\beta})\neq 0$ and $c_l(\boldsymbol{\beta})\neq 0$. Now for any root $\boldsymbol{\beta}$, the set of simple roots $\boldsymbol{\alpha}_i$ such that $c_i(\boldsymbol{\beta})\neq 0$ is connected on the Dynkin diagram of g.[6] Hence, there is a chain of nodes $\{i_1\ldots i_n\}$, on the Dynkin diagram of g with

[6]Suppose there are s connected components to the set of $\boldsymbol{\alpha}_i$ with $c_i(\boldsymbol{\beta})$ nonzero. Let $\boldsymbol{\beta}_t$ be the sum of the $c_i(\boldsymbol{\beta})\boldsymbol{\alpha}_i$ with $\boldsymbol{\alpha}_i$ restricted to the t^{th} component, so that $\boldsymbol{\beta}=\sum_{t=1}^s\boldsymbol{\beta}_t$. Since each $\boldsymbol{\beta}_t$ lies on the root lattice, $|\boldsymbol{\beta}_t|^2\geq 2$; and since the $\boldsymbol{\beta}_t$ are sums of roots on mutually disconnected portions of the Dynkin diagram, $\boldsymbol{\beta}_t\cdot\boldsymbol{\beta}_{t'}=0$ for $t\neq t'$. Thus $|\boldsymbol{\beta}|^2=\sum_{t=1}^s|\boldsymbol{\beta}_t|^2\geq 2s$. But $\boldsymbol{\beta}$ is a root, so $|\boldsymbol{\beta}|^2=2$ and hence $s=1$, as claimed.

$\boldsymbol{\alpha}_{i_1} = \boldsymbol{\alpha}_k$, $\boldsymbol{\alpha}_{i_n} = \boldsymbol{\alpha}_l$, $c_{i_p}(\boldsymbol{\beta}) \neq 0$ for $p = 1 \ldots n$, and with $\{i_p\,,\, i_{p+1}\}$ neighbouring nodes on the Dynkin diagram for $p = 1 \ldots n{-}1$. This means that whenever $m_k m_l \cosh(\sigma_k{-}\sigma_l)$ appears in one of the sums (3.6), it is inevitably accompanied by the terms

$$m_{i_p} m_{i_q} \cosh(\sigma_{i_p}{-}\sigma_{i_q})\,, \quad p, q = 1 \ldots n\,, \tag{3.10}$$

and $m_k m_l \cosh(\sigma_k{-}\sigma_l)$ must be larger than all of these numbers if it is not to be swamped. Taking square roots, the condition for the scale m_{kl} not to be hidden by the other scales that always appear with it is that

$$m_{kl} \ggg m_{i_p i_q} \quad \forall\ p, q \in \{1 \ldots n\} \quad \text{with} \quad \{p, q\} \neq \{1, n\}\,, \tag{3.11}$$

where the roots $\{\boldsymbol{\alpha}_{i_1} \ldots \boldsymbol{\alpha}_{i_n}\}$ form the unique chain of simple roots on the Dynkin diagram of g joining $\boldsymbol{\alpha}_k$ to $\boldsymbol{\alpha}_l$. (The chain is unique since non-affine Dynkin diagrams are trees.)

Conversely, suppose that (3.11) is satisfied for (k, l). Then, with $\{\boldsymbol{\alpha}_{i_1} \ldots \boldsymbol{\alpha}_{i_n}\}$ again the chain of roots joining $\boldsymbol{\alpha}_k$ to $\boldsymbol{\alpha}_l$, $\boldsymbol{\beta} = \boldsymbol{\alpha}_{i_1} + \cdots + \boldsymbol{\alpha}_{i_n}$ is a root of g, and $m_k m_l \cosh(\sigma_k{-}\sigma_l)$ is realised as the squared mass scale for the classical particles associated with $\boldsymbol{\beta}$ – by (3.11), it dominates all other terms in the expression (3.6) for $m^2_{\boldsymbol{\beta}}$. Thus, (3.11) gives a necessary and sufficient condition for m_{kl} to be realised as the mass scale of a set of classical particle states in the model.

There is a simple graphical method to check all of the conditions (3.11) at once. Start by drawing a series of horizontal lines, or 'telegraph wires', one for each root in the chain $\{\boldsymbol{\alpha}_{i_1} \ldots \boldsymbol{\alpha}_{i_n}\}$. Give each wire a coordinate x running from $-\infty$ to $+\infty$, and for each $p = 1 \ldots n$, paint those parts of the p^{th} wire with $|x| > \ln(m_{kl}) - \ln(m_{i_p})$ a different colour, red say.

Without loss of generality, assume that $\sigma_k \geq \sigma_l$; otherwise relabel the chain so that $i_1 = l$ and $i_n = k$. Now draw a zig-zag line between the wires, starting at the point $x_1 = -\ln(m_{kl}) + \ln(m_{i_1})$ on the first wire ($p = 1$, $i_1 = k$) and then moving horizontally by an amount $\sigma_{i_p} - \sigma_{i_{p+1}}$ going from the p^{th} to the $(p{+}1)^{\text{th}}$ wire. This way, the p^{th} segment of the line joins the point $x_p = x_1 - \sigma_{i_p} + \sigma_{i_1}$ on the p^{th} wire to the point $x_{p+1} = x_1 - \sigma_{i_{p+1}} + \sigma_{i_1}$ on the $(p{+}1)^{\text{th}}$ wire. By the time the last wire has been reached, the total horizontal shift is $\sigma_{i_1} - \sigma_{i_n} = \sigma_k - \sigma_l$, and the zig-zag terminates at $x_n = x_1 - \sigma_l + \sigma_k = +\ln(m_{kl}) - \ln(m_{i_n})$, on the n^{th} wire.

Then condition (3.11) is equivalent to the following demand:

Apart from at its beginning and end, the zig-zag remains far from all red-painted regions of wire.	(3.12)

This can be proved as follows.

Moving from wire p to wire q, the total horizontal shift of the zig-zag is $\sigma = \sigma_{i_p} - \sigma_{i_q}$. For this to fit between the red-painted regions of wires p and q, the absolute value of σ must be less than the horizontal separation of these two regions, which is $2\ln(m_{kl}) - \ln(m_{i_p}) - \ln(m_{i_q})$. Hence

$$|\sigma_{i_p} - \sigma_{i_q}| \ll 2\ln(m_{kl}) - \ln(m_{i_p}) - \ln(m_{i_q}) \tag{3.13}$$

and so, recalling (3.8),

$$2\ln(m_{i_p i_q}) \ll 2\ln(m_{kl}) \tag{3.14}$$

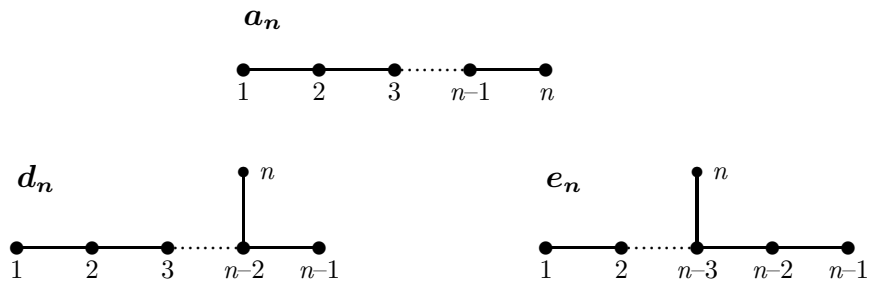

Figure 2: Dynkin diagrams of the simply-laced Lie algebras. The numbers show our labelling convention for the nodes.

For the zig-zag to remain far from all red-painted regions, this condition must be met for all $1 \leq p, q \leq n$ with $\{p, q\} \neq \{1, n\}$. (Note we include the cases $p = q$, for which (3.13) reduces to the requirement that there be a non-zero gap between the red-painted regions of the p^{th} wire.) Dividing (3.14) by 2 and exponentiating, (3.11) is recovered.

To see the condition in action, consider the d_4, or $SO(8)$, case. The Lie algebra d_4 has 4 simple roots, $\boldsymbol{\alpha}_1 \ldots \boldsymbol{\alpha}_4$, and 12 positive roots; we label the simple roots as in figure 2. For this example we shall take the masses of the four stable particles equal, and set the parameters σ_i as follows:

$$\begin{aligned} &m_1 = m_2 = m_3 = m_4 = m \ ; \\ &\sigma_1 = 100 \, , \quad \sigma_2 = 80 \, , \quad \sigma_3 = 45 \, , \quad \sigma_4 = 0 \, . \end{aligned} \tag{3.15}$$

These correspond to the following values of the three original S-matrix resonance parameters: $\sigma_{12} = 20$, $\sigma_{23} = 35$ and $\sigma_{24} = 80$.

Grouping the roots together according to their heights, the squared masses implied by (3.3) and (3.6) are

$$\begin{aligned}
\text{Height } 1: \quad & m^2_{\boldsymbol{\alpha}_1} = m^2_{\boldsymbol{\alpha}_2} = m^2_{\boldsymbol{\alpha}_3} = m^2_{\boldsymbol{\alpha}_4} = m^2 \ ; \\
\text{Height } 2: \quad & m^2_{\boldsymbol{\alpha}_1+\boldsymbol{\alpha}_2} = m^2(e^{20} + 2 + e^{-20}) \, , \\
& m^2_{\boldsymbol{\alpha}_2+\boldsymbol{\alpha}_3} = m^2(e^{35} + 2 + e^{-35}) \, , \\
& m^2_{\boldsymbol{\alpha}_2+\boldsymbol{\alpha}_4} = m^2(e^{80} + 2 + e^{-80}) \, ; \\
\text{Height } 3: \quad & m^2_{\boldsymbol{\alpha}_1+\boldsymbol{\alpha}_2+\boldsymbol{\alpha}_3} = m^2(e^{55} + e^{35} + e^{20} + 3 + e^{-20} + e^{-35} + e^{-55}) \, , \\
& m^2_{\boldsymbol{\alpha}_1+\boldsymbol{\alpha}_2+\boldsymbol{\alpha}_4} = m^2(e^{100} + e^{80} + e^{20} + 3 + e^{-20} + e^{-80} + e^{-100}) \, , \\
& m^2_{\boldsymbol{\alpha}_3+\boldsymbol{\alpha}_2+\boldsymbol{\alpha}_4} = m^2(e^{80} + e^{45} + e^{35} + 3 + e^{-35} + e^{-45} + e^{-80}) \, ; \\
\text{Height } 4: \quad & m^2_{\boldsymbol{\alpha}_1+\boldsymbol{\alpha}_2+\boldsymbol{\alpha}_3+\boldsymbol{\alpha}_4} = m^2(e^{100} + e^{80} + e^{55} + e^{45} + e^{35} + e^{20} + 4 \\
& \qquad\qquad + e^{-20} + e^{-35} + e^{-45} + e^{-55} + e^{-80} + e^{-100}) \, ; \\
\text{Height } 5: \quad & m^2_{\boldsymbol{\alpha}_1+2\boldsymbol{\alpha}_2+\boldsymbol{\alpha}_3+\boldsymbol{\alpha}_4} = m^2(e^{100} + 2e^{80} + e^{55} + e^{45} + 2e^{35} + 2e^{20} + 7 \\
& \qquad\qquad + 2e^{-20} + 2e^{-35} + e^{-45} + e^{-55} + 2e^{-80} + e^{-100}) \, .
\end{aligned} \tag{3.16}$$

Dropping subleading terms and taking square roots, the theory therefore has six separated

mass scales:

$$\begin{aligned}
m_{ii} &= m && (\sim m_{\boldsymbol{\alpha}_1},\ m_{\boldsymbol{\alpha}_2},\ m_{\boldsymbol{\alpha}_3},\ m_{\boldsymbol{\alpha}_4}) \\
m_{12} &= me^{10} && (\sim m_{\boldsymbol{\alpha}_1+\boldsymbol{\alpha}_2}) \\
m_{23} &= me^{17.5} && (\sim m_{\boldsymbol{\alpha}_2+\boldsymbol{\alpha}_3}) \\
m_{13} &= me^{27.5} && (\sim m_{\boldsymbol{\alpha}_1+\boldsymbol{\alpha}_2+\boldsymbol{\alpha}_3}) \\
m_{24} &= me^{40} && (\sim m_{\boldsymbol{\alpha}_2+\boldsymbol{\alpha}_4},\ m_{\boldsymbol{\alpha}_3+\boldsymbol{\alpha}_2+\boldsymbol{\alpha}_4}) \\
m_{14} &= me^{50} && (\sim m_{\boldsymbol{\alpha}_1+\boldsymbol{\alpha}_2+\boldsymbol{\alpha}_4},\ m_{\boldsymbol{\alpha}_1+\boldsymbol{\alpha}_2+\boldsymbol{\alpha}_3+\boldsymbol{\alpha}_4},\ m_{\boldsymbol{\alpha}_1+2\boldsymbol{\alpha}_2+\boldsymbol{\alpha}_3+\boldsymbol{\alpha}_4})
\end{aligned} \tag{3.17}$$

Comparing with the masses following from (3.8), one is missing, namely $m_{34} = me^{22.5}$. The reason for its absence is that, while $(m_{34})^2 = m^2e^{45}$ does appear in certain of the sums in (3.16), it does not dominate any of them, and hence m_{34} is always hidden underneath other scales; in particular, any $m^2_{\boldsymbol{\beta}}$ which might contain m^2_{34} also contains m^2_{24}, and $m_{24} \ggg m_{34}$. In other words, for the choice (3.15) of parameters, the scale m_{34} is *shielded* by m_{24}. To see that this shielding also follows from condition (3.12), figure 3 below shows the 'telegraph wire' diagrams for the chains of simple roots relevant for the mass scales m_{14}, m_{13} and m_{34}. (For those viewing the figures in black-and-white, the red sections of wire have been made thicker than the other parts.)

Clearly, figures 3a and 3b meet condition (3.12), while figure 3c does not. In the next section this rephrasing of the shielding criterion will be used to show in complete generality that the separated mass scales in the quantum theory, as seen in the finite-size crossover effects described by the TBA equations, precisely match those of the classical theory.

4 The quantum theory

4.1 The TBA equations

The thermodynamic Bethe ansatz (TBA) is an exact method for the calculation of the ground state energy of an integrable quantum field theory on a circle of circumference R or, equivalently, the free energy of the same theory at finite temperature $T = R^{-1}$ [24]. This allows the theory to be studied non-perturbatively at all length scales, by varying the value of R. The key input to the method is the set of two-particle S-matrix elements for the scattering of stable particle states, and these were proposed for the simply-laced HSG models in [3]. The masses of the one-particle states are given by the formula (2.4), with M an overall (quantum) mass scale. The scattering is diagonal, and to emphasise the similarities that the resulting TBA systems have with those which had previously arisen in the contexts of perturbed coset theories [25, 26, 27] and staircase models [28, 29], we shall rewrite the S-matrix elements of [3] in a slightly modified notation. Borrowing from [28], define two functions

$$S^{\min}_{ab}(\theta) = \prod_{x \in A_{ab}} \{x\}(\theta)\,, \qquad S^{F}_{ab}(\theta) = \prod_{x \in A_{ab}} (x)(\theta)\,, \tag{4.1}$$

where A_{ab} is the set of integers $\{a+b+1-2l\}_{l=1}^{\min(a,b)}$, and the blocks

$$\{x\} = (x{-}1)(x{+}1)\,, \qquad (x)(\theta) = \frac{\sinh\frac{1}{2}(\theta + i\frac{\pi x}{k})}{\sinh\frac{1}{2}(\theta - i\frac{\pi x}{k})} \tag{4.2}$$

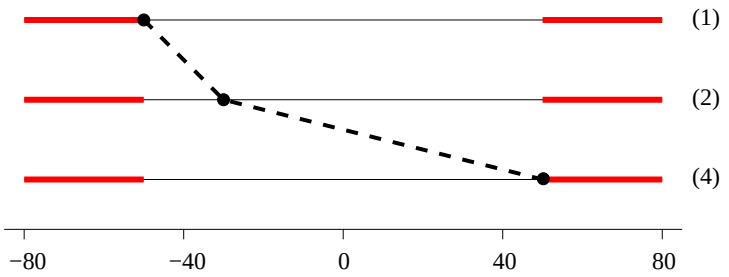

3a) The chain for m_{14} .

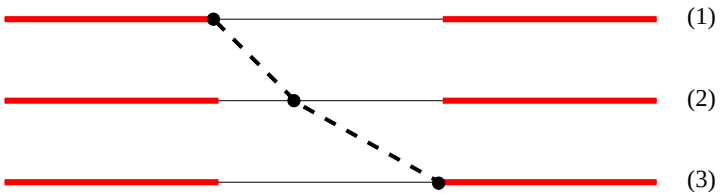

3b) The chain for m_{13} .

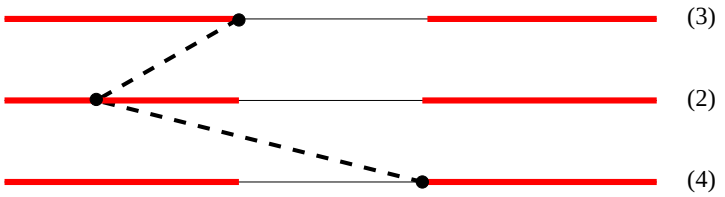

3c) The chain for m_{34} .

Figure 3: Telegraph wire diagrams for the would-be scales m_{14}, m_{13} and m_{34} in the d_4 example of section 3.

are as in [30]. The two-particle scattering amplitudes are then

$$S_{ab}^{i\,i}(\theta) = S_{ab}^{\min}(\theta) \tag{4.3}$$

$$S_{ab}^{i\,j}(\theta) = \left[(\eta_{ij})^{ab}\, S_{ab}^{F}(\theta+\sigma_{ij})\right]^{-I_{ij}^{g}} \quad \text{for} \quad i \neq j\,, \tag{4.4}$$

where θ is the rapidity, I^g is the incidence matrix of g, and $\eta_{ij} = \eta_{ji}^{-1}$ are arbitrary (fixed) k^{th} roots of -1. Recall that the functions $S_{ab}^{\text{F}}(\theta)$ sometimes fail, by a sign, to satisfy the bootstrap and crossing equations holding for $S_{ab}^{\min}(\theta)$ [28]; in contrast, the scattering amplitudes $S_{ab}^{i\,j}(\theta)$ do satisfy them due to the constant factors η_{ij} [3]. The numbers $\sigma_{ij} = -\sigma_{ji} = \sigma_i - \sigma_j$ are the real-valued resonance parameters seen earlier; since they need only be defined for $I_{ij}^g = 1$, there is an independent resonance parameter for each of the $r_g - 1$ links on the Dynkin diagram of g. An integral representation for these scattering amplitudes was given in [5].

Unlike the resonance parameters, the relative mass scales do not appear explicitly in the S-matrix. Instead, they emerge when the TBA equations are introduced. These equations have the standard form for a diagonal scattering theory, though care is needed in their derivation owing to the parity-breaking of the model [5]. There is a pseudoenergy

$\varepsilon_a^i(\theta)$ for each of the $(k-1) \times r_g$ stable particles; the mass scales m_i influence them via $(k-1) \times r_g$ energy terms

$$\nu_a^i(\theta) = M_a^i R \, \cosh\theta = m_i \mu_a r \, \cosh\theta \tag{4.5}$$

where $\mu_a = \sin(\pi a/k)/\sin(\pi/k)$ as before, and r is a dimensionless overall crossover scale:

$$r = MR \,. \tag{4.6}$$

Defining $L_a^i(\theta) = \ln(1 + \mathrm{e}^{-\varepsilon_a^i(\theta)})$, the pseudoenergies solve the TBA equations

$$\varepsilon_a^i(\theta) = \nu_a^i(\theta) - \sum_{b=1}^{k-1} \left(\phi_{ab} * L_b^i(\theta) + \sum_{j=1}^{r_g} I_{ij}^g \, \psi_{ab} * L_b^j(\theta - \sigma_{ji}) \right) \tag{4.7}$$

where '$*$' denotes the rapidity convolution

$$f * g(\theta) = \int_{-\infty}^{+\infty} \frac{d\theta'}{2\pi} \, f(\theta - \theta') \, g(\theta') \,, \tag{4.8}$$

and the TBA kernel functions ϕ and ψ are

$$\phi_{ab}(\theta) = -i \frac{\mathrm{d}}{\mathrm{d}\theta} \ln S_{ab}^{i\,i}(\theta) = -i \frac{\mathrm{d}}{\mathrm{d}\theta} \ln S_{ab}^{\min}(\theta) \,,$$

$$\psi_{ab}(\theta) = -i \frac{\mathrm{d}}{\mathrm{d}\theta} \ln S_{ab}^{i\,j}(\theta + \sigma_{ji}) = +i \frac{\mathrm{d}}{\mathrm{d}\theta} \ln S_{ab}^{\mathrm{F}}(\theta) \,, \quad \text{for} \quad I_{ij}^g = 1 \,. \tag{4.9}$$

The dimensionless effective central charge $c(r)$ for the theory at scale r is expressed in the standard way in terms of the energy terms and the solutions to the TBA equations:

$$c(r) = \frac{3}{\pi^2} \sum_{i=1}^{r_g} \sum_{a=1}^{k-1} \int_{-\infty}^{+\infty} d\theta \, \nu_a^i(\theta) \, L_a^i(\theta) \,, \tag{4.10}$$

and the ground state energy $E(R)$ is related to this through

$$E(R) = -\frac{\pi}{6R} \, c(MR) \,. \tag{4.11}$$

A bulk term linear in R may also contribute to $E(R)$, but this need not concern us here – most of the physically-relevant information from the point of view of RG flows is already contained in $c(r)$. Note that $c(r)$ depends not only on r, but also on the r_g mass scales $\{m_i\}$ and the $r_g - 1$ resonance parameters $\{\sigma_{ij}\}$: $c(r) = c(r, \{m_i\}, \{\sigma_{ij}\})$. However, since

$$c(r, \{m_i\}, \{\sigma_{ij}\}) = c(\alpha r, \{\alpha^{-1} m_i\}, \{\sigma_{ij}\}) \tag{4.12}$$

the effective central charge depends non-trivially on just $(2r_g - 1)$ parameters, one of which can be chosen to be the dimensionless overall crossover scale.

The limiting value of $c(r)$ as $r \to 0$ with all other parameters fixed is equal, in unitary cases such as these, to the central charge of the conformal field theory which is the far UV limit of the theory. For the HSG theories this was calculated in [5], with the result

$$\lim_{r \to 0} c(r) = \frac{k-1}{k+h_g} \, h_g r_g \,, \tag{4.13}$$

which is the central charge of the $G_k/U(1)^{r_g}$ coset CFT. This holds for any fixed choice of the r_g relative mass scales $0 < m_i < +\infty$ and the $r_g - 1$ resonance parameters $-\infty < \sigma_{ij} < +\infty$. In the opposite, $r \to \infty$, limit, $c(r)$ tends to zero, as expected for a massive theory.

4.2 The staircase flow

The value of the central charge in the far UV is not the only information hidden inside the HSG TBA equations. For intermediate values of r, depending on the values taken by the $\{m_i\}$ and the $\{\sigma_{ij}\}$, numerical work has shown that the scaling function $c(r)$ can have a characteristic 'staircase' pattern, hinting at a renormalisation group flow which passes close to a number of other fixed points. In contrast to Zamolodchikov's original staircase model [31] and its generalizations in [28, 32, 29], the number of steps is always finite. Furthermore, for the HSG models the staircase pattern can be understood physically, as a consequence of the decoupling of those stable or unstable particles that are effectively heavy at the relative energy scale fixed by the temperature r^{-1}. This was demonstrated for the $SU(3)_k/U(1)^2$ HSG models in [5, 7], but these cases are too simple to be affected by the subtleties about separable mass scales and shielding that were discussed in the last section. Here we shall give a more general analysis, following a line of argument used for other staircase models in [28, 29]. This will allow a full understanding of the staircase pattern to be gained, subject only to mild assumptions about the form of the solutions to (4.7). These assumptions are no more severe than those made in the analysis of the UV limit of more-usual TBA systems, but we have nevertheless verified our predictions numerically in a number of particular cases. These checks, which also serve to illustrate the patterns of flows, will be reported in section 4.5.

We shall work at a fixed (finite) value of k. Since our interest is in scales which can be made arbitrarily well-separated, the constants $\mu_a = \sin(\pi a/k)/\sin(\pi/k)$ appearing in the energy terms $\nu_a^i(\theta) = m_i \mu_a r \cosh(\theta)$ can be taken to be of order one, and ignored for the rest of the discussion. The pseudoenergies are then controlled by two sets of numbers: the resonance parameters $\{\sigma_{ij}\}$, and the values of the stable mass scales relative to the (inverse) system size, $m_i r$, which are conveniently parametrised by defining

$$\theta_i(r) \equiv \ln(\tfrac{2}{m_i r}) \ . \tag{4.14}$$

For $|\theta| \gg \theta_i(r)$, the energy terms $\nu_a^i(\theta)$ completely dominate the TBA equations for the corresponding pseudoenergies, and as a result

$$\varepsilon_a^i(\theta) \ggg 1 \quad \text{for} \quad |\theta| \gg \theta_i(r) \ , \quad a = 1 \ldots k{-}1 \, . \tag{4.15}$$

This causes the functions $L_a^i(\theta)$ to suffer a double exponential decay in this region, and to the level of approximation to which we are working,

$$L_a^i(\theta) \approx 0 \quad \text{for} \quad |\theta| \gg \theta_i(r) \ , \quad a = 1 \ldots k{-}1 \, . \tag{4.16}$$

An important special case is

$$L_a^i(\theta) \approx 0 \quad \forall\, \theta \quad \text{if } \theta_i(r) \ll 0 \, . \tag{4.17}$$

In this event the pseudoenergy $\varepsilon_a^i(\theta)$ contributes neither directly to the effective central charge, nor indirectly via any influence on the values of the other pseudoenergies. This happens when $2/r \lll m_i$; physically, it corresponds to the energy scale set by the system size, $R^{-1} = M/r$, being so much less than the mass scale of the (stable) particles of type i, Mm_i, that these particles are effectively decoupled. Such decouplings have the effect of splitting the original HSG model into smaller HSG models.

Such cases apart, there will be a region $|\theta| \ll \theta_i(r)$ within which the energy terms $\nu_i^a(\theta)$ are exponentially small, allowing them to be dropped from the TBA equations:

$$\nu_a^i(\theta) \approx 0 \quad \text{for} \quad |\theta| \ll \theta_i(r)\ , \quad a = 1 \ldots k-1\,. \tag{4.18}$$

In this region no immediate conclusion can be drawn about the values of the pseudoenergies $\varepsilon_a^i(\theta)$, as they continue to interact with other pseudoenergies via the convolution terms. The key feature [28] of this interaction is that it is *localised* in rapidity-space: for real values of θ, the kernels $\phi_{ab}(\theta)$ and $\psi_{ab}(\theta)$ are peaked about $\theta = 0$, and fall exponentially to zero outside a region of order one. In the absence of the resonance parameters σ_{ji}, this implies that, apart from the driving energy term, the value of any pseudoenergy near a given value of θ is only influenced by the values of the other pseudoenergies near that same value of θ. (This lies behind the presence of 'kink' solutions in even the simplest TBA systems [24].) For the HSG models, as for the earlier examples of staircase models, non-zero values of the resonance parameters cause the interactions between pseudoenergies to be shifted, so that, for $I_{ij}^g \neq 0$, the TBA equations (4.7) couple $\varepsilon_a^i(\theta_0)$ not to $\varepsilon_b^j(\theta)$ near $\theta = \theta_0$, but near $\theta = \theta_0 - \sigma_{ji}$. In turn, each $\varepsilon_b^j(\theta_0 - \sigma_{ji})$ interacts with further pseudoenergies $\varepsilon_c^k(\theta)$ near $\theta = \theta_0 - \sigma_{ji} - \sigma_{kj} = \theta_0 - \sigma_{ki}$, for all k such that $I_{jk}^g \neq 0$. Continuing, it is clear that in the absence of the energy terms the TBA equations couple all pairs of pseudoenergies, with $\varepsilon_a^i(\theta)$ near $\theta = \theta_0$ interacting with $\varepsilon_b^j(\theta)$ near $\theta = \theta_0 - \sigma_{ji}$ via a unique sequence of pairwise interactions along the links of the Dynkin diagram.

The fact that the non-affine Dynkin diagrams are trees, together with the antisymmetry of σ_{ij}, means that the set of rapidities $\theta_0 - \sigma_{ji}$ with which the pseudoenergy $\varepsilon_a^i(\theta)$ at $\theta \approx \theta_0$ interacts is finite. This contrasts with the original staircase models of [31, 32, 28, 29], where for non-zero values of the resonance parameter and in the absence of energy terms the psedoenergies are coupled at infinitely-many shifted values of θ. This distinction is the reason why the TBA equations for the original staircase models can show an infinite number of steps, while for the HSG models the number of steps is always finite[7].

We now return to the effect of the energy terms, which bring the scale-dependence into the TBA equations. Select a pair of nodes i and j on the Dynkin diagram, and suppose that r is such that

$$\theta_i(r) \gg 0 \quad \text{and} \quad \theta_j(r) \gg 0\,, \tag{4.19}$$

so that neither node is decoupled. For $\theta \approx \pm\theta_i(r)$, the energy term $\nu_a^i(\theta)$ entering the TBA equation for ε_a^i is of the same order as the convolution term; at these values of θ, $\varepsilon_a^i(\theta)$ has a non-trivial behaviour, and at generic values of r has the form of a so-called 'kink solution' [24] of the TBA equations. Likewise, $\varepsilon_a^j(\theta)$ generally has a kink behaviour for $\theta \approx \mp\theta_j(r)$. However, these two would-be kinks may influence each other via the chains of convolution terms just discussed. For values of r such that this occurs, the solution of the TBA system will depend on r in a non-trivial way, causing the value of the effective central charge to change and signalling a crossover in the finite-size behaviour of the model.

[7] It may be instructive to make the relationship between the spiral staircase models constructed in [29] and the HSG models more explicit. Each spiral staircase model is associated with a simply-laced Lie algebra $\mathcal{G}$ and a cyclic group $\mathbb{Z}_n$, which can be viewed as the Dynkin diagram of the affine algebra $a_{n-1}^{(1)}$. Then, for $\mathcal{G} = a_{k-1}$, the TBA equations defining the spiral staircase model can be seen as the TBA equations of the $SU(n)_k/U(1)^{n-1}$ HSG model with a particular (limiting) choice for the energy terms and resonance parameters, and with a_{n-1} replaced by $a_{n-1}^{(1)}$.

Two conditions must be satisfied for the interaction to occur. Taking the shift σ_{ij} moving from node i to node j into account, the first is that either

$$\theta_i(r) - \sigma_{ji} \approx -\theta_j(r) \qquad \text{or} \qquad -\theta_i(r) - \sigma_{ji} \approx \theta_j(r)\,, \tag{4.20}$$

depending on whether $\sigma_{ji} > 0$ or $\sigma_{ji} < 0$, respectively. Both cases are summarised by

$$\theta_i(r) + \theta_j(r) \approx |\sigma_{ij}|\,, \tag{4.21}$$

where the presence of the modulus sign is consistent with the requirement that both $\theta_i(r)$ and $\theta_j(r)$ be non-negative. Rearranging, the condition is

$$\frac{2}{r} \approx \sqrt{m_i m_j}\,\mathrm{e}^{\,|\sigma_{ij}|/2}\,. \tag{4.22}$$

In other words, $r \approx 2/m_{ij}$, and the physical system size R is of the order of the length-scale set by Mm_{ij}. Taken over all values of i and j, this yields exactly the set of crossover scales that one would predict on the basis of a naïve analysis of the set (3.8) of classical mass scales.

However, the simple picture of a crossover for every pair of pseudoenegies, caused by the interaction between the corresponding pairs of kink systems, can break down once the effects of other energy terms are taken into consideration. According to (4.16), the energy terms force the functions $L_a^l(\theta)$ to zero for $|\theta| \gg \theta_l(r)$, irrespective of the values of any other pseudoenergies. To take this into account, an additional condition is required to ensure that the chain of interactions connecting the kinks for $\varepsilon_a^i(\theta)$ and $\varepsilon_a^j(\theta)$ near to $\theta = \pm\theta_i(r)$ and $\theta = \mp\theta_j(r)$ is actually effective. Suppose that $\sigma_{ji} > 0$, and let $\{i_1 \ldots i_n\}$ be the unique chain of adjacent nodes on the Dynkin diagram joining nodes i and j, so that $i_1 = i$ and $i_n = j$. Then, for any $p = 2 \ldots n{-}1$, the value of $\varepsilon_a^i(\theta)$ at $\theta \approx \theta_i(r)$ is coupled to the value of $\varepsilon_b^{i_p}(\theta)$ at $\theta \approx \theta_i(r) - \sigma_{i_p i}$ provided that $|\theta_i(r) - \sigma_{i_p i}| \ll \theta_{i_p}(r)$. Therefore, taking (4.22) into account, the required interaction between kinks will only take place if

$$|\theta_i(r) - \sigma_{i_p i}| \ll \theta_{i_p}(r) \qquad \forall\, p = 2 \ldots n{-}1 \qquad \text{at} \quad r \approx \frac{2}{m_{ij}}\,. \tag{4.23}$$

This is identical to the classical condition summarised by eq. (3.12), which ensures that the (classical) scale m_{ij} is not shielded, and really does appear as the dominant term in the mass of some classical particle. Therefore, we deduce that there is a crossover in the finite-size behaviour of the quantum model at $r \approx 2/m_{ij}$ for each *unshielded* mass scale m_{ij} within the set of numbers given by eq. (3.8), where m_i and σ_i are now the (quantum) TBA parameters. This is one of our main results: for given values of the parameters, the set of distinct mass scales picked up by the finite-size crossover behaviour as the system size varies from zero to infinity is exactly the same as would have been predicted from an examination of the full set of classical particle masses, stable and unstable. This match includes the shielding of classical scales that was discussed in section 3, and holds for all values of k, and not just semiclassically. Otherwise stated, for the quantum theory, the set of scales at which crossover phenomena occur is not $\{m_{ij}, i, j = 1 \ldots r_g\}$, but rather $\{m_{\boldsymbol{\beta}},\, \boldsymbol{\beta} \in \Phi_g^+\}$, just as in the classical theory.

These non-perturbative results also provide a quantitative test for the accuracy of the identifications of M_ρ and M_{R}, as defined in section 2, with the physical mass scales

of the unstable particles. Take two neighbouring nodes on the Dynkin diagram of g, say $\{i, j\}$, and consider the simple pole of the amplitude $S_{11}^{ij}(\theta)$ at $\theta_{\mathrm{R}_{ij}} = \sigma_{ji} - i\pi/k$. As explained just after (2.8), when $\sigma_{ji} > 0$ this pole is expected to be the trace of the unstable particle associated with the root $\boldsymbol{\alpha}_i + \boldsymbol{\alpha}_j$, of height two. At level $k = 2$ in the limit $\sigma_{ji} \gg \ln(m_i^2 + m_j^2)/m_i m_j$, the two standard candidates to characterise the mass of this particle, from (2.9), are:

$$M_{\rho_{ij}} = M\sqrt{m_i^2 + m_j^2} \quad \text{and} \quad M_{\mathrm{R}_{ij}} \approx M\sqrt{\frac{m_i m_j}{2}}\, \mathrm{e}^{\,\sigma_{ji}/2} = \frac{M m_{ij}}{\sqrt{2}}\,. \tag{4.24}$$

For this range of parameters, the mass scale m_{ij} is unshielded, so $m_{\boldsymbol{\alpha}_i+\boldsymbol{\alpha}_j} \approx m_{ij}$. Moreover, according to our results, the finite-size behaviour of the quantum model has a crossover at $1/r \approx m_{ij}/2$, a consequence of the decoupling of the unstable particles associated with the root $\boldsymbol{\alpha}_i + \boldsymbol{\alpha}_j$. This singles out $M m_{\boldsymbol{\alpha}_i+\boldsymbol{\alpha}_j} \approx M m_{ij}$ as the physical mass scale of the unstable particle and, comparing with (4.24) and taking into account the approximate nature of the mass scales provided by the study of finite-size effects, shows that $M_{\mathrm{R}_{ij}}$ provides the correct value for the mass scale of this unstable particle. In contrast, the value of $M_{\rho_{ij}}$ can be made arbitrarily far from the value of $M m_{\boldsymbol{\alpha}_i+\boldsymbol{\alpha}_j}$ by letting σ_{ji} tend to infinity. In this case, our results clearly favour the use of $M_{\mathrm{R}} = \mathrm{Re}(\sqrt{s_R})$ to characterise the mass scale of the unstable particles against the more standard choice $M_\rho = \sqrt{\mathrm{Re}(s_R)}$.

For $k > 2$, and for the same values of the parameters, the position of the pole on the complex s-plane is $s_{\mathrm{R}_{ij}} \approx (M m_{ij})^2 e^{-i\frac{\pi}{k}}$ (see (2.8)). This leads to the following values of the two candidate masses:

$$M_{\rho_{ij}} \approx M m_{\boldsymbol{\alpha}_i+\boldsymbol{\alpha}_j}\sqrt{\cos\frac{\pi}{k}} \quad \text{and} \quad M_{\mathrm{R}_{ij}} \approx M m_{\boldsymbol{\alpha}_i+\boldsymbol{\alpha}_j}\cos\frac{\pi}{2k}\,, \tag{4.25}$$

which coincide in the large k limit, as expected. However, even at finite values of $k \geq 3$, and in contrast to the $k = 2$ case, it is not possible to make an unambiguous choice between M_ρ and M_R .

4.3 The central charges on the plateaux

At a crossover, the value of the effective central charge $c(r)$ changes rapidly; between any two separated crossovers it remains approximately constant. The next task is to calculate this constant, as it will help us to identify the fixed point being visited by the staircase flow. The calculation is largely standard; for the aspects peculiar to staircase models, see also [28, 29].

To place ourselves far from all crossovers, we suppose that $|\ln(\frac{2}{r}) - \ln m_{ij}| \gg 0$ for all i, j such that the scale m_{ij} is unshielded. (Since we are anticipating that some of the scales m_{ij} may be well-separated, this does not exclude $\ln(\frac{2}{r})$ lying between two different crossover scales.) In addition, to simplify the initial analysis we suppose that the parameters are such that there are no 'accidental' degeneracies between unshielded scales of the form $m_{ii} \approx m_{ij}$. (The precise reasons for these conditions, and what happens when they are broken, will be discussed in section 4.4 below.)

The effective central charge is given by (4.10), which we rewrite as

$$c(r) = \sum_{p=1}^{r_g} c_p(r) \tag{4.26}$$

where

$$c_p(r) = \frac{3}{\pi^2} \sum_{a=1}^{k-1} \int_{-\infty}^{+\infty} d\theta \, \nu_a^p(\theta) \, L_a^p(\theta) \tag{4.27}$$

is the direct contribution of the p^{th} set of pseudoenergies to $c(r)$. Since $\nu_a^p(\theta) \approx 0$ for $|\theta| \ll \theta_p(r)$, and $L_a^p(\theta) \approx 0$ for $|\theta| \gg \theta_p(r)$, this integral is dominated by the values taken by $L_a^p(\theta)$ at $\theta \approx \pm\theta_p(r)$ if $\theta_p(r) \gg 0$, and is zero if $\theta_p(r) \ll 0$. (Note, $\theta_p(r) \approx 0$ corresponds to $|\ln(\frac{2}{r}) - \ln m_{pp}|$ being small. Since m_{pp} is never shielded, this is already excluded by the requirement that r be far from all crossover values.)

Suppose that $\theta_p(r) \gg 0$. Since $\nu_a^p(\theta) = m_p \mu_a r \cosh\theta$, we have

$$c_p(r) = c_p^-(r) + c_p^+(r) \,, \tag{4.28}$$

where

$$c_p^\pm(r) = \frac{3}{2\pi^2} \sum_{a=1}^{k-1} \int_{-\infty}^{+\infty} d\theta \, m_p \mu_a r e^{\pm\theta} L_a^p(\theta) = \frac{3}{\pi^2} \sum_{a=1}^{k-1} \int_{-\infty}^{+\infty} d\theta \, \mu_a e^{-\theta_p(r)\pm\theta} L_a^p(\theta) \tag{4.29}$$

are the 'left' and 'right' contributions of the p^{th} pseudoenergy to the effective central charge: $c_p^-(r)$ is dominated by the values of $L_a^p(\theta)$ near $\theta = -\theta_p(r)$, and $c_p^+(r)$ by the values near $\theta = +\theta_p(r)$. The approximate values of $L_a^p(\theta)$ in these two regions are determined by a pair of 'effective' kink TBA systems. These can be found using again the facts that the kernel functions couple pseudoenergies which are adjacent on the Dynkin diagram of g at values of θ shifted by the resonance parameters, and that these chains of interacting pseudoenergies are cut whenever other energy terms force the functions $L_a^j(\theta)$ to zero. To specify the effective systems precisely, let $\widetilde{g}_p^\pm(r, \{m_i\}, \{\sigma_{ij}\})$ be the (possibly disconnected) Dynkin diagram obtained by deleting all nodes j on the Dynkin diagram of g for which $|\pm\theta_p(r) - \sigma_{jp}| \gg \theta_j(r)$, and let $g_p^\pm(r, \{m_i\}, \{\sigma_{ij}\})$ be the connected component of $\widetilde{g}_p^\pm(r, \{m_i\}, \{\sigma_{ij}\})$ containing the node p. Then, for all nodes $i \in g_p^\pm$ and to leading approximation,

$$\begin{aligned} L_a^i(\theta)\big|_{\theta\approx\pm\theta_p(r)-\sigma_{ip}} &\approx L_a^i(\theta \mp \theta_p(r) + \sigma_{ip})^\pm \,; \\ \varepsilon_a^i(\theta)\big|_{\theta\approx\pm\theta_p(r)-\sigma_{ip}} &\approx \varepsilon_a^i(\theta \mp \theta_p(r) + \sigma_{ip})^\pm \,, \end{aligned} \tag{4.30}$$

where $L_a^i(\theta)^\pm = \ln(1 + e^{\varepsilon_a^i(\theta)^\pm})$ and the effective TBA system solved by the 'kink pseudoenergies' $\varepsilon_a^i(\theta)^\pm$ is found by substituting the definitions (4.30) into (4.7) and dropping all subleading terms:

$$\varepsilon_a^i(\theta)^\pm = \delta_{ip} \, \mu_a e^{\pm\theta} - \sum_{b=1}^{k-1} \left(\phi_{ab} * L_b^i(\theta)^\pm + \sum_{j \in g_p^\pm} I_{ij}^{g_p^\pm} \, \psi_{ab} * L_b^j(\theta)^\pm \right). \tag{4.31}$$

Here $I_{ij}^{g_p^\pm}$ is the incidence matrix of the reduced Dynkin diagram $g_p^\pm$. (Note, $g_p^\pm$ in fact depends on r, $\{m_i\}$ and $\{\sigma_{ij}\}$, but this has been left implicit to avoid overburdening the notation.) In terms of the kink pseudoenergies, $c_p^\pm(r)$ is simply

$$c_p^\pm(r) = \frac{3}{\pi^2} \sum_{a=1}^{k-1} \int_{-\infty}^{+\infty} d\theta \, \mu_a e^{\pm\theta} L_a^p(\theta)^\pm \,. \tag{4.32}$$

The rapidity shifts in (4.30) serve to eliminate all relative rapidity shifts in the effective TBA system (4.31), though of course these shifts still influence the system indirectly, via their role in the determination of the diagram $g_p^{\pm}$. With all shifts removed, the effective TBA is exactly the kink form of a 'Dynkin' TBA system, of the sort discussed in [27]. Notice that there is no explicit r-dependence – the value of r only enters via its effect on $g_l^{\pm}(r, \{m_i\}, \{\sigma_{ij}\})$. This does not change between crossovers, and so the expected plateau structure is confirmed.

The integral in (4.32) can be evaluated exactly as a sum of dilogarithms. Such sums have been well-studied (see, for example, [33]), and their values can be expressed in terms of Lie-algebraic data, as follows. Let $g_p^{\pm}$ be defined as above, and let $\widehat{g}_p^{\pm}$ be the (possibly disconnected) Dynkin diagram formed by deleting the node p from $g_p^{\pm}$. For any connected Dynkin diagram $g \in a, d, e$ with rank r and Coxeter number h, define $C_k(g)$ by

$$C_k(g) = \frac{k-1}{k+h}\, hr \tag{4.33}$$

and if g is disconnected, define $C_k(g)$ to be the sum of (4.33) over all connected components of g. Then

$$c_p^{\pm} = \tfrac{1}{2}(C_k(g_p^{\pm}) - C_k(\widehat{g}_p^{\pm}))\,. \tag{4.34}$$

Note, $C_k(g)$ is the central charge of the $G_k/U(1)^r$ coset; the factor of $\frac{1}{2}$ appears in (4.34) because the full effective central charge is the sum of two contributions, one from the left and one from the right kink system. As we shall see in an example shortly, the parity-breaking of the HSG models means that in general the individual terms c_p^+ and c_p^- are not directly related, a contrast to the behaviour of more usual systems. However, the effective central charge $c(r)$ is not sensitive to parity-breaking, in the sense that the total 'left' and 'right' contributions are equal; *i.e.*,

$$\sum_{p=1}^{r_g} c_p^+(r) = \sum_{p=1}^{r_g} c_p^-(r)\,, \tag{4.35}$$

which is proved in appendix A.

The rules we have given here allow the unambiguous calculation of $c(r)$ in generic situations, away from any crossovers. The calculation of the plateau values is not exact because, for finite values of the $\theta_i(r)$ and σ_{ij}, the pseudoenergies approximated by the different effective kink TBA systems actually interact with each other, as they correspond to the behaviours in different regions of a single set of functions. If a limit could be taken such that the separation between these different regions became infinite, then the plateau value for the effective central charge would be exact. This cannot be achieved simply by taking r to zero – this would just reproduce the far UV central charge of the model in every case. Instead, to capture the intermediate plateaux, a more subtle 'multiple scaling limit' should be taken. The simplest choice is to settle on a finite set of parameters $\{\theta_i(r), \sigma_{ij}\}$ away from any crossover, and then rescale as

$$\{\theta_i(r), \sigma_{ij}\} \to \{\rho\theta_i(r), \rho\sigma_{ij}\} \tag{4.36}$$

for some positive real number ρ. In the limit $\rho \to \infty$, the plateau values of the effective central charge, calculated using the above rules, become exact. In terms of the original infrared parameters this limit is essentially

$$\{r, m_i, \sigma_{ij}\} \to \{2\left(\frac{r}{2}\right)^{\rho}, m_i^{\rho}, \rho\sigma_{ij}\} \quad ; \quad \rho \to \infty. \tag{4.37}$$

It is interesting that a single TBA system can hide such a variety of exact limits. Similar remarks in the simpler context of the traditional staircase models were made in [28, 29].

4.4 Effective TBA systems for the crossovers

The appearance of just a single 'driving term' $\delta_{ip}\,\mu_a e^{\pm\theta}$ in each kink TBA system (4.31) is a consequence of the conditions that r should be far from any crossovers, and that there should be no accidental degeneracies between unshielded scales of the form $m_{ii} \approx m_{ij}$. This can be shown as follows. Consider the value of $\varepsilon_a^p(\theta)$ near $\theta = \pm\theta_p(r)$, where the balance between the energy and convolution terms in its TBA equation causes it to have a non-trivial form. Via a chain of links on the Dynkin diagram of g, this form might be influenced by $\varepsilon_a^q(\theta)$ near $\theta = \pm\theta_p(r) - \sigma_{qp}$ (here q labels another node on the Dynkin diagram of g). Now if $|\pm\theta_p(r) - \sigma_{qp}| \gg \theta_q(r)$ then $\varepsilon_a^q(\theta)$ is completely dominated by the energy term at these values of θ, and the chain is cut; and if $|\pm\theta_p(r) - \sigma_{qp}| \ll \theta_q(r)$, then the energy term is effectively zero at these same values of θ, and so no energy term for $\varepsilon_a^q(\theta)^\pm$ should be included in the effective TBA system. The extra energy term needs only be included explicitly if $|\pm\theta_p(r) - \sigma_{qp}| \approx \theta_q(r)$, with the chain linking p to q uncut. There are two cases: (a) $\theta_p(r) \mp \sigma_{qp} \approx \theta_q(r)$, or (b) $-\theta_p(r) \pm \sigma_{qp} \approx \theta_q(r)$. Case (b) has already appeared in eq. (4.20) above, and is ruled out if r is far from any crossover scale. Case (a) translates as $m_q/m_p e^{\mp\sigma_{qp}} \approx 1$. Since $(m_{pq}/m_{qq})^2 = (m_p/m_q)e^{|\sigma_{qp}|}$ and $(m_{pp}/m_{pq})^2 = (m_p/m_q)e^{-|\sigma_{qp}|}$, this is ruled out by the condition on coincidental mass scales.

When the conditions are not met, the decoupling of the full TBA into separate effective systems, one for each still-active energy term, is not complete. The effective TBA systems for any set of energy terms which have not been disentangled must be combined into one, which itself has more than one driving term. Suppose for illustration that just one extra driving term, coming from $\varepsilon_a^q(\theta)$, needs to be included in the effective TBA system governing the form of $\varepsilon_a^p(\theta)$ near $\theta = \theta_p(r)$. (The modifications to the discussion when an extra term is instead needed for the system governing $\varepsilon_a^p(\theta)$ near $\theta = -\theta_p(r)$, or when larger numbers of extra energy terms are involved, should then be clear.) Case (a) corresponds to $\theta_p(r) - \sigma_{qp} \approx \theta_q(r)$, and it follows from the definitions made just before eq. (4.30) that the reduced diagrams $g_p^+(r, \{m_i\}, \{\sigma_{ij}\})$ and $g_q^+(r, \{m_i\}, \{\sigma_{ij}\})$ coincide. The effective TBA systems governing $\varepsilon_a^p(\theta)$ near $\theta = \theta_p(r)$ and $\varepsilon_a^q(\theta)$ near $\theta = \theta_q(r)$ should therefore be merged. Defining kink pseudoenergies as in (4.30), there are two energy terms which cannot be discarded and the effective system is

$$\varepsilon_a^i(\theta)^+ = \delta_{ip}\,\mu_a e^\theta + \delta_{iq}\,\mu_a \frac{m_q}{m_p} e^{-\sigma_{qp}} e^\theta - \sum_{b=1}^{k-1} \left(\phi_{ab} * L_b^i(\theta)^+ + \sum_{j \in g_l^\pm} I_{ij}^{g_l^\pm}\ \psi_{ab} * L_b^j(\theta)^+ \right) \quad (4.38)$$

and the separate contributions of $c_p^+(r)$ and $c_q^+(r)$ to the total effective central charge should be replaced by

$$c_{p+q}^+(r) = \frac{3}{\pi^2} \sum_{a=1}^{k-1} \int_{-\infty}^{+\infty} d\theta\ \left(\mu_a e^\theta L_a^p(\theta)^+ + \mu_a \frac{m_q}{m_p} e^{-\sigma_{qp}} e^\theta L_a^q(\theta)^+ \right). \quad (4.39)$$

Note that the 'coincidence condition' $\theta_p(r) - \sigma_{qp} \approx \theta_q(r)$ implies that $(m_q/m_p)e^{-\sigma_{qp}}$ is of order 1. This term cannot be eliminated from the equations without reintroducing

a rapidity shift for the second convolution term in (4.38), but the apparent asymmetry between p and q can be removed by making an overall shift $\theta \to \theta + \ln m_p + \sigma_{qp}/2$. The value of c^+_{p+q} is calculated as for the generic plateau case discussed in the last section, the only difference being that the diagram $\widehat{g}^+_p$ is now found by deleting both nodes p and q from g^+_p, instead of just node p. From this it follows that the value of $c^\pm_{p+q}$ is in fact independent of $(m_q/m_p)e^{-\sigma_{qp}}$, and it is easy to check from the rules for calculation given above that its value is consistent with the value of $c^\pm_p + c^\pm_q$ found when $(m_q/m_p)e^{-\sigma_{qp}}$ becomes large (or small) and the p and q kink systems decouple. Physically this is as it should be – the approximate equality of the scales m_{pp} and m_{pq} will only be seen in the finite-size behaviour of the system at the corresponding crossovers, and the scale r at which this calculation has been performed is away from all crossovers.

For case (b), the story is different and gives the archetypal approximation for the finite-size behaviour during a crossover. We have $\theta_p(r) - \sigma_{qp} \approx -\theta_q(r)$, with $\sigma_{qp} > 0$ since we have already supposed that both $\theta_p(r)$ and $\theta_q(r)$ be positive. The reduced diagrams g^+_p and g^-_q coincide, and the effective TBA systems governing $\varepsilon^p_a(\theta)$ near $\theta = \theta_p(r)$ and $\varepsilon^q_a(\theta)$ near $\theta = -\theta_q(r)$ should be merged. As the first system involves e^θ in its energy term and the second $e^{-\theta}$, it is no longer possible to eliminate all r-dependence by an overall shift in θ. If kink pseudoenergies are again defined as in (4.30), the effective system is

$$\varepsilon^i_a(\theta)^+ = \delta_{ip}\,\mu_a e^\theta + \delta_{iq}\,\mu_a \frac{m_p m_q}{4} e^{\sigma_{qp}} r^2\, e^{-\theta} - \sum_{b=1}^{k-1} \left(\phi_{ab} * L^i_b(\theta)^+ + \sum_{j \in g^\pm_p} I^{g^\pm_p}_{ij}\ \psi_{ab} * L^j_b(\theta)^+ \right) \tag{4.40}$$

Using $m^2_{pq} = m_p m_q e^{\sigma_{qp}}$ (recall that σ_{qp} is positive), shifting $\theta \to \theta + \ln(m_{pq}/2)$ and redefining the pseudoenergies appropriately, this can be put in the more symmetrical form

$$\varepsilon^i_a(\theta)^+ = \tfrac{1}{2}\delta_{ip}\,\mu_a m_{pq} r\, e^\theta + \tfrac{1}{2}\delta_{iq}\,\mu_a m_{pq} r\, e^{-\theta} - \sum_{b=1}^{k-1} \left(\phi_{ab} * L^i_b(\theta)^+ + \sum_{j \in g^\pm_p} I^{g^\pm_p}_{ij}\ \psi_{ab} * L^j_b(\theta)^+ \right). \tag{4.41}$$

The contribution to the effective central charge, which replaces $c^+_p(r) + c^-_q(r)$, is then[8]

$$c^+_{p+q}(r) = \frac{3}{\pi^2} \sum_{a=1}^{k-1} \int_{-\infty}^{+\infty} d\theta\ \left(\tfrac{1}{2}\mu_a m_{pq} r\, e^\theta L^p_a(\theta)^+ + \tfrac{1}{2}\mu_a m_{pq} r\, e^{-\theta} L^q_a(\theta)^+ \right). \tag{4.42}$$

These equations make it particularly clear that the crossover scale is m_{pq}. Considered on their own, these HSG crossover TBA systems generalise massless TBAs discussed in [27], in that there is no requirement for the nodes p and q to be symmetrically-placed on the Dynkin diagram of g. This greater freedom is related to the fact that the HSG models can break parity, an option not treated in [27]. Note also that we only discussed the simplest cases here; by suitably tuning the parameters it can be arranged for more driving terms to be present in the effective TBA systems, giving, for example, new multiparameter families of massless flows which may or may not break parity.

[8]Beware that the '+' label we associated with this effective TBA system is potentially misleading, as it actually arises from the merging of a '+' kink system with a '−' kink system, but for the sake of simplicity we do not introduce a further notation.

4.5 Examples

We now outline some specific examples, starting with the $SU(4)_2/U(1)^3$ HSG model, for which a number of numerically-obtained plots are shown in figure 4.

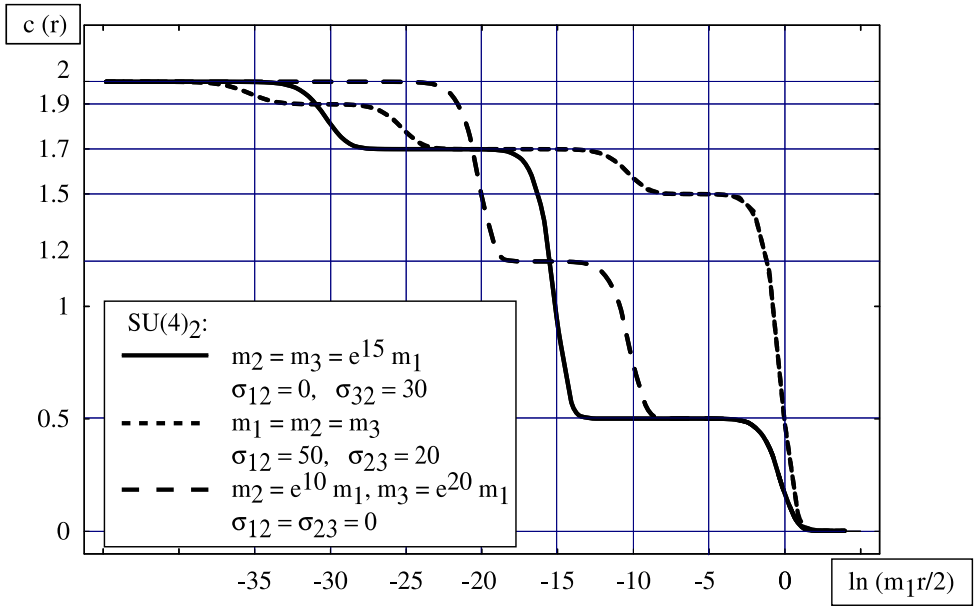

Figure 4: The TBA scaling functions for the $SU(4)_2/U(1)^3$ HSG model.

Simplest to describe is the flow with both resonance parameters zero: $\sigma_{12} = \sigma_{23} = 0$, drawn as a dashed line on the plot. The mass scales are such that $m_1 \lll m_2 \lll m_3$.[9] As r varies from 0 and $+\infty$, the effective central charge exhibits three plateaux corresponding to the regions $2r^{-1} \ggg m_3$ (the deep UV limit), $m_2 \lll 2r^{-1} \lll m_3$, and $m_1 \lll 2r^{-1} \lll m_2$, before it reaches the massive region for $2r^{-1} \lll m_1$ where $c(r)$ vanishes. Within each region, $c(r)$ matches the central charges of the following coset CFTs:

$$\text{(UV)} \quad \frac{SU(4)_k}{U(1)^3} \xrightarrow{m_3} \frac{SU(3)_k}{U(1)^2} \xrightarrow{m_2} \frac{SU(2)_k}{U(1)} \xrightarrow{m_1} \text{Massive} \quad \text{(IR)}\,. \tag{4.43}$$

The central charges can be recovered using the rules given above as follows. We return to the 'telegraph wire' diagrams of the last section, but this time allow them to depend on r (the previous 'chain' diagrams occur as subdiagrams when r is placed at the relevant crossover scale). Draw a wire for every node of the Dynkin diagram of g (in this case, that for a_3), give each wire a coordinate θ, and paint red those parts of the l^{th} wire with $|\theta| > \theta_l(r)$, for $l = 1 \ldots r_g$. The diagram $g_l^{\pm}$ is found by first drawing a node for the 'driving' point $\theta = \pm\theta_l(r)$ on the l^{th} wire. (If $\theta_l(r)$ is negative, then $\varepsilon_a^l(\theta)$ is already decoupled, and no node need be drawn.) Then move from wire to wire of the diagram according to the connectivity of the Dynkin diagram, shifting in θ by σ_{ij} when moving from wire i to wire j. So long as the points reached lie on unpainted sections of wire, then they should be included in $g_l^{\pm}$. It is easily checked that this graphical technique matches the rule for the construction of $g_l^{\pm}$ given just before (4.30).

[9] We continue to use the conventions of fig. 2 for numbering the nodes of the Dynkin diagram of g.

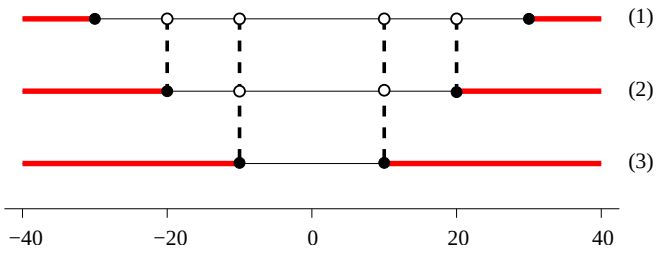

5a) $\ln(m_1 r/2) = -30$.

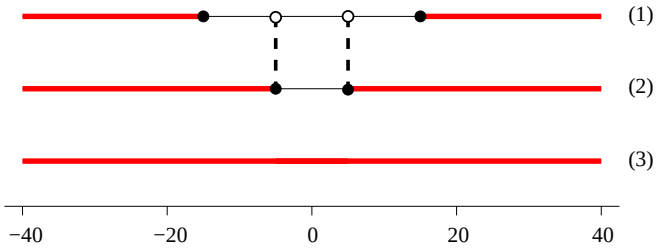

5b) $\ln(m_1 r/2) = -15$.

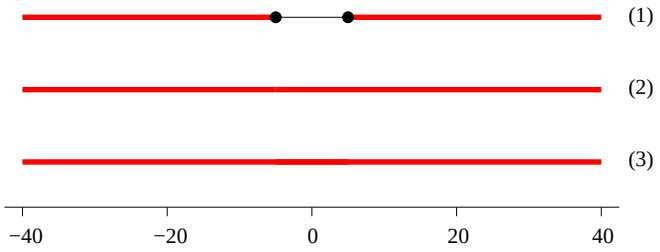

5c) $\ln(m_1 r/2) = -5$.

Figure 5: Effective TBA systems for the dashed-line flow in figure 4.

Figure 5a shows the resulting collection of kink TBA systems for the dashed-line flow at $\ln(m_1 r/2) = -30$. The systems are symmetrical between left and right, so $c_l^+ = c_l^-$ for each l and $c_l = 2c_l^\pm = C_k(g_l^\pm) - C_k(\widehat{g}_l^\pm)$. Hence the total central charge is

$$c = C_k(a_1) + (C_k(a_2) - C_k(a_1)) + (C_k(a_3) - C_k(a_2)) = C_k(a_3) \tag{4.44}$$

as expected for the far UV limit.

If instead $\ln(m_1 r/2) = -15$, the relevant diagram is drawn in figure 5b. The pseudoenergies ε_a^3 have decoupled, and the central charge is

$$c = C_k(a_1) + (C_k(a_2) - C_k(a_1)) = C_k(a_2)\,. \tag{4.45}$$

Finally, at $\ln(m_1 r/2) = -5$ all pseudoenergies but ε_a^1 have decoupled; the diagram is shown in figure 5c and the central charge is

$$c = C_k(a_1). \tag{4.46}$$

In contrast, had the mass scales been chosen such that $m_1 \simeq m_3 \lll m_2$, then $c(r)$

would have exhibited only two plateaux with effective central charges matching a flow

$$\text{(UV)} \quad \frac{SU(4)_k}{U(1)^3} \xrightarrow{m_2} \frac{SU(2)_k}{U(1)} \times \frac{SU(2)_k}{U(1)} \xrightarrow{m_1 \simeq m_3} \text{Massive} \quad \text{(IR)}\,. \tag{4.47}$$

We leave it to the reader to verify this using the diagrammatic approach.

Parenthetically, for any HSG model, we remark that if all the resonance parameters vanish then the mass scales can be adjusted so as to permit the existence of a regime in the RG flow from UV to IR where

$$m_{i_1}, \ldots, m_{i_l} \lll 2r^{-1} \lll m_{i_{l+1}}, \ldots, m_{i_{r_g}}\,. \tag{4.48}$$

In this portion of the flow all the particles of types 'i_{l+1}', ..., 'i_{r_g}' have already decoupled, with $L_a^{i_{l+1}}(\theta), \ldots, L_a^{i_{r_g}}(\theta) \approx 0$. This leaves us with the TBA equations corresponding to the HSG model associated with the coset $G_k^{[i_{l+1}\ldots i_{r_g}]}/U(1)^{r_g}$, where $G^{[i_{l+1}\ldots i_{r_g}]}$ denotes the subgroup of G associated with the (possibly disconnected) Dynkin diagram obtained by removing the $i_{l+1}, \ldots, i_{r_g}$–th nodes from the Dynkin diagram of g, times a $U(1)^{r_g-l}$ factor associated with those nodes. Physically, these staircase patterns reflect the decoupling of the stable particles when they are heavy compared to the relative energy scale fixed by the temperature r^{-1}, and the possible splitting of the initial HSG model into a number of decoupled components.

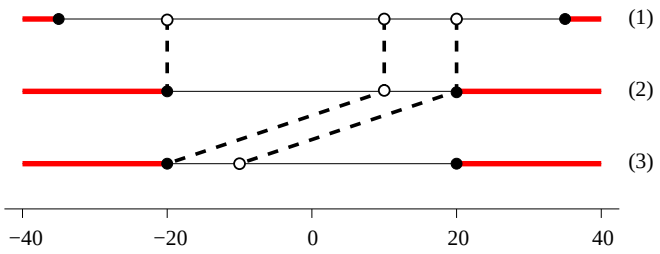

6a) $\ln(m_1 r/2) = -35$.

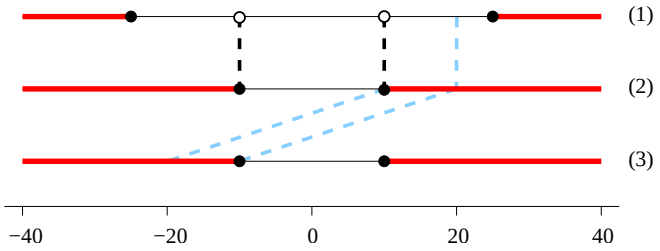

6b) $\ln(m_1 r/2) = -25$.

Figure 6: Effective TBA systems for the solid-line flow in figure 4.

Returning to the $SU(4)_2/U(1)^3$ examples of figure 4, we now analyse the flow shown as a solid line on figure 4, which breaks parity. In the far UV, which for this set of parameters can be found for $\ln(m_1 r/2) = -35$, the set of kink TBA systems is shown in figure 6a. Notice that, this time, the evident left-right symmetry has been lost. The calculation of c goes otherwise as before, with the same (expected) result: $c = C_k(a_3)$.

Increasing r through the first crossover, there is no decoupling of stable pseudoenergies, but the effective kink systems determining the values of c_3^- and c_2^+ change, as can be seen on figure 6b. (We have also shown, lightly-shaded, the parts of the kink systems which have been lost in the crossover.) Now $c = C_k(a_1) + (C_k(a_2) - C_k(a_1)) + C_k(a_1) = C_k(a_2) + C_k(a_1)$. Again this is easily understood physically – the crossover corresponds to the unstable particle corresponding to the root $\boldsymbol{\alpha}_2 + \boldsymbol{\alpha}_3$ becoming relatively heavy and decoupling; this splits the $SU(4)_k/U(1)^3$ HSG model into two decoupled parts, HSG models for $SU(3)_k/U(1)^2$ and $SU(2)_k/U(1)$, and makes it natural to conjecture that the full flow is

$$\text{(UV)}\quad \frac{SU(4)_k}{U(1)^3} \xrightarrow{m_{23}} \frac{SU(3)_k}{U(1)^2} \times \frac{SU(2)_k}{U(1)} \xrightarrow{m_2=m_3} \frac{SU(2)_k}{U(1)} \xrightarrow{m_1} \text{Massive}\quad \text{(IR)}\,. \tag{4.49}$$

Notice that the effective TBA system (4.41) governing the crossover at $r^{-1} \approx m_{23}$ is of massless type, but, since the driving terms are asymmetrically placed on the a_3 Dynkin diagram, it lies outwith the class of massless Dynkin TBA systems discussed in [27].

Finally, figure 7 shows the sets of effective kink TBA systems for the four plateaux of the flow shown as a dotted line in figure 4, which are separated by crossovers at $\ln(m_1 r/2) \approx -35$, -25, -10 and 0.

A coset identification for the fixed points visited by the flow is

$$\begin{aligned}\text{(UV)}\quad \frac{SU(4)_k}{U(1)^3} &\xrightarrow{m_{13}} \frac{SU(3)_k}{SU(2)_k \times U(1)} \times \frac{SU(3)_k}{U(1)^2} \xrightarrow{m_{12}} \frac{SU(2)_k}{U(1)} \times \frac{SU(3)_k}{U(1)^2} \\ &\xrightarrow{m_{23}} \left[\frac{SU(2)_k}{U(1)}\right]^{\times 3} \xrightarrow{m_{ii}} \text{Massive}\quad \text{(IR)}\,.\end{aligned} \tag{4.50}$$

This is the simplest example which inevitably involves a coset CFT not of parafermionic type: here, $\frac{SU(3)_k}{SU(2)_k \times U(1)}$. By level-rank duality [34], this is $\frac{SU(k)_2 \times SU(k)_1}{SU(k)_3}$, the coset which might have been more naturally suggested by a comparison of the effective TBA governing the crossover with the results of [25, 26]. Note also that the step at highest energy (that furthest into the UV) involves the mass scale m_{13} associated with the root $\boldsymbol{\alpha}_1 + \boldsymbol{\alpha}_2 + \boldsymbol{\alpha}_3$, which is of height 3, and so corresponds to an unstable particle which is not seen directly in the two-particle S-matrix elements. Even so, the TBA picks it up with no problems, as expected given our general analysis.

In general, a knowledge of the effective central charge is not enough to identify a coset unambiguously. In particular, parity-breaking in the HSG models brings with it a number of interesting phenomena, to which we shall return in section 6 and appendix A. However, the examples discussed above are sufficiently simple that these issues do not arise.

Some flows for the two rank 4 simply-laced Lie algebras, $a_4 \equiv SU(5)$ and $d_4 \equiv SO(8)$, are shown in figure 8. Again, the locations and heights of the steps all agree with the predictions of the rules formulated above. These flows were already presented in [10, 11], where conjectures for the fixed points visited by each of them can be found. More about the d_4 case can be found around eq. (6.36) below, in the context of the Lagrangian treatment of the flows.

Notice that the two a_4 flows have a different number of steps: 7 for the solid line, and only 6 for the dashed line. This is a simple consequence of the fact that $m_{12} = m_{24}$ for the choice of parameters corresponding to the dashed-line flow, while the mass scales m_{ij}, $i \neq j$, are all different for the solid line. A more subtle feature, not seen on the previous

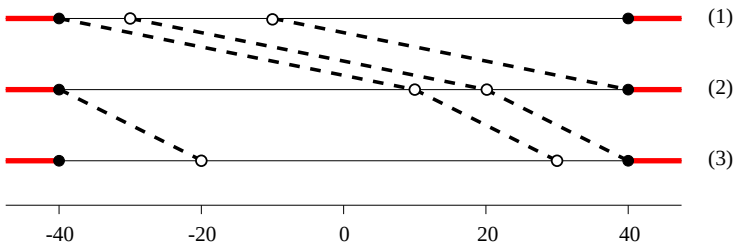

7a) $\ln(m_1 r/2) = -40$.

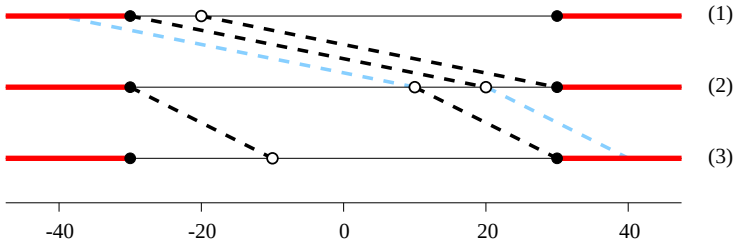

7b) $\ln(m_1 r/2) = -30$.

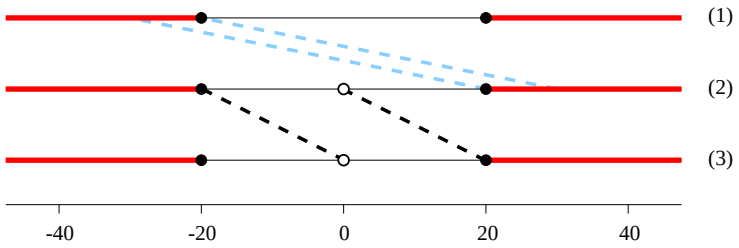

7c) $\ln(m_1 r/2) = -20$.

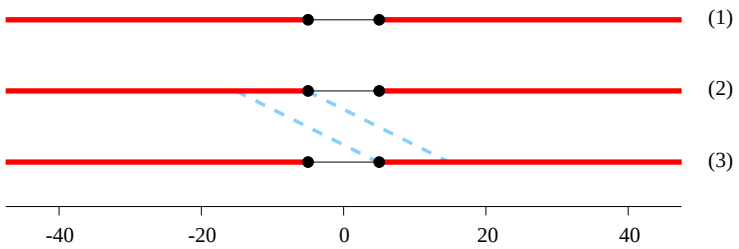

7d) $\ln(m_1 r/2) = -5$.

Figure 7: Effective TBA systems for the dotted-line flow in figure 4.

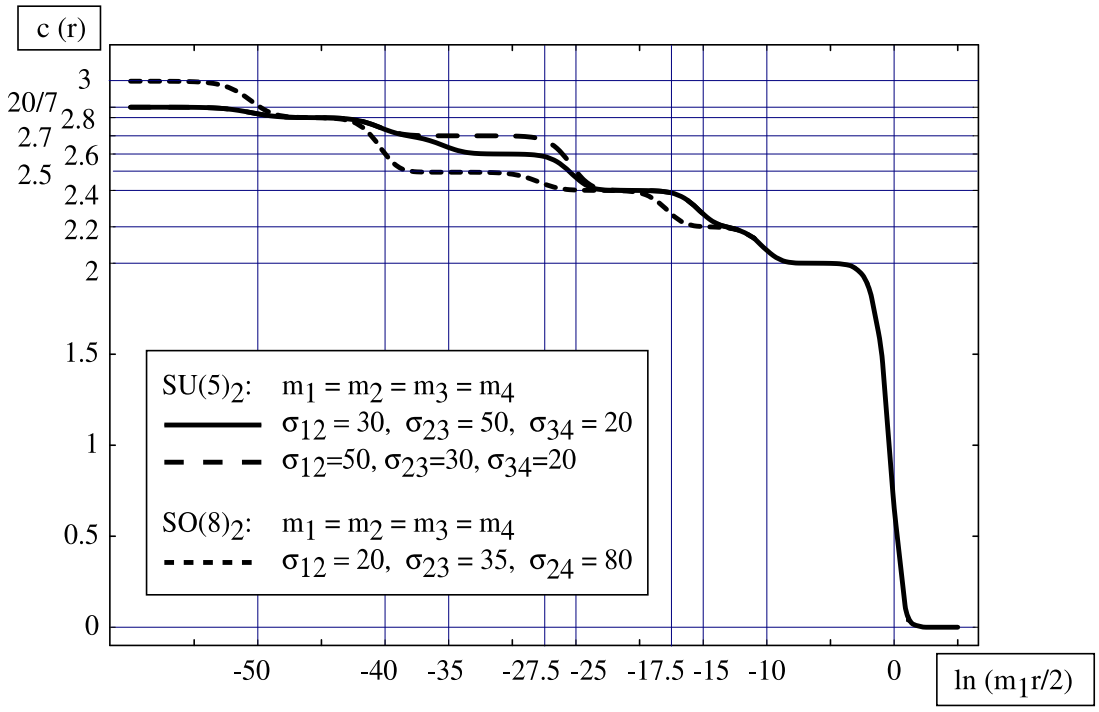

Figure 8: The TBA scaling function for the $SU(5)_2/U(1)^4$ and $SO(8)_2/U(1)^4$ HSG models.

collection of plots, concerns the d_4 flow, for which the quantum parameters were chosen to match the set of classical parameters analysed in section 3, eq. (3.15). All of the mass scales m_{ij}, $i \neq j$, are different, and yet there are only 6 steps. A naïve analysis would have predicted a crossover at $\ln(m_1 r/2) = \ln(m_1/m_{34}) = -22.5$, but this step is absent. This absence is exactly as predicted by our analysis of shielding.

By separating the stable mass scales we can add 3 more steps to each flow, making a total of 10 for the a_4 example corresponding to the solid line but only 9 for d_4. Now, in spite of the phenomenon of shielding, one might have expected that the *maximal* number of steps for a given algebra would equal the maximal possible number of distinct scales m_{ij} in every case, which for rank 4 is $r_g(r_g+1)/2 = 10$. Might a different choice of parameters for d_4 avoid the shielding, and produce a flow with the 10 steps we have already seen for a_4? In fact the answer to this question is no, as we now show.

5 The maximal number of steps

In this section, we find, for a generic simply-laced Lie algebra, the maximal number of well-separated scales that can be found in the set of numbers $\{m_{\boldsymbol{\beta}}\,,\ \boldsymbol{\beta} \in \Phi_g^+\}$, as the $2r_g - 1$ parameters are varied. This is equal to the maximal number of well-separated steps that can be found in the flow of the effective central charge of the corresponding quantum field theories.

By the results of section 3, the number of well-separated scales in $\{m_{\boldsymbol{\beta}}\,,\ \boldsymbol{\beta} \in \Phi_g^+\}$ for any given set of values of the parameters $\{m_i\}$ and $\{\sigma_j\}$ is equal to the number of *unshielded* well-separated scales in $\{m_{ij}\,,\ i,j = 1 \ldots r_g\}$. Our strategy will be to start by maximising the number of scales from this latter set which are unshielded, and only then

to worry about separating the unshielded scales so as to avoid any degeneracies.

We first take $g = a_n$, whose Dynkin diagram is simply a chain $\{1 \dots n\}$ of n nodes, where $\{j, j+1\}$ are neighbours for $j = 1 \dots n-1$ (see fig. 2). This case is rather trivial: consider the particular choice $m_j = \mathrm{e}^{\,ja}$ and $\sigma_j = jb$, for two real numbers $a, b \gg 0$ such that a/b is irrational. If we take $a \ll b$, it is straightforward to check that the constraints (3.11) are satisfied for all k, l, and so all of the m_{kl} are unshielded. Furthermore, as in (3.9), these scales can be made arbitrarily far apart by taking a and b large. Therefore, for $g = a_n$, the maximal number of well-separated scales is equal to $n(n+1)/2$, which is also the number of positive roots.

The d and e cases are more tricky, and we shall exploit the fact that their Dynkin diagrams always contain a–type subdiagrams. As a preliminary, we claim that a necessary condition for all of the scales m_{kl} associated with an a_n diagram (or subdiagram) to be unshielded is that the resonance parameters $\{\sigma_i\}$ and the stable-particle mass scales $\{m_i\}$ should satisfy

- $\left|\ln\left(m_i/m_{i+1}\right)\right| \ll \left|\sigma_i - \sigma_{i+1}\right| \quad \forall\, i = 1 \dots n-1$ (5.1)

and

- either $\quad \sigma_1 \gg \sigma_2 \gg \cdots \gg \sigma_n \quad$ or $\quad \sigma_1 \ll \sigma_2 \ll \cdots \ll \sigma_n$ (5.2)

In order to prove this, notice that, from (3.11), the relevant conditions to ensure that all the scales m_{kl} be unshielded are

$$m_{kl} \lll m_{pq} \quad \forall\, k, l, p, q \;\text{ such that }\; 1 \le k \le p \le q \le l \le n \;\text{ with }\; \{p, q\} \neq \{k, l\}\,. \tag{5.3}$$

These ensure that each m_{kl} appears as the dominating term in $m_{\boldsymbol{\beta}}$ for the positive root $\boldsymbol{\beta} = \sum_{i=k}^{l} \boldsymbol{\alpha}_i$. Taking logs and rearranging, the inequality in (5.3) is equivalent to

$$|\sigma_k - \sigma_l| - |\sigma_p - \sigma_q| \gg \ln(m_p/m_k) + \ln(m_q/m_l) \tag{5.4}$$

Then, the need for (5.1) follows from (5.4) on setting $k = p = q = i$, $l = i+1$, and then $k = i$, $p = q = l = i+1$. The first choice gives

$$|\sigma_i - \sigma_{i+1}| \gg \ln(m_i/m_{i+1}) \tag{5.5}$$

and the second

$$|\sigma_i - \sigma_{i+1}| \gg \ln(m_{i+1}/m_i)\,. \tag{5.6}$$

Combining the two, (5.1) is recovered. To see the need for (5.2), suppose that the condition does *not* hold. Then there must be a sequence σ_i, σ_{i+1}, σ_{i+2} such that either

$$\sigma_i \gg \sigma_{i+1} \ll \sigma_{i+2} \tag{5.7}$$

or

$$\sigma_i \ll \sigma_{i+1} \gg \sigma_{i+2} \tag{5.8}$$

(Note, $\sigma_i \sim \sigma_{i+1}$ and $\sigma_{i+1} \sim \sigma_{i+2}$ are excluded by (5.1), which has already been established.) Consider (5.7), and suppose that $\sigma_i \ge \sigma_{i+2}$. Then

$$|\sigma_i - \sigma_{i+2}| = \sigma_i - \sigma_{i+2} = \sigma_i - \sigma_{i+1} + \sigma_{i+1} - \sigma_{i+2} = |\sigma_i - \sigma_{i+1}| - |\sigma_{i+1} - \sigma_{i+2}| \tag{5.9}$$

and so

$$|\sigma_i - \sigma_{i+2}| - |\sigma_i - \sigma_{i+1}| = -|\sigma_{i+1} - \sigma_{i+2}| \ll -|\ln(m_{i+1}/m_{i+2})| \tag{5.10}$$

using (5.1) for the final inequality. On the other hand, (5.4) for $k = p = i$, $q = i{+}1$, $l = i{+}2$ is

$$|\sigma_i - \sigma_{i+2}| - |\sigma_i - \sigma_{i+1}| \gg \ln(m_{i+1}/m_{i+2}) \tag{5.11}$$

The contradiction with (5.10) rules out (5.7) with $\sigma_i \geq \sigma_{i+2}$; the other options are dealt with similarly, establishing the necessity of (5.2).

Parenthetically we remark that not only are (5.1) and (5.2) necessary conditions for the $n(n+1)/2$ scales $\{m_{kl}\}$ to be unshielded; they are also sufficient. Suppose that the first option of (5.2) holds. (The argument is trivially rewritten for the second option.) Then the LHS of (5.4) is equal to $\sigma_k - \sigma_p + \sigma_q - \sigma_l$, while, using (5.1),

$$\begin{aligned} \ln(m_p/m_k) &\leq |\ln(m_k/m_p)| \\ &\leq |\ln(m_k/m_{k+1})| + |\ln(m_{k+1}/m_{k+2})| + \cdots + |\ln(m_{p-1}/m_p)| \\ &\ll \sigma_k - \sigma_p \,. \end{aligned} \tag{5.12}$$

Likewise, $\ln(m_q/m_l) \ll \sigma_q - \sigma_l$, and so $\ln(m_p/m_k) + \ln(m_q/m_l) \ll \sigma_k - \sigma_p + \sigma_q - \sigma_l$, which is the required result.

Once the necessity of (5.1) and (5.2) has been established, it is easy to see that at least one scale m_{kl} must be shielded for the d and e cases. Condition (5.2) implies that the sequence $\{\sigma_{i_k}\}$ for any chain of nodes $\{i_k\}$ on the Dynkin diagram must be monotonic, since otherwise one of the scales $m_{i_k i_l}$ associated with that chain will be shielded. Now the d and e Dynkin diagrams are forked, and it is clearly impossible to enforce simultaneous monotonicity for the three maximal chains of nodes including the fork node. (For $g = d_n$, these are the chains $\{1 \ldots n{-}1\}$, $\{1 \ldots n{-}2, n\}$, and $\{n{-}1, n{-}2, n\}$ in the labelling of fig. 2; for $g = e_n$, $\{1 \ldots n{-}1\}$, $\{1 \ldots n{-}3, n\}$, and $\{n{-}1, n{-}2, n{-}3, n\}$.) Hence, the number of unshielded scales certainly cannot exceed $n(n{+}1)/2 - 1$. To show that this number can be attained, and that the resulting $n(n{+}1)/2 - 1$ unshielded scales can be separated, we resort again to explicit examples. For $g = d_n$, one can take

$$\begin{aligned} &\sigma_i = ib \quad \forall i = 1 \ldots n{-}1 \,, \qquad \sigma_n = \sigma_{n-2} \,, \\ &m_i = \mathrm{e}^{\,ja} \quad \forall j = 1 \ldots n{-}1 \,, \qquad m_n = \mathrm{e}^{\,(n+1)a} \,, \end{aligned} \tag{5.13}$$

and for $g = e_n$,

$$\begin{aligned} &\sigma_i = ib \quad \forall i = 1 \ldots n{-}1 \,, \qquad \sigma_n = \sigma_{n-3} \,, \\ &m_j = \mathrm{e}^{\,ja} \quad \forall j = 1 \ldots n{-}1 \,, \qquad m_n = \mathrm{e}^{\,na} \,, \end{aligned} \tag{5.14}$$

where in all cases a and b are real numbers, $\gg 0$, such that a/b is irrational, and $b \gg 4a$. It is easy to check that the constraints (3.11) are satisfied for all k, l, with the only exceptions being $\{k, l\} = \{n{-}2, n\}$ for $g = d_n$, or $\{k, l\} = \{n{-}3, n\}$ for $g = e_n$. This means that the scale $m_{n-2,n}$ (for $g = d_n$) or $m_{n-3,n}$ (for $g = e_n$) is shielded. Moreover, all the unshielded scales m_{kl} can be given arbitrarily well-separated magnitudes by choosing a and b large enough. Therefore, for $g = d_n$ and $g = e_n$, the maximal number of well-separated mass scales is $n(n+1)/2 - 1$.

For $g = d_n$, there is another generic way to arrange the parameters such that only one scale is shielded: suppose that

$$\begin{array}{lll} \text{either} & \sigma_1 \ll \sigma_2 \ll \cdots \ll \sigma_{n-1} & \text{and} \quad \sigma_{n-2} \ll \sigma_n \\ \text{or} & \sigma_1 \gg \sigma_2 \gg \cdots \gg \sigma_{n-1} & \text{and} \quad \sigma_{n-2} \gg \sigma_n \,, \end{array} \tag{5.15}$$

and in addition

$$\left|\ln\left(m_i/m_j\right)\right| \ll \left|\sigma_i - \sigma_j\right| \tag{5.16}$$

for each pair of neighbouring nodes $\{i, j\}$. Then, all the scales m_{ij} with $i, j = 1 \ldots n-1$, and m_{in} with $i = 1 \ldots n-2, n$ are unshielded. In contrast, the number $m_{n-1\,n}$ is always swamped by other scales in the sums (3.6). All these numbers can be separated, as shown by the particular choice of parameters used in (3.9) with $a \ll b$.

A similar trick does not succeed for $g = e_n$ because the shortest maximal chain including the fork node has length 4 rather than 3. In this case, the only choices of $\{m_i, \sigma_i\}$ leading to the maximal number of unshielded scales are those that satisfy the following constraints. First, the parameters associated with the chain of nodes $\{1 \ldots n-1\}$ have to satisfy the conditions (5.1) and (5.2), to ensure that all the scales m_{kl} with $k, l = 1 \ldots n-1$ are unshielded. Second, σ_n and m_n have to be chosen such that

$$\begin{aligned} & m_n \lll m_{n-3} \,, \quad |\sigma_{n-3} - \sigma_n| \lesssim |\ln(m_{n-3}/m_n)| \,, \\ & |\sigma_{n-1} - \sigma_n| - |\sigma_{n-2} - \sigma_n| \gg \ln(m_{n-2}/m_{n-1}) \,, \\ & |\sigma_i - \sigma_n| \gg \ln(m_n/m_i) \quad i = n-4, n-2 \,, \\ & |\sigma_i - \sigma_n| - |\sigma_i - \sigma_{n-3}| \gg \ln(m_{n-3}/m_n) \quad \forall i = 1 \ldots n-1 \,,\ i \neq n-3 \,, \\ & |\sigma_i - \sigma_n| - |\sigma_{i+1} - \sigma_n| \gg \ln(m_{i+1}/m_i) \quad \forall i = 1 \ldots n-5 \,. \end{aligned} \tag{5.17}$$

The proof of these conditions is based on the characterisation of the choices of parameters such that all but one of the scales associated with a given chain are unshielded, which can be easily derived from (5.1) and (5.2). Since it is rather involved, it will be omitted. It is straightforward to check that the values (5.14) satisfy (5.17).

Our results for the maximal number of separable mass scales are summarised in table 1. (Note that this table corrects an error in the result for $g = e_n$ reported in [11].)

g	Maximal number of separable scales
a_n	$n(n+1)/2 \,, \quad n \geq 1$
d_n	$n(n+1)/2 - 1 \,, \quad n \geq 4$
e_n	$n(n+1)/2 - 1 \,, \quad n = 6, 7, 8$

Table 1: The maximal number of separable scales for the HSG models associated with the different simply-laced Lie groups (see also the comments in the last two paragraphs of section 5).

Sometimes, it is of interest to consider choices of the parameters with all the stable-particle mass scales equal, so that $m_i = m_j \quad \forall i, j$. For such cases it is clear that the maximal number of well-separated scales cannot be larger that the number quoted in table 1, minus $(n-1)$. For $g = a_n$ and d_n, this number can be attained, as can be shown via an explicit example. In both cases, take

$$\sigma_i = 2^i b \quad \forall i = 1 \ldots n \,, \tag{5.18}$$

where b is a real number $\gg 0$. For $g = a_n$, this choice satisfies (5.1) and (5.2), and for $g = d_n$, (5.15) and (5.16). All of the resulting unshielded scales m_{kl} can be given arbitrarily well-separated values by choosing b large enough.

However, for $g = e_n$, eq. (5.17) shows that $m_n \ggg m_{n-3}$ is a necessary condition to achieve the maximal number of unshielded scales. Therefore, by taking all the stable-particle mass scales to be equal we lose at least one extra unshielded scale, and the resulting maximal number of well-separated scales cannot be larger than the number quoted in table 1 minus n. For an explicit example where this number is attained, one can again take (5.18), which makes all of the scales m_{kl} with $k \neq l$ unshielded with the only exception of $m_{n-2\,n}$ and $m_{n-1\,n}$, and well-separated, by choosing b large enough.

6 Crossovers from the Lagrangian approach

The original formulation of the HSG theories was in terms of a gauged WZW action modified by a potential [1, 2]. This explicit Lagrangian definition provides a more physical interpretation of the crossovers observed in the study of finite-size effects using the TBA, allowing them to be seen as consequences of changes in the number of the field configurations that remain effectively massless at the given finite-size (RG) scale. In addition, this interpretation turns out to be very useful in elucidating the precise nature of the effective field theories between well-separated crossovers. While such a semiclassical analysis is rather naïve, it turns out to be surprisingly powerful.

The HSG theories corresponding to perturbations of the coset $G_k/U(1)^{r_g}$ have actions

$$S_{\rm HSG}[\gamma, A_\pm] = k\Big(S_{\rm gWZW}[\gamma, A_\pm] \; - \int d^2x\, V(\gamma)\Big)\,. \tag{6.1}$$

Here, $\gamma = \gamma(t,x)$ is a bosonic field that takes values in some faithful representation of the compact Lie group G, and $A_\pm$ are non-dynamical gauge fields taking values in the Cartan subalgebra of g associated with $H \simeq U(1)^{r_g}$, a maximal torus of G. Then, $S_{\rm gWZW}$ is the gauged WZW action corresponding to the coset G/H [35, 36]. The potential is

$$V(\gamma) = \frac{m_0^2}{4\pi}\,\langle \Lambda_+, \gamma^\dagger \Lambda_- \gamma\rangle\,, \tag{6.2}$$

where m_0^2 is a bare overall mass scale, $\langle\ ,\ \rangle$ is the Killing form of g, and $\Lambda_\pm = i\boldsymbol{\lambda}_\pm \cdot \boldsymbol{h}$ are two arbitrary elements in the Cartan subalgebra of g associated with the maximal torus H, specified by two r_g-dimensional vectors $\boldsymbol{\lambda}_+$ and $\boldsymbol{\lambda}_-$. In this context, $S_{\rm HSG}$ is a Lagrangian action defined on 1+1 Minkowski space. (In contrast, eq. (2.2) defines the model as a perturbed conformal field theory in two-dimensional Euclidean space with role of the potential $V(\gamma)$ being taken by the perturbing operator $\mu\,\phi_{\boldsymbol{\lambda},\overline{\boldsymbol{\lambda}}}$.) The field γ in (6.1) has $\dim(G) = (h_g{+}1)r_g$ degrees of freedom. However, $S_{\rm HSG}$ is invariant under a group of abelian gauge transformations generated by H. This built-in gauge symmetry removes r_g degrees of freedom, and $S_{\rm HSG}$ is actually defined on the coset manifold G/H of dimension $r_g h_g$. The positive integer k is known as the 'level' [37]. Classically, it plays the role of an inverse coupling constant, and both the weak-coupling (perturbative) and semiclassical regimes are recovered when k is large. $kS_{\rm gWZW}$ provides an action for the $G_k/U(1)^{r_g}$ coset conformal field theory, and the potential is a composite field that can be identified with a (gauge invariant) matrix element of the WZW field γ taken in the

adjoint representation [17]. This is the spinless relevant primary field that defines the perturbation, and the resulting theory is massive for any choice of $\boldsymbol{\lambda}_+$ and $\boldsymbol{\lambda}_-$ such that $\boldsymbol{\lambda}_\pm \cdot \boldsymbol{\alpha} \neq 0$ for all roots $\boldsymbol{\alpha}$ of g; for these cases quantum integrability was checked in [2].

Without loss of generality, $\boldsymbol{\lambda}_+$ and $\boldsymbol{\lambda}_-$ can be restricted to live in the same Weyl chamber [1], which ensures that $V(\gamma)$ has a minimum at $\gamma = \mathbb{I}$ [10]. In the following, we shall assume that the simple roots have been chosen so that this chamber is the fundamental Weyl chamber. Then, $\boldsymbol{\lambda}_+$ and $\boldsymbol{\lambda}_-$ specify the classical masses and resonance parameters of the solitons associated with the positive roots $\boldsymbol{\beta}$ via the formulae [3, 9]

$$M_{\boldsymbol{\beta}}^2 = m_0^2 (\boldsymbol{\beta}\cdot\boldsymbol{\lambda}_+)(\boldsymbol{\beta}\cdot\boldsymbol{\lambda}_-) \quad \text{and} \quad \sigma_{\boldsymbol{\beta}} = \frac{1}{2}\ln\frac{\boldsymbol{\beta}\cdot\boldsymbol{\lambda}_+}{\boldsymbol{\beta}\cdot\boldsymbol{\lambda}_-}\,, \tag{6.3}$$

and, up to the overall bare mass scale, $M_{\boldsymbol{\beta}}^2$ coincides with (2.6). These equations can be solved for $\boldsymbol{\lambda}_+$ and $\boldsymbol{\lambda}_-$ as functions of $m_i = M_{\boldsymbol{\alpha}_i}/m_0$ and $\sigma_i = \sigma_{\boldsymbol{\alpha}_i}$ to recover (2.5). When substituted in (6.2), this provides the following decomposition of the potential:

$$V(\gamma) = \frac{m_0^2}{4\pi}\sum_{i,j=1}^{r_g} \mu_{ij}^2\,\Gamma_{ij}(\gamma)\,, \tag{6.4}$$

where

$$\mu_{ij}^2 = m_i\, m_j\, \mathrm{e}^{\,\sigma_i-\sigma_j} \qquad \text{and} \qquad \Gamma_{ij}(\gamma) = -\Big\langle (\boldsymbol{\lambda}_i\cdot\boldsymbol{h})\,,\ \gamma^\dagger\,(\boldsymbol{\lambda}_j\cdot\boldsymbol{h})\,\gamma\Big\rangle\,. \tag{6.5}$$

This shows that the potential depends on the $r_g h_g$ gauge-invariant degrees of freedom of the fundamental field γ through the r_g^2 composite fields $\Gamma_{ij}(\gamma)$. All the dependence on the parameters $\{m_i, \sigma_i\}$ is concentrated in the real positive coupling constants μ_{ij}. Notice that m_{ij}, as defined in (3.8), is equal to $\max(\mu_{ij}, \mu_{ji})$. Recall also that the parity symmetry of the unperturbed gauged WZW theory is implemented by the simultaneous transformations $x \to -x$, $\gamma \to \gamma^\dagger$. Since $\Gamma_{ij}(\gamma^\dagger) = \Gamma_{ji}(\gamma)$, the condition for this symmetry to be respected by the perturbation is $\mu_{ij} = \mu_{ji}$. The composite fields $\Gamma_{ij}(\gamma)$ are independent of the parameters and, since the group G is compact, their size is bounded and can be taken to be of order one. Eq. (6.4) provides an explicit realisation of the general parametrisation of the perturbing operator given in (2.1), as

$$V(\gamma) = \frac{m_0^2}{4\pi}\sum_{i,j=1}^{r_g} \mu_{ij}^2\,\Gamma_{ij}(\gamma) \;\equiv\; \mu\sum_{p,q=1}^{r_g}\lambda_p\overline{\lambda}_q\,\phi^{\mathrm{adj},\,\mathrm{adj}}_{p\,,\,q} = \mu\,\phi_{\boldsymbol{\lambda},\overline{\boldsymbol{\lambda}}}\,. \tag{6.6}$$

Noticing that $\mu_{ij}^2 = (\boldsymbol{\lambda}_+\cdot\boldsymbol{\alpha}_i)(\boldsymbol{\lambda}_-\cdot\boldsymbol{\alpha}_j)$, this shows that the two vectors $\boldsymbol{\lambda}$ and $\overline{\boldsymbol{\lambda}}$ correspond to $\boldsymbol{\lambda}_+$ and $\boldsymbol{\lambda}_-$ in the semiclassical limit.

The decomposition (6.4) provides a simple physical explanation for the pattern of crossover effects observed in the TBA analysis. All of the coupling constants $(m_0^2/4\pi)\,\mu_{ij}^2$ have the dimension of a squared mass scale. Therefore, along the RG trajectory corresponding to the action (6.1), they are relatively small in the UV region, and large in the IR. In massive theories with just one coupling constant, of the type most often discussed

[10] The group of gauge transformations can be taken to be of axial form, *i.e.*, $\gamma \to \alpha\gamma\alpha$ with $\alpha = \alpha(t,x)$ taking values in H, which makes the minimum of the potential at $\gamma = \mathbb{I}$ unique, modulo gauge transformations.

in the perturbed conformal field theory literature, there is only one independent mass scale and the passage from the UV to the IR involves just one transition. In contrast, for the HSG theories, the various mass scales $(m_0^2/4\pi)\,\mu_{ij}^2$ can be given very different values by varying the parameters $\{m_i, \sigma_i\}$. As the RG scale passes any of these scales, a new transition may potentially occur; from the Lagrangian point of view, this underlies the observed staircase trajectories.

However, when the scale associated with a given coupling is reached, it could be that all fields involved in the corresponding interaction have already decoupled. To avoid this issue in our initial discussion, suppose that the values of the parameters are such that one coefficient, say μ_{ij}, is much larger than all of the others. One way to achieve this is to choose the parameters

$$m_k = \mathrm{e}^{\,a\delta_{k,i}}\,, \quad \sigma_k = 0, \qquad \forall\, k = 1 \ldots r_g \tag{6.7}$$

for $i = j$, or

$$m_k = 1\,, \quad \sigma_k = a\big(\delta_{k,i} - \delta_{k,j}\big), \qquad \forall\, k = 1 \ldots r_g \tag{6.8}$$

for $i \neq j$, with $a \gg 0$ in both cases. Then, starting from the UV where all couplings are effectively zero and all fields effectively massless, at the squared mass scale $(m_0^2/4\pi)\,\mu_{ij}^2$, only μ_{ij} has become effectively nonzero. This coupling governs the separation between the UV and the IR regions for all configurations of the field γ such that $\Gamma_{ij}(\gamma)$ is non-trivial; *i.e.*, for those γ such that $\Gamma_{ij}(\gamma) \not\approx \Gamma_{ij}(\mathbb{1})$, where $\gamma = \mathbb{1}$ is the absolute minimum of the potential. Defining a dimensionless RG scale $\overline{\Lambda} = \frac{\sqrt{4\pi}}{m_0}\,\Lambda$, the effect of $\Gamma_{ij}(\gamma)$ is negligible for $\overline{\Lambda} \ggg \mu_{ij}$, and only those field configurations such that $\Gamma_{ij}(\gamma) \approx \Gamma_{ij}(\mathbb{1})$ remain in the effective theory for $\overline{\Lambda} \lll \mu_{ij}$. Since μ_{ij} was assumed to be larger than all of the other coefficients, it is in particular larger than μ_{ji}, and so $\mu_{ij} = m_{ij}$ and this crossover happens at one of the classical mass scales.

To solve the condition $\Gamma_{ij}(\gamma) \approx \Gamma_{ij}(\mathbb{1})$, we first recall that every element γ of a compact connected Lie group lies in a one-parameter subgroup, so that $\gamma = \exp X$ for some $X \in g$. Introducing a Cartan-Weyl basis for the complexification of g, consisting of a Cartan subalgebra $\{h_1 \ldots h_{r_g}\}$ and step generators $E_{\boldsymbol{\alpha}}$, X is of the general form

$$X = i\boldsymbol{t}\cdot\boldsymbol{h} + \sum_{\boldsymbol{\alpha}\in\Phi^+} (\phi_{\boldsymbol{\alpha}} E_{\boldsymbol{\alpha}} - \phi^*_{\boldsymbol{\alpha}} E_{-\boldsymbol{\alpha}}) = -X^\dagger\,, \tag{6.9}$$

where $\boldsymbol{t}$ is real, and the $\phi_{\boldsymbol{\alpha}}$ are complex. Then

$$\begin{aligned}\Gamma_{ij}(\exp X) - \Gamma_{ij}(\mathbb{1}) &= -\sum_{n\geq 2} \frac{1}{n!} \Big\langle (\mathrm{ad}X)^n(\boldsymbol{\lambda}_i\cdot\boldsymbol{h})\,,\ \boldsymbol{\lambda}_j\cdot\boldsymbol{h}\Big\rangle \\ &= \sum_{\boldsymbol{\alpha}\in\Phi^+} (\boldsymbol{\alpha}\cdot\boldsymbol{\lambda}_i)(\boldsymbol{\alpha}\cdot\boldsymbol{\lambda}_j)\,\langle E_{\boldsymbol{\alpha}}, E_{-\boldsymbol{\alpha}}\rangle\,|\phi_{\boldsymbol{\alpha}}|^2 - \sum_{n\geq 3} \frac{1}{n!} \Big\langle (\mathrm{ad}X)^n(\boldsymbol{\lambda}_i\cdot\boldsymbol{h})\,,\ \boldsymbol{\lambda}_j\cdot\boldsymbol{h}\Big\rangle\,. \end{aligned} \tag{6.10}$$

At the level of the quadratic (leading) term, the condition $\Gamma_{ij}(\gamma) = \Gamma_{ij}(\mathbb{1})$ is therefore solved by restricting the sum in (6.9) to the roots $\boldsymbol{\alpha}$ of g that satisfy $(\boldsymbol{\alpha}\cdot\boldsymbol{\lambda}_i)(\boldsymbol{\alpha}\cdot\boldsymbol{\lambda}_j) = 0$, and this gives the possible flat (effectively massless) directions away from the identity. Notice that the condition to quadratic order is symmetrical in i and j: the flat directions for Γ_{ij} and Γ_{ji} coincide at the identity.

However, to match the non-perturbative TBA results, the full vacuum manifold for the effective theory should be mapped out. In order to do this, we first recall the notation introduced just after (4.48): $g^{[i_1,\ldots,i_n]}$ denotes the Dynkin diagram obtained by deleting the nodes $i_1 \ldots i_n$ from the Dynkin diagram of g, and $G^{[i_1,\ldots,i_n]}$ the compact subgroup of G associated with $g^{[i_1,\ldots,i_n]}$ times a $U(1)^n$ factor associated with those nodes. We shall also use the superscript $^{[i_1,\ldots,i_n]}$ to indicate that a field configuration takes values in this group. With this notation in place, we show that $\Gamma_{ij}(\gamma)$ is invariant under the action of $G_L^{[j]} \times G_R^{[i]}$, by which we mean that

$$\Gamma_{ij}(\phi^{[j]}\,\gamma\,\psi^{[i]}) = \Gamma_{ij}(\gamma), \qquad \forall \phi^{[j]} \in G^{[j]} \quad \text{and} \quad \psi^{[i]} \in G^{[i]}. \tag{6.11}$$

This follows from the fact that, if $\psi = \exp X$ with X of the form (6.9), then

$$\psi(\boldsymbol{\lambda}_i \cdot \boldsymbol{h})\psi^\dagger = \boldsymbol{\lambda}_i \cdot \boldsymbol{h} - \sum_{\boldsymbol{\alpha}\in\Phi^+} (\boldsymbol{\alpha}\cdot\boldsymbol{\lambda}_i) \sum_{n\geq 1} \frac{1}{n!} (\mathrm{ad}X)^{n-1}(\phi_{\boldsymbol{\alpha}} E_{\boldsymbol{\alpha}} + \phi^*_{\boldsymbol{\alpha}} E_{-\boldsymbol{\alpha}})\,. \tag{6.12}$$

If $\psi = \psi^{[i]} \in G^{[i]}$, the sum (6.9) for the corresponding X is restricted to the roots $\boldsymbol{\alpha}$ of g such that $\boldsymbol{\alpha}\cdot\boldsymbol{\lambda}_i = 0$, and so $\psi^{[i]}(\boldsymbol{\lambda}_i\cdot\boldsymbol{h})\psi^{[i]\,\dagger} = \boldsymbol{\lambda}_i\cdot\boldsymbol{h}$. Similarly, if $\phi^{[j]} \in G^{[j]}$ then $\phi^{[j]\dagger}(\boldsymbol{\lambda}_j\cdot\boldsymbol{h})\phi^{[j]} = \boldsymbol{\lambda}_j\cdot\boldsymbol{h}$. Combining these two facts is enough to prove (6.11), and to show, in particular, that $\Gamma_{ij}(\phi^{[j]}\,\mathbb{1}\,\psi^{[i]}) = \Gamma_{ij}(\mathbb{1})$. Adding the already-performed identification of the flat directions at the identity, the final conclusion is that the configurations connected to the identity which satisfy $\Gamma_{ij}(\gamma) = \Gamma_{ij}(\mathbb{1})$ live in the submanifold of G

$$G^{[j]}\cdot G^{[i]} = \{\phi^{[j]}\,\psi^{[i]} \,|\, \phi^{[j]} \in G^{[j]}, \psi^{[i]} \in G^{[i]}\}. \tag{6.13}$$

These fields participate in the effective theory in the regime $\mu_{ij} \ggg \overline{\Lambda} \ggg \mu_{pq}$ in situations where $\mu_{ij} \ggg \mu_{pq}$ for all $(p,q) \neq (i,j)$. Near to the identity they correspond to the effectively massless fluctuations, and are symmetrical in i and j. However, it is important to appreciate that the full manifolds of effective field configurations left unfrozen by Γ_{ij} and Γ_{ji} can be different, reflecting the breaking of parity, even though this asymmetry never shows up in the quadratic approximation to (6.10).

This characterisation of the effective theory provides useful information about the fixed point visited by the RG flow after the first crossover has occurred. This fixed point is associated with the gauged WZW action in (6.1), S_{gWZW}, restricted to the manifold $G^{[j]}\cdot G^{[i]}$, whose conformal field theory interpretation will be investigated in the following paragraphs.

We start with the case when $i = j$. Then, the manifold of effective field configurations is $G^{[i]}\cdot G^{[i]} = G^{[i]}$, which is a subgroup of G that splits into a product of simple groups associated with the (possibly disconnected) Dynkin diagram $g^{[i]}$, times a $U(1)$ factor. Recall that the HSG model was originally defined not on G, but on the coset manifold G/H, where $H \simeq U(1)^{r_g}$ is a maximal torus of G. Therefore, the fixed point is specified by the restriction of S_{gWZW} to the manifold $G^{[i]}/H$, which is in agreement with the TBA results presented just after (4.48). Since, by construction, the $U(1)$ factor in $G^{[i]}$ is contained in H, the restriction of the gauged WZW action to $G^{[i]}/H$ splits into a number of decoupled parafermionic theories, one for each simple factor in $G^{[i]}$, and all of them at level k.

The case with $i \neq j$ is more involved. We start by characterising the manifold of effective field configurations $G^{[j]}\cdot G^{[i]}$ as a coset manifold. First, we note that there is

an obvious map from $G^{[j]} \times G^{[i]}$ into $G^{[j]} \cdot G^{[i]}$ given by $(\phi^{[j]}, \psi^{[i]}) \to \phi^{[j]}\psi^{[i]}$. However this is not one-to-one, since $\phi^{[j]}\psi^{[i]}$ is invariant under $\phi^{[j]} \to \phi^{[j]}\rho^{-1}$ and $\psi^{[i]} \to \rho\psi^{[i]}$, for any $\rho \in G^{[i,j]} = G^{[j]} \cap G^{[i]}$, and so this action should be factored out. This provides the following coset realisation of the manifold of effective field configurations:

$$G^{[j]} \cdot G^{[i]} \simeq \frac{G^{[j]} \times G^{[i]}}{G^{[i,j]}} \,, \tag{6.14}$$

where the action of $G^{[i,j]}$ on $G^{[j]} \times G^{[i]}$ is $(\phi^{[j]}, \psi^{[i]}) \to (\phi^{[j]}\rho^{-1}, \rho\psi^{[i]})$, for any $\rho \in G^{[i.j]}$. Parenthetically, we point out that this coset is a particular example of those considered by Guadagnini *et al.* in [38] (see also [39]), which is one of the first papers dealing with N/D coset models where different left and right actions of D on N are gauged: the so-called 'asymmetric cosets'. Models of this type, and their generalisations, are examples of 'heterotic' conformal field theories and have been of some interest in string theory; in addition to the papers just mentioned, refs. [40, 41, 42, 43, 44, 45] give a sample of work in this direction.

However, in our case, not all the field configurations $\gamma \in G^{[j]} \cdot G^{[i]}$ are physical. The actions $S_{\rm gWZW}$ and $S_{\rm HSG}$ in (6.1) are invariant under a group of abelian gauge transformations generated by a maximal torus $H \simeq U(1)^{r_g}$ of G, and they are therefore defined on G/H. The precise form of the gauge group is $\gamma \to \alpha\,\gamma\,\widehat{\tau}(\alpha^{-1})$, $A_\pm \to \alpha(A_\pm + \partial_\pm)\alpha^{-1}$, which is parametrised by the lift $\widehat{\tau}$ of a suitable orthogonal $O(r_g)$ transformation τ acting on the Cartan subalgebra into H [1, 2].[11] Taking all of this into account, the full manifold of *physical* effective field configurations left unfrozen by Γ_{ij} can be identified with the coset

$$\frac{G^{[j]} \times G^{[i]}}{G^{[i,j]} \times H} \;\simeq\; \frac{G^{[j]} \times G^{[i]}}{G^{[i,j]} \times U(1)^{r_g}} \,, \tag{6.15}$$

where the action of $G^{[i,j]} \times H$ on $G^{[j]} \times G^{[i]}$ is

$$\begin{aligned} \big(\phi^{[j]}, \psi^{[i]}\big) &\to \big(\alpha\,\phi^{[j]}\,\rho^{-1}, \rho\,\psi^{[i]}\,\widehat{\tau}(\alpha^{-1})\big) \\ &= \big(\alpha, \rho\big)\,\big(\phi^{[j]}\,, \psi^{[i]}\big)\,\big(\rho^{-1}, \widehat{\tau}(\alpha^{-1})\big)\,, \quad \forall\,\rho \in G^{[i,j]} \;\text{ and }\; \alpha \in H\,. \end{aligned} \tag{6.16}$$

Next, consider the gauged WZW action corresponding to the coset (6.15) and the (anomaly free) group of gauge transformations $h \to \epsilon_L(u)\,h\,\epsilon_R(u^{-1})$, where $h = (\phi, \psi) \in G^{[j]} \times G^{[i]}$, $u = (\rho, \alpha) \in G^{[i,j]} \times H$, and $\epsilon_{L/R} : G^{[i,j]} \times H \to G^{[j]} \times G^{[i]}$ are two group homomorphisms defined by

$$\epsilon_L(\rho, \alpha) = (\alpha, \rho) \quad \text{and} \quad \epsilon_L(\rho, \alpha) = \big(\rho, \widehat{\tau}(\alpha)\big)\,, \tag{6.17}$$

which descend to embeddings of the corresponding Lie algebras. The action is given by [39, 40, 35] (see also [2] for the normalisation)

$$\begin{aligned} kS^{[i,j]}_{\rm gWZW}[h, \mathcal{A}_\pm] = kS^{[i,j]}_{\rm WZW}[h] + \frac{k}{\pi}\int d^2x\,\Big(&-\langle\epsilon_L(\mathcal{A}_+), \partial_- h h^{-1}\rangle \\ &+\langle\epsilon_R(\mathcal{A}_-), h^{-1}\partial_+ h\rangle + \langle h^{-1}\epsilon_L(\mathcal{A}_+)h, \epsilon_R(\mathcal{A}_-)\rangle - \langle\epsilon_L(\mathcal{A}_+), \epsilon_L(\mathcal{A}_-)\rangle\Big)\,, \end{aligned} \tag{6.18}$$

where $kS^{[i,j]}_{\rm WZW}[h]$ is the WZW action at level k for the field h in $G^{[j]} \times G^{[i]}$, and $\mathcal{A}_\pm = (a_\pm, A_\pm)$ are non-dynamical gauge fields taking values in the Lie algebra of $G^{[i,j]} \times H$.

[11] In particular, taking $\tau = +I$ or $-I$ leads to gauge transformations of vector or axial type, respectively.

More precisely, $a_\pm \in g^{[i,j]} \oplus u(1)^2$ and $A_\pm \in u(1)^{r_g}$, where all the explicit $u(1)$ factors are embedded in the Cartan subalgebra into H, and we have denoted by $g^{[i,j]}$ both the Dynkin diagram defined just after (4.48) and the corresponding (compact semisimple) Lie algebra. We have also used the same notation for the invariant bilinear form of g and its trivial extension to $\left(g^{[i,j]} \oplus u(1)^2\right) \oplus u(1)^{r_g}$:

$$\langle (u,v),(r,s)\rangle \equiv \langle u,r\rangle + \langle v,s\rangle \,. \tag{6.19}$$

Writing $h = (\phi,\psi)$ and expanding (6.18), we obtain

$$\begin{aligned} kS^{[i,j]}_{\rm gWZW}[h,\mathcal{A}_\pm] = {}& kS_{\rm WZW}[\phi] + kS_{\rm WZW}[\psi] \\ & + \frac{k}{\pi}\int d^2x \,\Big(-\langle a_+, \partial_-\psi\psi^{-1}\rangle + \langle a_-, \phi^{-1}\partial_+\phi\rangle + \langle a_+, \psi\tau(A_-)\psi^{-1}\rangle \\ & \quad + \langle a_-, \phi^{-1}A_+\phi\rangle - \langle a_+, a_-\rangle \\ & \quad - \langle A_+, \partial_-\phi\phi^{-1}\rangle + \langle \tau(A_-), \psi^{-1}\partial_+\psi\rangle - \langle A_+, A_-\rangle \Big) \,, \end{aligned} \tag{6.20}$$

where $kS_{\rm WZW}$ is the WZW action at level k corresponding to the group G. The dependence of this action on the non-dynamical gauge fields $a_\pm$ is very simple, allowing them to be integrated out by solving their equations of motion. The result is

$$\begin{aligned} k\widetilde{S}^{[i,j]}_{\rm gWZW}[h,A_\pm] = {}& kS_{\rm WZW}[\phi] + kS_{\rm WZW}[\psi] - \frac{k}{\pi}\int d^2x \,\langle \phi^{-1}\partial_+\phi, \partial_-\psi\psi^{-1}\rangle \\ & + \frac{k}{\pi}\int d^2x \,\Big(-\langle A_+, \partial_-(\phi\psi)(\phi\psi)^{-1}\rangle + \langle \tau(A_-), (\phi\psi)^{-1}\partial_+(\phi\psi)\rangle \\ & \quad + \langle (\phi\psi)^{-1}A_+(\phi\psi), \tau(A_-)\rangle - \langle A_+, A_-\rangle \Big) \,. \end{aligned} \tag{6.21}$$

Finally, using the Polyakov-Wiegmann formula

$$kS_{\rm WZW}[\phi\psi] = kS_{\rm WZW}[\phi] + kS_{\rm WZW}[\psi] - \frac{k}{\pi}\int d^2x \,\langle \phi^{-1}\partial_+\phi, \partial_-\psi\psi^{-1}\rangle \,, \tag{6.22}$$

it is straightforward to check that $k\widetilde{S}^{[i,j]}_{\rm gWZW}[h,A_\pm]$ coincides with the gauged WZW action in (6.1), $S_{\rm gWZW}[\gamma,A_\pm]$, for $\gamma = \phi\,\psi$.

Therefore, for $i \neq j$, the fixed point visited by the RG flow after the first crossover has occurred corresponds to the gauged WZW action of the 'asymmetric coset' (6.15), where different left and right actions of $G^{[i,j]} \times H$ on $G^{[j]} \times G^{[i]}$, specified by the two group homomorphisms (6.17), are gauged. This means that the holomorphic and anti-holomorphic sectors of the resulting effective field theory correspond to different cosets sharing the same central charge [39, 40, 35]. Taking the form of $\epsilon_{L/R}$ into account, the left and right cosets can be written as

$$\frac{G^{[j]}_k}{U(1)^{r_g}} \times \frac{G^{[i]}_k}{G^{[i,j]}_k} \quad \text{and} \quad \frac{G^{[j]}_k}{G^{[i,j]}_k} \times \frac{G^{[i]}_k}{U(1)^{r_g}} \,, \tag{6.23}$$

which are uniquely defined by the inclusion of $g^{[i,j]}$ into $g^{[j]}$ and $g^{[i]}$, respectively. In retrospect, this result is not surprising: the HSG models generically break parity, and

this can make the relationship between the holomorphic and anti-holomorphic sectors in any intermediate-scale conformal field theories non-trivial. Our discussion has made this explicit by showing that, for $i \neq j$, and $\mu_{ij} \ggg \mu_{pq}\ \forall (p,q) \neq (i,j)$, the fixed point visited by the RG flow after the first crossover has occurred corresponds to a 'heterotic' conformal field theory where parity is broken, unless the two cosets in (6.23) are isomorphic.

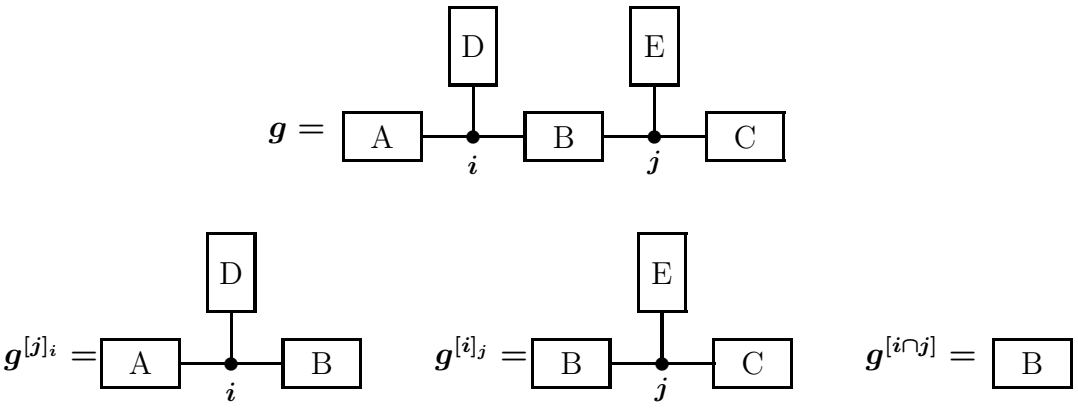

Figure 9: The generic form of the Dynkin diagrams of g, $g^{[j]_i}$, $g^{[i]_j}$, and $g^{[i\cap j]}$ defined just before eq. (6.24). The boxes A, B, C, D, E stand for Dynkin subdiagrams connected to either node 'i' or 'j'. Some of these boxes can be empty. In particular, B is empty if i and j are neighbouring nodes.

Although the notation used in (6.23) looks simple, it can be misleading because the subgroups $G^{[j]}$, $G^{[i]}$, and $G^{[i,j]}$ may split into products of simple groups and $U(1)$ factors, yielding common factors in the numerators and denominators that can be cancelled out. This prompts us to write the cosets in a more detailed way, to clarify their structure. We start by introducing the following notation: let $g^{[i]_j}$ be the connected component of the Dynkin diagram $g^{[i]}$ containing the node j, $r^{[i]_j}$ be the rank of $g^{[i]_j}$, and $g^{[i\cap j]} = g^{[i]_j} \cap g^{[j]_i}$. Correspondingly, let $G^{[i]_j}$, $G^{[j]_i}$, and $G^{[i\cap j]}$ denote the simple compact Lie groups whose Dynkin diagrams are $g^{[i]_j}$, $g^{[j]_i}$, and $g^{[i\cap j]}$, respectively. Taking into account the form of the Dynkin diagram of g, which is sketched in figure 9 in a non-standard but convenient way for our purposes, it is easy to prove that any field configuration of the form $\gamma = \phi^{[j]}\psi^{[i]}$ can always be written as the product of a element in $G^{[j]_i} \times U(1)^{r_g - r^{[j]_i}}$ times an element in $G^{[i]_j} \times U(1)^{r_g - r^{[i]_j}}$, where $U(1)^{r_g - r^{[j]_i}}$ and $U(1)^{r_g - r^{[i]_j}}$ are subsets of H; *i.e.*,

$$G^{[j]} \cdot G^{[i]} = \{\phi^{[j]}\psi^{[i]}\} = \{\widetilde{\phi}^{[j]_i}\,\widetilde{\psi}^{[i]_j}\} = \left(G^{[j]_i} \times U(1)^{r_g - r^{[j]_i}}\right) \cdot \left(G^{[i]_j} \times U(1)^{r_g - r^{[i]_j}}\right) . \quad (6.24)$$

As a direct consequence of this,

$$\Gamma_{ij}(\gamma) = \Gamma_{ij}(\mathbb{1}) \Rightarrow \Gamma_{kl}(\gamma) = \Gamma_{kl}(\mathbb{1}) \quad \forall\, k \notin g^{[i]_j} \quad \text{and} \quad l \notin g^{[j]_i} . \quad (6.25)$$

This ensures that, once the crossover at the scale μ_{ij} has taken place, no further crossovers will be observed at μ_{kl} for any $k \notin g^{[i]_j}$ and $l \notin g^{[j]_i}$, and provides the Lagrangian version of the shielding mechanism.

Notice that $\widetilde{\phi}^{[j]_i}\,\widetilde{\psi}^{[i]_j}$ is invariant under $\widetilde{\phi}^{[j]_i} \to \widetilde{\phi}^{[j]_i}\rho$ and $\widetilde{\psi}^{[i]_j} \to \rho^{-1}\widetilde{\psi}^{[i]_j}$ for any $\rho \in G^{[i\cap j]} \times U(1)^{r_g - r^{[i\cap j]}}$, where $r^{[i\cap j]} = r^{[i]_j} + r^{[j]_i} - r_g$ is the rank of $g^{[i\cap j]}$. Then, repeating the

arguments used in the previous paragraphs, the cosets (6.23) that specify the holomorphic and anti-holomorphic sectors of the effective field theory can be written as

$$\frac{(G^{[j]_i})_k}{U(1)^{r^{[j]_i}}} \times \frac{(G^{[i]_j})_k}{(G^{[i\cap j]})_k \times U(1)^{r_g - r^{[j]_i}}} \quad \text{and} \quad \frac{(G^{[j]_i})_k}{(G^{[i\cap j]})_k \times U(1)^{r_g - r^{[i]_j}}} \times \frac{(G^{[i]_j})_k}{U(1)^{r^{[i]_j}}} \,, \tag{6.26}$$

and these cosets are uniquely defined by the inclusions $g^{[i\cap j]} \subset g^{[i]_j}$ and $g^{[i\cap j]} \subset g^{[j]_i}$. When i and j are neighbours on the Dynkin diagram of g, the box B in figure 9 is empty, $G^{[i\cap j]}$ is trivial, and the conjectured effective field theory consists of two decoupled parafermionic theories specified by the cosets $(G^{[i]_j})_k/U(1)^{r^{[i]_j}}$ and $(G^{[j]_i})_k/U(1)^{r^{[j]_i}}$. This particular decoupling could have been anticipated from the structure of the two-particle scattering amplitudes that define the $G_k/U(1)^{r_g}$ HSG model, given by (4.4). In the limit $|\sigma_{ij}| \to \infty$, they split into the amplitudes corresponding to the direct sum of the $(G^{[i]_j})_k/U(1)^{r^{[i]_j}}$ and $(G^{[j]_i})_k/U(1)^{r^{[j]_i}}$ HSG models, provided we restrict ourselves to rapidity values $|\theta| \ll |\sigma_{ij}|$. Eq. (6.26) also shows that whenever $\{i, j\}$ are not neighbours on the Dynkin diagram of g, the effective field theory involves a coset CFT that is not of parafermionic type.

The predictions obtained using the explicit formulation of the HSG models in terms of gauged WZW models can be checked against the TBA results. The TBA equations can also be used to find candidates for the effective field theory, as explained in appendix A. As a manifestation of parity breaking, the TBA equations (4.7) are not always symmetrical under $\theta \to -\theta$ and, consequently, they generically lead to different 'left' and 'right' candidates that share the same central charge. In the cases that we have analysed, this matches the results obtained using the gauged WZW formulation, where different cosets specify the holomorphic and anti-holomorphic sectors of the conformal field theory corresponding to the fixed point visited.

More quantitative tests are provided by the central charges of the fixed points visited by the RG flow, which can be calculated as in section 4. Consider a set of TBA parameters chosen as in (6.7) or (6.8), so that one scale, m_{ij}, is larger than all the others. Then $2r^{-1} \ggg m_{ij}$ corresponds to the deep UV limit, where $c(r) \approx C_k(g)$, and increasing the value of r through the first crossover, we get to the regime where $m_{pq} \lll 2r^{-1} \lll m_{ij}$, for all $(p, q) \neq (i, j)$. The effective value of $c(r)$ is specified by $\widetilde{g}_l^{\pm}(r, \{m_i\}, \{\sigma_{ij}\})$, which are the subsets of the Dynkin diagram of g defined just before eq. (4.30). Taking into account that for this range of values of r the pseudoenergies ε_a^i are effectively independent of the pseudoenergies ε_b^j, the Dynkin diagram $\widetilde{g}_l^{\pm}$ satisfies the following relations:

$$\begin{aligned}
&i) \quad \text{if} \quad i \in \widetilde{g}_l^{\pm} \,, \quad \text{then} \quad j \notin \widetilde{g}_l^{\pm} \,, \quad \widetilde{g}_l^{\pm} = \widetilde{g^{[j]}}_l^{\pm} \,, \quad \text{and} \quad \widetilde{g^{[i]}}_l^{\pm} = \widetilde{g^{[i,j]}}_l^{\pm} \,, \\
&ii) \quad \text{if} \quad j \in \widetilde{g}_l^{\pm} \,, \quad \text{then} \quad i \notin \widetilde{g}_l^{\pm} \,, \quad \widetilde{g}_l^{\pm} = \widetilde{g^{[i]}}_l^{\pm} \,, \quad \text{and} \quad \widetilde{g^{[j]}}_l^{\pm} = \widetilde{g^{[i,j]}}_l^{\pm} \,, \\
&iii) \quad \text{if} \quad i, j \notin \widetilde{g}_l^{\pm} \,, \quad \text{then} \quad \widetilde{g}_l^{\pm} = \widetilde{g^{[i]}}_l^{\pm} = \widetilde{g^{[j]}}_l^{\pm} = \widetilde{g^{[i,j]}}_l^{\pm} \,,
\end{aligned} \tag{6.27}$$

for all $l = 1 \dots r_g$. Therefore, using (4.26), (4.28), and (4.34), the TBA equations lead to the behaviour

$$c(r) \approx \begin{cases} C_k\big(g\big) \,, & \text{for} \;\; 2r^{-1} \ggg m_{ij}, \\ C_k\big(g^{[i]}\big) + C_k\big(g^{[j]}\big) - C_k\big(g^{[i,j]}\big) \,, & \text{for} \;\; m_{pq} \lll 2r^{-1} \lll m_{ij} \,, \quad \forall \, \{p, q\} \neq \{i, j\}, \end{cases} \tag{6.28}$$

where $C_k\big(g\big)$ has been defined in (4.33) for $g \in a, d, e$ with rank r_g; it denotes the central charge of the $G_k/U(1)^{r_g}$ coset conformal field theory. For g disconnected, it is the sum of (4.33) over all connected components of g. Notice that $C_k\big(g^{[i]}\big) + C_k\big(g^{[j]}\big) - C_k\big(g^{[i,j]}\big)$ is the central charge of the conformal field theory specified by the cosets (6.23). Therefore, if we identify the Lagrangian parameters $\{m_i, \sigma_i\}$ with the TBA parameters such that $m_{ij} = \mu_{ij}$, and the dimensionless RG scale $\overline{\Lambda}$ with $2r^{-1}$, the behaviour predicted using the gauged WZW formulation matches the plateau value of c calculated from the TBA.

Eq. (6.28) resembles a decoupling rule suggested in [46] to describe the behaviour of the models in the $\sigma_{ij} \to \infty$ limit. However, the embeddings necessary to define the cosets were not discussed in that paper, and in particular the possible left-right asymmetry of the relevant theories was missed.

So far in this section we have restricted ourselves to cases when one coefficient, say μ_{ij}, is larger than all of the others, and we have discussed the fixed point visited by the RG flow just after the crossover associated with μ_{ij} has occurred. More generally, in this formalism, crossovers are associated with the decoupling of field configurations that become effectively heavy at a given RG scale. The relevant mass scales are just the classical masses (2.6), since, using (6.10), they determine the (quadratic) leading term of the potential

$$V(\exp X) = \frac{m_0^2}{4\pi} \sum_{i,j=1}^{r_g} \mu_{ij}^2\, \Gamma_{ij}(\exp X) = \frac{m_0^2}{4\pi} \sum_{\boldsymbol{\alpha}\in\Phi^+} m_{\boldsymbol{\alpha}}^2\, \langle E_{\boldsymbol{\alpha}}, E_{-\boldsymbol{\alpha}}\rangle\, |\phi_{\boldsymbol{\alpha}}|^2 + \cdots \,. \tag{6.29}$$

Consequently, the resulting pattern of crossover scales is the same as deduced in section 3, and we will not discuss it again here. Instead, we shall briefly discuss the identification of the fixed points visited by the RG flow corresponding to the plateaux observed in the effective central charge $c(r)$. According to the results in sections 3 and 4, a plateau will occur whenever, for particular values of the parameters, the dimensionless mass scales $\{m_{\boldsymbol{\alpha}},\ \boldsymbol{\alpha} \in \Phi^+\}$ split into two well-separated sets $\mathcal{E}_{\rm light}$ and $\mathcal{E}_{\rm heavy}$, with $m_{\boldsymbol{\alpha}} \lll m_{\boldsymbol{\beta}}$ for any $m_{\boldsymbol{\alpha}} \in \mathcal{E}_{\rm light}$ and $m_{\boldsymbol{\beta}} \in \mathcal{E}_{\rm heavy}$. The plateau occurs for RG scales between these two sets,

$$m_{\boldsymbol{\alpha}} \lll \overline{\Lambda} \lll m_{\boldsymbol{\beta}} \qquad \forall\, m_{\boldsymbol{\alpha}} \in \mathcal{E}_{\rm light} \quad \text{and} \quad m_{\boldsymbol{\beta}} \in \mathcal{E}_{\rm heavy}\,, \tag{6.30}$$

and the corresponding fixed point is expected to be specified by the field configurations which are left unfrozen by the components of the potential associated with $\mathcal{E}_{\rm heavy}$. This is, by the field configurations that satisfy the conditions

$$\Gamma_{ij}(\gamma) = \Gamma_{ij}(\mathbb{1}) \qquad \forall\,(i,j) \quad \text{such that} \quad \mu_{ij} \sim m_{\boldsymbol{\alpha}} \quad \text{with} \quad m_{\boldsymbol{\alpha}} \in \mathcal{E}_{\rm heavy}\,. \tag{6.31}$$

The general solution of these conditions and their detailed comparison with the TBA results deserve further study, which is beyond the scope of this paper.

In the following, we will just illustrate their use in a concrete example. Consider the same $d_4 \equiv SO(8)$ case studied in section 3, corresponding to the parameters in (3.15). The scales $\mu_{ij} = m_{ij}$ are ordered as follows

$$\mu_{14} \ggg \mu_{24} \ggg \mu_{13} \ggg \mu_{34} \ggg \mu_{23} \ggg \mu_{12} \ggg \mu_{11} = \mu_{22} = \mu_{33} = \mu_{44}\,, \tag{6.32}$$

and the relationship between the classical mass scales $m_{\boldsymbol{\alpha}}$ and the coefficients μ_{ij} can be worked out from (3.16) and (3.17). Consider first the regime $\overline{\Lambda} \ggg m_{14} = \mu_{14}$. This

corresponds to the deep UV limit, where all the field configurations are effectively massless, the potential can be completely neglected, and the effective field theory is described by the unperturbed $SO(8)_k/U(1)^4$ coset conformal field theory.

Notice that the coefficient μ_{14} is larger than all of the others, which means that the effective theory after the first crossover has occurred is determined by left and right cosets of the form (6.26). To be concrete, for the range of energies $m_{24} = \mu_{24} \lll \overline{\Lambda} \lll m_{14}$ only the field configurations that satisfy $\Gamma_{14}(\gamma) = \Gamma_{14}(\mathbb{1})$ remain effectively massless, which are of the form $\gamma = \phi^{[4]}\,\psi^{[1]}$. In this case, the Dynkin diagrams $g^{[1]_4}$ and $g^{[4]_1}$ defined just before (6.24) are the a_3 Dynkin subdiagrams associated to the nodes $\{2,3,4\}$ and $\{1,2,3\}$, respectively, while $g^{[1\cap 4]}$ is the a_2 subdiagram corresponding to $\{2,3\}$. Then, the two cosets (6.26) coincide with

$$\frac{SU(4)_k}{SU(3)_k \times U(1)} \times \frac{SU(4)_k}{U(1)^3}\,. \tag{6.33}$$

Taking (3.17) into account, in this regime all the field configurations associated with the roots $\boldsymbol{\alpha}_1 + \boldsymbol{\alpha}_2 + \boldsymbol{\alpha}_4$, $\boldsymbol{\alpha}_1 + \boldsymbol{\alpha}_2 + \boldsymbol{\alpha}_3 + \boldsymbol{\alpha}_4$, and $\boldsymbol{\alpha}_1 + 2\boldsymbol{\alpha}_2 + \boldsymbol{\alpha}_3 + \boldsymbol{\alpha}_4$ are decoupled.

Next, we consider the energy scales $m_{13} = \mu_{13} \lll \overline{\Lambda} \lll m_{24}$, where all the field configurations associated with the roots $\boldsymbol{\alpha}_2 + \boldsymbol{\alpha}_4$ and $\boldsymbol{\alpha}_3 + \boldsymbol{\alpha}_2 + \boldsymbol{\alpha}_4$ become decoupled too. According to (6.31), the corresponding fixed point is determined by the simultaneous solutions to $\Gamma_{14}(\gamma) = \Gamma_{14}(\mathbb{1})$ and $\Gamma_{24}(\gamma) = \Gamma_{24}(\mathbb{1})$. Remarkably, taking (6.25) into account, the condition $\Gamma_{24}(\gamma) = \Gamma_{24}(\mathbb{1})$ already implies $\Gamma_{14}(\gamma) = \Gamma_{14}(\mathbb{1})$ and $\Gamma_{34}(\gamma) = \Gamma_{34}(\mathbb{1})$, which has two direct consequences. First, the effective theory in this regime is specified by left and right cosets of the form (6.26) with $i = 2$ and $j = 4$, which in our case read

$$\frac{SU(4)_k}{U(1)^3} \times \frac{SU(2)_k}{U(1)}\,, \tag{6.34}$$

and correspond to two decoupled parafermionic theories.

The second consequence is that there is no crossover at the scale $m_{34} = \mu_{34}$, exactly as predicted by our analysis of shielding in section 3. Therefore, the next regime is $m_{23} = \mu_{23} \lll \overline{\Lambda} \lll m_{13}$, where all the field configurations associated with the root $\boldsymbol{\alpha}_1 + \boldsymbol{\alpha}_2 + \boldsymbol{\alpha}_3$ become decoupled. In this case, the fixed point is determined by the solutions to $\Gamma_{24}(\gamma) = \Gamma_{24}(\mathbb{1})$ and $\Gamma_{13}(\gamma) = \Gamma_{13}(\mathbb{1})$, which are of the form $\gamma = \phi^{[3,4]}\psi^{[1,4]}\omega^{[1,2,3]}$. Using similar arguments to those that lead to (6.31), the corresponding manifold of effective field configurations can be realised as a coset manifold in terms of $G^{[3,4]} \times G^{[1,4]} \times G^{[1,2,3]}$. Since $g^{[1,2,3,4]}$ is trivial, $G^{[1,2,3,4]} = H$ and one has to take into account the invariance of γ under $\phi^{[3,4]} \to \phi^{[3,4]}\rho$, $\psi^{[1,4]} \to \rho^{-1}\,\psi^{[1,4]}\beta$, and $\omega^{[1,2,3]} \to \beta^{-1}\omega^{[1,2,3]}$ for each $\rho \in G^{[1,3,4]}$ and $\beta \in H$, which leads to the identification of the fixed point as a coset conformal field theory associated with

$$\frac{SU(3)_k}{SU(2)_k \times U(1)} \times \frac{SU(3)_k}{U(1)^2} \times \frac{SU(2)_k}{U(1)}\,. \tag{6.35}$$

In this particular case, the left and right cosets coincide.

We can keep considering smaller and smaller energy scales until we reach the deep IR limit $\overline{\Lambda} \lll m_{ii}$ for all $i = 1 \ldots 4$, where all the field configurations are decoupled. The resulting flow of effective field theories is summarised by

$$\gamma \equiv \left(\frac{SO(8)_k}{U(1)^4}\right)^{<3>} \xrightarrow[\Gamma_{14}]{m_{14}} \phi^{[4]}\,\psi^{[1]} \equiv \left(\frac{SU(4)_k}{SU(3)_k \times U(1)} \times \frac{SU(4)_k}{U(1)^3}\right)^{<\frac{14}{5}>}$$

$$\xrightarrow[\Gamma_{24}]{m_{24}} \phi^{[4]}\,\psi^{[1,2,3]} \equiv \left(\frac{SU(4)_k}{U(1)^3}\times\frac{SU(2)_k}{U(1)}\right)^{<\frac{5}{2}>}$$

$$\xrightarrow[\Gamma_{13}]{m_{13}} \phi^{[3,4]}\,\psi^{[1,4]}\,\omega^{[1,2,3]} \equiv \left(\frac{SU(3)_k}{SU(2)_k\times U(1)}\times\frac{SU(3)_k}{U(1)^2}\times\frac{SU(2)_k}{U(1)}\right)^{<\frac{12}{5}>}$$

$$\xrightarrow[\Gamma_{23}]{m_{23}} \phi^{[3,4]}\,\psi^{[1,2,4]}\,\omega^{[1,2,3]} \equiv \left(\frac{SU(3)_k}{U(1)^2}\times\left[\frac{SU(2)_k}{U(1)}\right]^{\times 2}\right)^{<\frac{11}{5}>}$$

$$\xrightarrow[\Gamma_{12}]{m_{12}} \phi^{[2,3,4]}\,\psi^{[1,3,4]}\,\omega^{[1,2,4]}\,\chi^{[1,2,3]} \equiv \left(\left[\frac{SU(2)_k}{U(1)}\right]^{\times 4}\right)^{<2>}$$

$$\xrightarrow[\Gamma_{ii}]{m_{ii}} \phi^{[1,2,3,4]} \equiv \text{Massive}^{\,<0>}\,. \tag{6.36}$$

Strictly speaking, the Lagrangian action (6.1) should only be expected to give a full description of the theory in the semiclassical (large k) limit. However, the resulting values of the effective central charge reproduce the approximate values calculated using the TBA equations for any value of k. In particular, in (6.36), the superscripts $^{<\,>}$ provide the central charges of the corresponding coset conformal field theories for level $k = 2$. They match the TBA results illustrated in figure 8, despite the fact that this value of the level is far from the semiclassical regime. The same occurs for the other examples discussed along the paper.

7 Comments on form factor calculations

There is another context where crossover phenomena can be seen, namely the behaviour of correlation functions. It is natural to ask whether, and to what extent, the results we have obtained from a study of finite-size effects can be reproduced. In integrable theories, this can be addressed using the form-factor approach, which provides an infrared series expansion for correlation functions that typically has good convergence properties down to short distances. The method was first applied to the HSG models associated with $SU(N)_2/U(1)^{N-1}$ for $N = 3$ in [6, 7], and for $N \geq 4$ in [8]. However, while crossover effects for unstable particles of height 2 were observed in [7, 8], no transitions associated with roots of height greater than 2 were found. This is as expected for the $SU(3)_2/U(1)^2$ case of [7] since $SU(3)$ has no roots of height greater than 2 anyway, but it is more puzzling for the cases discussed in [8]. Indeed, the plot shown in [8] for $SU(4)_2/U(1)^3$ with $\sigma_{12} = 50$ and $\sigma_{23} = 20$ should qualitatively match the corresponding flow presented in [10, 11] and in figure 4 above, while in fact even the number of steps is different. Similarly, the plotted $SU(5)_2/U(1)^4$ flows in [8] do not match our predictions. These discrepancies between form-factor and finite-size results were first remarked in [10] (see [11]), and for these particular instances they were later traced [46] to a misattribution in the signs of the resonance parameters as originally given in [8] – so, for example, the $SU(4)$ plot is actually for $\sigma_{12} = 50$ and $\sigma_{23} = -20$. Using our terminology, the scale m_{13} is then shielded by m_{12} and this resolves the immediate mismatch. However, it remains the case that crossovers associated with roots of heights greater than 2 have yet to seen

using the form-factor approach. In this section we shall argue that the reasons for this run, at least in part, deeper than a simple question of the correct allocation of the signs of the resonance parameters in the form factors, and that they have a bearing on a claimed slow-down in the convergence of the form factor approach for the HSG models.

The investigation of HSG RG flows in [7, 8] was based on the numerical evaluation of Zamolodchikov's c-function [47] using Cardy's sum rule [48], expanding the relevant two-point functions of the trace of the energy-momentum tensor in terms of n-particle form factors. In practice, such calculations must always be truncated at some point. Usually, while this affects the accuracy of results to some – albeit small [49] – extent, no important information is lost provided one calculates at least as far as the two-particle contributions. However, as we now show, in theories with unstable particles there are good reasons to predict that the effects of early truncation can be more dramatic, sometimes obscuring physically-relevant crossovers, and sometimes leading to misleading values for the ultraviolet central charge.

Form factors are matrix elements of some local operator $\mathcal{O}$ between a multiparticle in-state and the vacuum. They can be written as

$$F_n^{\mathcal{O}|\mu_1\dots\mu_n}(\theta_1,\dots,\theta_n) = \langle 0 \mid \mathcal{O}(0,0) \mid V_{\mu_1}(\theta_1)\dots V_{\mu_n}(\theta_n)\rangle_{\text{in}}\,, \tag{7.1}$$

where the symbol $V_\mu(\theta)$ represents a particle of species μ and rapidity θ. Two-point functions can then be obtained by inserting a complete set of asymptotic states between the two operators involved, resulting in a sum over (integrated) one-, two- and higher-particle contributions. Only stable particles appear directly in the asymptotic states, and so this raises the question of how and in what way the form-factor expansion can be influenced by the existence of any unstable particles. Taking the particle interpretation as a guiding principle, we conjecture that two conditions must be met for the n^{th}-order term associated with the form factor (7.1) to be sensitive to an unstable state $\tilde{\mu}_R$. The first condition is that it must be possible to form $\tilde{\mu}_R$ as a bound state of some subset $\{\mu_{i_1}\dots\mu_{i_m}\}$ of the particles $\{\mu_1\dots\mu_n\}$; the second, apparently trivial but as we shall see important, is that $F_n^{\mathcal{O}|\mu_1\dots\mu_n}$ should not be identically zero. Notice that the second condition will often require that n be strictly larger than m.

All HSG form factor calculations to date have been performed for level $k = 2$, and for simplicity we restrict to such cases here too. Then the quantum number a of single-particle states (i, a) is always equal to 1 and can be dropped, while i labels a simple root $\boldsymbol{\alpha}_i$ of g. The remaining, unstable, particles are similarly indexed by the positive roots $\boldsymbol{\beta} = \sum n_i\boldsymbol{\alpha}_i$ of height ≥ 2. The condition that it be possible to form the unstable particle $\boldsymbol{\beta}$ from some subset of the set $\{\boldsymbol{\alpha}_{i_1}\dots\boldsymbol{\alpha}_{i_n}\}$ of stable particles is that it should contain n_1 times $\boldsymbol{\alpha}_1$, n_2 times $\boldsymbol{\alpha}_2$, and so on.

The second condition, the non-vanishing of the relevant form factors, can be partially analysed using a spin-zero conserved charge. As in the unperturbed theory of level-k G-parafermions [13], the HSG theory associated with the coset $G_k/U(1)^{r_g}$ possesses a discrete conserved charge taking values in Λ_g modulo $k \times \Lambda_g$, where Λ_g is the root lattice of g. This generalises the $\mathbb{Z}_k$ charge of the usual parafermions, which is recovered for $G = SU(2)$. Stable particles correspond to states of definite charge, and the particle (i, a) carries the charge $a\boldsymbol{\alpha}_i$ [3]. Taking this into account, a necessary condition to ensure that a given form factor is non-vanishing is that the total charge of the multiparticle state matches the charge of the local operator $\mathcal{O}$. In the particular case of neutral operators

such as the trace of the energy-momentum tensor, Θ, this implies that the form factor associated with a multiparticle state $(i_1, a_1)....(i_n, a_n)$ will vanish unless

$$\sum_{j=1}^{n} a_j \boldsymbol{\alpha}_{i_j} \in k \times \Lambda_g \tag{7.2}$$

Therefore, for $k = 2$, the only form factors of neutral operators that can be non-vanishing are those corresponding to multiparticle states where each simple root appears an even number of times. For Θ, this general rule is in agreement with the results of [6,8].

Consider now the calculation of Zamolodchikov's c-function for the HSG theories at $k = 2$. This requires the two-point function of Θ, and hence the form factors $F_n^{\Theta|\boldsymbol{\alpha}_{i_1}\dots\boldsymbol{\alpha}_{i_n}}$. Combining our two conditions, we conclude that the effects of unstable resonance states associated with the roots $\boldsymbol{\beta}$ of height $\mathrm{ht}(\boldsymbol{\beta})$ will only be seen in the n^{th}-order term in the form factor expansion if $n \geq 2\,\mathrm{ht}(\boldsymbol{\beta})$. Since the numerical calculations of [8] went up to 6-particle form factor contributions, this means that they are not expected to be sensitive to unstable particles associated with roots of height larger that 3.

All of this leads to the following predictions. For $SU(4)_2/U(1)^3$, the calculation of Zamolodchikov c-function for the values of the resonance parameters originally quoted in [8], using the form factor expansion up to the 6^{th}-order term, should qualitatively match the dotted line in figure 4 and detect the crossover transition at the scale fixed by $m_{\boldsymbol{\alpha}_1+\boldsymbol{\alpha}_2+\boldsymbol{\alpha}_3}$. In contrast, for $SU(5)_2/U(1)^4$, it should only find the transitions associated with the scales $m_{\boldsymbol{\alpha}_1+\boldsymbol{\alpha}_2+\boldsymbol{\alpha}_3}$ and $m_{\boldsymbol{\alpha}_2+\boldsymbol{\alpha}_3+\boldsymbol{\alpha}_4}$, but no crossover transition associated with the maximal root alone, which in this case is of height 4. In general, for $SU(N)_2/U(1)^{N-1}$ the maximal number of crossovers that can be observed when truncating the form factor series at the 6-particle contribution is $3(N-2)$, the number of roots of height ≤ 3, while the maximal number of separable scales quoted in table 1 for $g = a_{N-1}$ is $N(N-1)/2$. Hence for $N \geq 5$ there will always be choices of the parameters for which some crossovers are missed completely, if the form factor expansion is not pushed further.

On the other hand, if the parameters are chosen such that no new physical crossover scales are associated with roots of height greater than two, so that all crossovers are already noticed by the low-lying roots, then another, more subtle, effect comes into play – while a crossover will be seen at the appropriate energy scale, the change in the effective central charge will be wrong, as not all relevant states will have been taken into account. Recall that the pattern of crossovers observed in the HSG models can be viewed as a consequence of the change in the number of field configurations that remain effectively massless at the RG scale, both stable and unstable. According to our analysis, a similar, but not identical, effect is at work in the form factor expansion: truncating the series at a certain number of particles will suppress the contribution of some unstable particle states, which would otherwise have been seen once the energy scale became large enough. If we try to calculate the effective central charge in the far ultraviolet, then this effect is sure to show up, no matter what values are chosen for the S-matrix parameters. As will now be shown, this idea can be checked quantatively against previously-published data.

The central charge of the unperturbed theory can be recovered by integrating the derivative of Zamolodchikov's c-function not just up to some finite scale, but all the way to the far ultraviolet. Using the form factor approach, this leads to a series

$$c_{UV} = \sum_{n=1}^{\infty} \Delta c^{(n)} \tag{7.3}$$

for the UV central charge, where $\Delta c^{(n)}$ is the n-particle form factor contribution. This typically has excellent convergence properties, for which there are good analytic arguments [49]. However, in [8] this general understanding was called into question: a study of the truncations of the form factor series for the $SU(N)_2/U(1)^{N-1}$ HSG models up to 6 particles led to the suggestion that convergence was becoming slower and slower for increasing values of N. The proposed decoupling of unstable particle states from form factors involving a small number of particles allows an alternative understanding of the data presented in [8]: it is not that the calculated central charge is becoming more inaccurate, it is just that it is no longer measuring the UV central charge of the full theory, but rather that of a subtheory in which certain particle states are decoupled. This phenomenon should be general to all theories with unstable particles, and we predict that once sufficiently-many terms have been included in the form factor expansion that no unstable particle contributions are artificially excluded, the good convergence properties argued for in [49] will be restored.

For $SU(N)_2/U(1)^{N-1}$, this idea can be tested against the numerical results of [8] for the would-be UV central charge. Let $c_{UV}^{(m)} \equiv \sum_{n=1}^{m} \Delta c^{(n)}$ denote the UV central charge computed from the series (7.3) truncated at the m-particle contribution. The prediction suggested by our analysis is that, for $m < 2(N-1)$, $c_{UV}^{(m)}$ should not approximate the UV central charge of the full theory, but rather that of the effective theory obtained by decoupling all unstable particles associated with the roots of height larger that $m/2$. In contrast, once $m \geq 2(N-1)$, the value of $c_{UV}^{(m)}$ should converge in the usual manner to the value of c_{UV}, which is $C_2(a_{N-1})$ in the notation of (4.33).

We start by quoting the individual n-particle form factor contributions to the value of c_{UV} for $SU(N)_2/U(1)^{N-1}$, as given in [8]:

$$\begin{aligned}
\Delta c^{(2)} &= (N-1) \times 0.5\,, \\
\Delta c^{(4)} &= (N-2) \times 0.197\,, \\
\Delta c^{(6)} &= (N-2) \times 0.002 + (N-3) \times 0.0924\,.
\end{aligned} \tag{7.4}$$

Substituted into the expansion, these lead to

$$\begin{aligned}
c_{UV}^{(2)} &= (N-1) \times 0.5\,, \\
c_{UV}^{(4)} &= N \times 0.697 - 0.894\,, \\
c_{UV}^{(6)} &= N \times 0.7914 - 1.1752\,.
\end{aligned} \tag{7.5}$$

Our claim is that these numbers should approximate the ultraviolet central charges of the effective theories obtained by decoupling all the unstable particles associated with the roots of height larger than χ, where $\chi = 1, 2, 3$ for $c_{UV}^{(2)}$, $c_{UV}^{(4)}$ and $c_{UV}^{(6)}$ respectively. For the $SU(N)_2/U(1)^{N-1}$ theories, there is an alternative way to realise the required effective theories, by choosing the S-matrix parameters as follows

$$m_i = 1 \quad \text{and} \quad \sigma_i = i\sigma \quad \forall\, i = 1, \ldots, N-1 \quad \Rightarrow \quad m_{ij} = \mathrm{e}^{\,|i-j|\sigma}\,, \tag{7.6}$$

with $\sigma \gg 0$, and examining the theory at scales $\mathrm{e}^{\,(\chi-1)\,\sigma/2} \lll 2r^{-1} \lll \mathrm{e}^{\,\chi\,\sigma/2}$, where all the field configurations associated with the roots of height larger than χ have been decoupled. Using the TBA analysis given earlier, for the parameters (7.6) the effective

central charge $c(r)$ has $N-1$ plateaux as r varies from 0 to ∞, matching the successive decoupling of roots of heights $N-1$, $N-2$, ..., 1:

$$c(r) \approx \begin{cases} c_{UV}\,, & \text{for } \; 2r^{-1} \ggg \mathrm{e}^{\,(N-2)\,\sigma/2}\,, \\ c_\chi\,, & \text{for } \; \mathrm{e}^{\,(\chi-1)\,\sigma/2} \lll 2r^{-1} \lll \mathrm{e}^{\,\chi\,\sigma/2}\,, \quad \chi = 1 \ldots N-2\,, \\ 0\,, & \text{for } \; 2r^{-1} \lll 1. \end{cases} \tag{7.7}$$

The plateau central charges c_χ can then be calculated using the results of section 4. The result is

$$c_\chi = (N-\chi)\,C_2(a_\chi) - (N-\chi-1)\,C_2(a_{\chi-1})\,, \quad \chi = 1 \ldots N-1\,, \tag{7.8}$$

where $c_{N-1} = c_{UV}$, and we have used $C_2(a_0) = 0$. For $\chi = 1, 2, 3$, this gives

$$c_1 = (N-1) \times \frac{1}{2}\,, \qquad c_2 = N \times \frac{7}{10} \; - \; \frac{9}{10}\,, \qquad c_3 = N \times \frac{4}{5} \; - \; \frac{6}{5}\,. \tag{7.9}$$

Comparing with (7.5), we see that while the difference between $c_{UV}^{(6)}$ and $c_{UV} = C_2(a_{N-1})$ becomes larger and larger with increasing values of N, with a relative error that reaches up to 20%, $c_{UV}^{(2\chi)}$ approximates c_χ with a relative error of less than 1% for any value of N. This offers strong support for our contention that the problems previously observed in form-factor results for the HSG models are not due to any general degrading of the convergence properties of the series, but rather to a controlled decoupling of states which could, in principle, be remedied by adding a *finite* number of further terms. The data is illustrated in table 2.

N	c_{UV}	$c_{UV}^{(6)}$	c_3	$c_{UV}^{(4)}$	c_2
4	2	1.9904	2	1.894	1.9
5	2.85714	2.7818	2.8	2.591	2.6
6	3.75	3.5732	3.6	3.288	3.3
10	7.5	6.7388	6.8	6.076	6.1
100	97.0588	77.9648	78.8	68.806	69.1

Table 2: The UV central charges of the $SU(N)_2/U(1)^{N-1}$ HSG models, c_{UV}, compared with form factor results, from [8], truncated at the 2χ-particle contribution, $c_{UV}^{(2\chi)}$, and with the plateau central charges c_χ corresponding to the decoupling of all the unstable particles associated with roots of heights larger than χ, for $\chi = 2, 3$.

8 Conclusions

In this paper, the patterns of crossover phenomena in the HSG models have been analysed in detail, principally through a study of finite-size effects using the thermodynamic Bethe ansatz. We have restricted our attention to simply-laced G, but we expect that similar results will hold for the non simply-laced cases too. For suitable values of the parameters, the finite-size scaling function $c(r)$ undergoes a series of well-separated

crossovers. The positions of these crossovers allowed us to identify scales associated with both stable and unstable quantum particles, and to show that they match semiclassical data, even far from that regime. Although only well-separated scales can be seen in this way, our results provide non-perturbative support for the idea that *all* of the semiclassical particles, both stable and unstable, survive in the quantum theory, for any value of k.

The crossovers corresponding to unstable particles associated with roots of height larger than two have yet to be observed in calculations based on the form factor approach [8]. While this lack is partially explained by the particular values of the parameters chosen for the computations performed to date [46], we pointed out that truncation effects in the form factor series should be particularly important in the presence of unstable particles, and proposed that this should lie behind previously-observed losses in accuracy in such calculations.

Our results imply the existence of a great variety of 'staircase' renormalisation group flows which, starting from the UV, pass close to a finite number of other fixed points before reaching their ultimate destinations. The multiparameter nature of the HSG models means that their flows in fact sweep out whole manifolds of integrability in the space of theories, and the staircases can be understood as lying near the boundaries of these manifolds. We have provided general rules to find the central charges of the fixed points visited by these flows, by calculating the plateau values of $c(r)$. We have also established the maximal number of steps for each model; owing to the shielding phenomenon, for the d and e algebras this number is less than might have been expected. It would be interesting to classify the different ways to realise the maximal number of steps, and more generally to find a more group-theoretical interpretation of the patterns of successive symmetry-breakings revealed by the TBA analysis.

At the crossovers, the models are described by a set of effective TBA systems that extends the class of massless TBAs discussed in [25, 26, 27], enabling the HSG models to unify these simpler flows within a common structure. This relationship can be used to deduce a Lagrangian formulation for some of these massless TBA systems from the formulation of the HSG models in terms of perturbed gauged WZW actions. Another interesting aspect of the HSG TBA staircase patterns is that the plateau values of the scaling function correspond to certain exact multiple scaling limits. The relationship between these limits and quantum group reduction merits further study, perhaps making use of ideas discussed in [50].

A final question, partially addressed in this paper, is the precise identification of the conformal field theories visited by the RG flows. We have investigated this using the TBA equations and the Lagrangian formulation, both of which lead to natural candidates for the relevant fixed points. In many cases these are heterotic conformal field theories [39, 40, 41]. To the best of our knowledge, this is the first time that the issue of RG flows to and from such conformal field theories has been raised[12], and it clearly deserves further work. As suggested in more general terms in [11], the full spectrum of excited states should provide important information in this regard, and a study of this using the TBA techniques developed in [52, 53] would be worthwhile.

[12]But note, *marginal* heterotic deformations are discussed in, for example, [45], while a perturbation with more extreme left-right asymmetry, for which even the perturbing dimensions on left and right differ, is treated in [51].

Acknowledgments

We would both like to thank Pascal Baseilhac, Peter Bowcock, Aldo Delfino, Terry Gannon, Werner Hoffmann, Angel Paredes, Volker Schomerus, Roberto Tateo and Jean-Bernard Zuber for helpful discussions during the course of this project, and SPhT Saclay for hospitality in its final stages. PED and JLM also thank USC and SISSA, respectively, for hospitality. The work was partly supported by the EC network "EUCLID", contract number HPRN-CT-2002-00325, and partly by a NATO grant PST.CLG.980424. JLM also thanks MCyT (Spain) and FEDER (BFM2002-03881 and FPA2002-01161), and Incentivos from Xunta de Galicia for financial support.

A Coset candidates and hints of heteroticity

The plateau values of the effective central charge calculated in section 4.3 provide partial, but not complete, information about the fixed points visited by the RG flows. At various points in this paper we have specified fixed points not by their central charges, but rather by giving candidate coset conformal field theories. In this appendix we review briefly how such candidates can be found directly from the structure of the TBA equations, and explain why they should be treated with particular caution for the HSG models.

The basic procedure is simple. In section 4.3, the plateau central charge was evaluated as a sum over the left and right active energy terms of contributions $c_p^\pm = \frac{1}{2}(C_k(g_p^\pm) - C_k(\widehat{g}_p^\pm))$. The first step is to identify $2c_p^\pm$ with the central charge of the coset conformal field theory

$$\frac{\left(G_p^\pm\right)_k}{\left(\widehat{G}_p^\pm\right)_k \times U(1)}\,, \tag{A.1}$$

where $G_p^\pm$ and $\widehat{G}_p^\pm$ are the compact subgroups of G specified by the Dynkin diagrams $g_p^\pm$ and $\widehat{g}_p^\pm$, respectively. By construction, $G_p^\pm$ is simple, and $\widehat{G}_p^\pm$ semisimple. These cosets are uniquely defined by the (regular) embeddings of $\widehat{G}_p^\pm$ into $G_p^\pm$ provided by the inclusion $\widehat{g}_p^\pm \subset g_p^\pm$, and the identification of the $U(1)$ factor with the one-dimensional subgroup generated by the Cartan element associated with the fundamental weight $\boldsymbol{\lambda}_p$. A candidate for the conformal field theory of the plateau is then obtained by tensoring all these terms,

$$\frac{\left(G_1^\pm\right)_k}{\left(\widehat{G}_1^\pm\right)_k \times U(1)} \times \frac{\left(G_2^\pm\right)_k}{\left(\widehat{G}_2^\pm\right)_k \times U(1)} \times \cdots \times \frac{\left(G_{r_g}^\pm\right)_k}{\left(\widehat{G}_{r_g}^\pm\right)_k \times U(1)}\,, \tag{A.2}$$

and reducing the resulting expression by means of the cancellation of those simple factors that appear associated with the same nodes of the Dynkin diagram of g both in the numerator and the denominator.

To see the procedure in action, consider the plateau whose effective TBA equations are summarised by figure 6a. The $\{c_p^-\}$ contributions lead to the following 'left' coset candidate:

$$\frac{SU(2)_k^{\{1\}}}{U(1)^{\{1\}}} \times \frac{SU(3)_k^{\{1,2\}}}{SU(2)_k^{\{1\}} \times U(1)^{\{2\}}} \times \frac{SU(4)_k^{\{1,2,3\}}}{SU(3)_k^{\{1,2\}} \times U(1)^{\{3\}}}, \tag{A.3}$$

where we have introduced the notation $G^{\{i_1 \dots i_n\}}$ to indicate that this group is associated with the nodes $i_1 \dots i_n$ of the Dynkin diagram of g. After the cancellation of the common terms of numerator and denominator, this coset simplifies to

$$\frac{SU(4)_k^{\{1,2,3\}}}{U(1)^{\{1\}} \times U(1)^{\{2\}} \times U(1)^{\{3\}}} \equiv \frac{SU(4)_k}{U(1)^3} \,. \tag{A.4}$$

Similarly, the $\{c_p^+\}$ contributions lead to the 'right' coset candidate

$$\frac{SU(2)_k^{\{1\}}}{U(1)^{\{1\}}} \times \frac{SU(4)_k^{\{1,2,3\}}}{SU(2)_k^{\{1\}} \times U(1)^{\{2\}} \times SU(2)_k^{\{3\}}} \times \frac{SU(2)_k^{\{3\}}}{U(1)^{\{3\}}} \,, \tag{A.5}$$

which, after the cancellations, also leads to $SU(4)_k/U(1)^3$. Notice that the cancellation performed in (A.3) and (A.5) takes place only between simple factors associated with the same nodes of the Dynkin diagram of g.

In this first example, the left and right candidates coincide, which should be expected since the effective TBA equations represented by figure 6a correspond to the deep UV limit of the $SU(4)_k/U(1)^3$ HSG model. This correspondence provides an *a posteriori* justification for the cancellations leading from (A.3) and (A.5) to the coset $SU(4)_k/U(1)^3$.

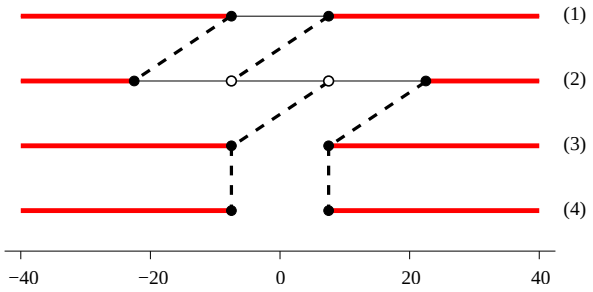

Figure 10: Effective TBA systems with asymmetric candidate cosets.

However, since the individual contributions c_p^+ and c_p^- are different in general, they often lead to different left and right candidates. This will be illustrated by our second example. Consider the effective TBA equations summarised by figure 10. In this case, some of the Dynkin diagrams $\{g_p^\pm\}$ coincide, namely $g_2^+ = g_3^+ = g_4^+$, $g_1^- = g_2^-$, $g_3^- = g_4^-$, and the general rules to calculate the plateau central charge have to be modified as described in section 4.4, so that the separate contributions $\{c_1^+ \dots c_4^+\}$ and $\{c_1^- \dots c_4^-\}$ to the total effective central charge are replaced by $\{c_1^+, c_{2+3+4}^+\}$ and $\{c_{1+2}^-, c_{3+4}^-\}$, respectively (see eq. (4.39)). Then, the value of, say, $c_{p_1+\dots+p_n}^\pm$ is calculated as for the generic case, the only difference being that the diagram $\widehat{g}_{p_1}^\pm$ is now found by deleting all the nodes $p_1 \dots p_n$ from $g_{p_1}^\pm$, instead of just p_1. Correspondingly, in our construction, $2c_{p_1+\dots+p_n}^\pm$ is identified with the central charge of the coset conformal field theory

$$\frac{\left(G_{p_1}^\pm\right)_k}{\left(\widehat{G}_{p_1}^\pm\right)_k \times U(1)^n} \,, \tag{A.6}$$

which generalises (A.1). The $\{c_p^-\}$ contributions lead to the coset candidate

$$\frac{SU(3)_k^{\{1,2\}}}{U(1)^{\{1\}} \times U(1)^{\{2\}}} \times \frac{SU(4)_k^{\{2,3,4\}}}{SU(2)_k^{\{2\}} \times U(1)^{\{3\}} \times U(1)^{\{4\}}} \equiv \frac{SU(3)_k}{U(1)^2} \times \frac{SU(4)_k}{SU(2)_k \times U(1)^2} \,, \tag{A.7}$$

while the candidate suggested by $\{c_p^+\}$ is

$$\frac{SU(3)_k^{\{1,2\}}}{SU(2)_k^{\{2\}}\times U(1)^{\{1\}}}\times\frac{SU(4)_k^{\{2,3,4\}}}{U(1)^{\{2\}}\times U(1)^{\{3\}}\times U(1)^{\{4\}}}\equiv\frac{SU(3)_k}{SU(2)_k\times U(1)}\times\frac{SU(4)_k}{U(1)^3}\,. \quad \text{(A.8)}$$

Clearly, for this case, our prescription indeed leads to different left and right coset conformal field theory candidates, although with the same central charge.

Since the different left and right candidates are constructed by analysing the left and right active energy term contributions, it is natural to identify the resulting candidates with the holomorphic and anti-holomorphic sectors of a conformal field theory. In cases where those candidates are different, one might predict that the corresponding fixed point visited by the RG flow should be of heterotic type. In the particular case of (A.7) and (A.8), they would correspond to an asymmetric coset conformal field theory [39, 40] associated with

$$\frac{SU(3)_k\times SU(4)_k}{SU(2)_k\times U(1)^4}\,, \quad \text{(A.9)}$$

where (A.7) and (A.8) specify the different left and right actions of $SU(2)\times U(1)^4$ on $SU(3)\times SU(4)$.

This matches the Lagrangian calculations of section 6. The effective TBA equations represented by figure 10 correspond to the $SU(4)_k/U(1)^3$ HSG model in the regime $\mu_{pq}\lll 2r^{-1}\lll\mu_{41}=\mu_{31}$, $\forall(p,q)\neq(4,1),(3,1)$. According to (6.31), the effective theory is specified by the field configurations of the form $\gamma=\phi^{[1]}\psi^{[3,4]}$, which can always be written as $\gamma=\widetilde{\phi}^{[1]}\widetilde{\psi}^{[3]}$. The two candidates (A.7) and (A.8) then coincide with the cosets in (6.26) for $i=3$ and $j=1$.

We finish this appendix by showing that, despite the fact that the left and right candidates can be different, they always have equal central charges. This follows from the general indentity

$$\sum_{p=1}^{r_g}c_p^+(r)=\sum_{p=1}^{r_g}c_p^-(r)\,, \quad \text{(A.10)}$$

which can be proved as follows. Eq. (4.29) and the TBA equations (4.7) lead to

$$\begin{aligned}\sum_{p=1}^{r_g}c_p^+(r)-\sum_{p=1}^{r_g}c_p^-(r) &= \frac{3}{\pi^2}\sum_{p=1}^{r_g}\sum_{a=1}^{k-1}\int_{-\infty}^{+\infty}d\theta\, m_i\mu_a r\,\sinh\theta\, L_a^p(\theta)\\ &= \frac{3}{\pi^2}\sum_{p=1}^{r_g}\sum_{a=1}^{k-1}\int_{-\infty}^{+\infty}d\theta\,\nu_a^{p\,\prime}(\theta)L_a^p(\theta)\\ &= \mathcal{J}(r)+\mathcal{I}_0(r)+\mathcal{I}_\sigma(r)\,, \quad \text{(A.11)}\end{aligned}$$

where $f'(\theta)=df(\theta)/d\theta$,

$$\mathcal{J}(r)=\frac{3}{\pi^2}\sum_{p=1}^{r_g}\sum_{a=1}^{k-1}\int_{-\infty}^{+\infty}d\theta\,\varepsilon_a^{p\,\prime}(\theta)L_a^p(\theta)\,,$$

$$\mathcal{I}_0(r)=\frac{3}{\pi^2}\sum_{p=1}^{r_g}\sum_{a,b=1}^{k-1}\int_{-\infty}^{+\infty}d\theta\,\phi'_{ab}*L_b^p(\theta)\,L_a^p(\theta)\,,$$

$$\mathcal{I}_\sigma(r) = \frac{3}{\pi^2}\sum_{p,j=1}^{r_g}\sum_{a,b=1}^{k-1}\int_{-\infty}^{+\infty} d\theta\, I^g_{pj}\, \psi'_{ab} * L^j_b(\theta-\sigma_{jp})\, L^p_a(\theta)\,. \tag{A.12}$$

All these contributions vanish. For instance, the first one is just

$$\mathcal{J}(r) = \frac{3}{\pi^2}\sum_{p=1}^{r_g}\sum_{a=1}^{k-1}\int_{\varepsilon^p_a(-\infty)}^{\varepsilon^p_a(+\infty)} d\varepsilon\, \ln(1+\mathrm{e}^{-\varepsilon}) = 0\,, \tag{A.13}$$

where we have used (4.15). The second is

$$\begin{aligned}
\mathcal{I}_0(r) &= \frac{3}{\pi^2}\sum_{p=1}^{r_g}\sum_{a,b=1}^{k-1}\int_{-\infty}^{+\infty} d\theta \int_{-\infty}^{+\infty}\frac{d\tilde\theta}{2\pi}\,\phi'_{ab}(\theta-\tilde\theta)L^p_b(\tilde\theta)\, L^p_a(\theta)\\
&= -\frac{3}{\pi^2}\sum_{p=1}^{r_g}\sum_{a,b=1}^{k-1}\int_{-\infty}^{+\infty} d\tilde\theta \int_{-\infty}^{+\infty}\frac{d\theta}{2\pi}\,\phi'_{ba}(\tilde\theta-\theta)L^p_a(\theta)\, L^p_b(\tilde\theta)\\
&= -\mathcal{I}_0(r) = 0\,,
\end{aligned} \tag{A.14}$$

where we have just swapped the integration variables[13] and used that $\phi_{ab}(\theta) = \phi_{ba}(-\theta)$. Similarly, it can be checked that $\mathcal{I}_\sigma(r)$ vanishes by using $\psi_{ab}(\theta) = \psi_{ba}(-\theta)$, $I^g_{pj} = I^g_{jp}$, and $\sigma_{jp} = -\sigma_{pj}$.

B An E_6 HSG flow with maximal number of steps.

As a confirmation of the results quoted in table 1 for $g = e_n$, we include, as a final example, an $(E_6)_2/U(1)^6$ HSG model that generates a flow with the predicted maximal number of steps, *i.e.* $20 = 6(6+1)/2 - 1$. Figure 11 shows the flow of the effective central charge for the following choice of parameters:

$$m_i = \mathrm{e}^{\,(i-1)a}\,,\quad \sigma_i = ib\,,\quad \forall i = 1\ldots 5\,,\quad m_6 = \mathrm{e}^{\,5a}\,,\quad \sigma_6 = \sigma_3 \tag{B.1}$$

with $a = 10$ and $b = 80$. Using the results of section 4.3, the central charges of the fixed points visited by the corresponding staircase flow are predicted to be

$$\begin{aligned}
\{e_6\} = \tfrac{36}{7} &\xrightarrow[180]{m_{15}} \{2d_5\}-\{d_4\} = 5 \xrightarrow[145]{m_{25}} \{d_5,a_4\}-\{a_3\} = \tfrac{34}{7}\\
&\xrightarrow[135]{m_{14}} \{d_4,2a_4\}-\{2a_3\} = \tfrac{33}{7} \xrightarrow[125]{m_{56}} \{d_4,a_4\}-\{a_2\} = \tfrac{163}{35}\\
&\xrightarrow[110]{m_{35}} \{d_4,a_4,a_2\}-\{a_3,a_1\} = \tfrac{319}{70} \xrightarrow[105]{m_{16}} \{d_4,a_3\}-\{a_1\} = \tfrac{9}{2}\\
&\xrightarrow[100]{m_{24}} \{3a_3\}-\{a_2,a_1\} = \tfrac{43}{10} \xrightarrow[90]{m_{13}} \{2a_3,a_2\}-\{2a_1\} = \tfrac{21}{5}\\
&\xrightarrow[80]{m_{46}} \{a_3,3a_2\}-\{3a_1\} = \tfrac{41}{10} \xrightarrow[75]{m_{45}} \{a_3,2a_2\}-\{a_1\} = \tfrac{39}{10}\\
&\xrightarrow[70]{m_{26}} \{4a_2\}-\{2a_1\} = \tfrac{19}{5} \xrightarrow[65]{m_{34}} \{3a_2\} = \tfrac{18}{5} \xrightarrow[55]{m_{23}} \{2a_2,2a_1\} = \tfrac{17}{5}
\end{aligned}$$

[13] The integral over the entire $\theta,\tilde\theta$ plane is not absolutely convergent, which might make a naive swap of integration variables lead to a wrong result. A more careful analysis of integrals of this kind has been performed in [28] (see eq. (3.14)), which in our case leads to the same results.

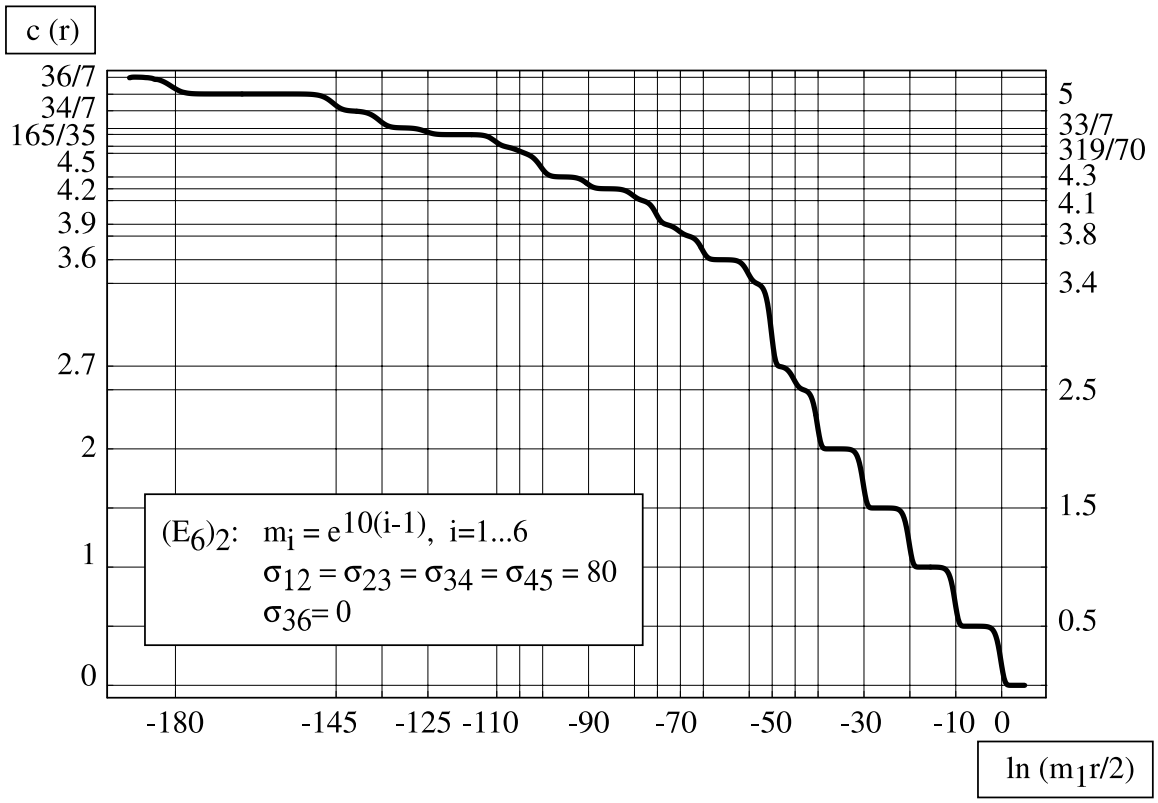

Figure 11: The TBA scaling function for the $(E_6)_2/U(1)^6$ HSG model.

$$\xrightarrow[50]{m_6} \{a_2, 3a_1\} = \tfrac{27}{10} \xrightarrow[45]{m_{12}} \{5a_1\} = \tfrac{5}{2} \xrightarrow[40]{m_5} \{4a_1\} = 2$$
$$\xrightarrow[30]{m_4} \{3a_1\} = \tfrac{3}{2} \xrightarrow[20]{m_3} \{2a_1\} = 1 \xrightarrow[10]{m_2} \{a_1\} = \tfrac{1}{2} \xrightarrow[0]{m_1} \text{Massive}\,, \quad \text{(B.2)}$$

where we have used the notation

$$\{p_1 g_1, \ldots, p_n g_n\} = p_1 C_2(g_1) + \cdots + p_n C_2(g_n)\,. \quad \text{(B.3)}$$

Here, $p_1 \ldots p_n$ are positive integers, $g_1 \ldots g_n$ are simple Lie algebras, and $C_k\big(g\big)$ is the central charge of the $G_k/U(1)^{r_g}$ coset conformal field theory, given by (4.33). Above and below the arrows, we have indicated the mass scale associated with each crossover, say m_{ij}, and the value of $-\ln(m_1 r/2)$ at $r = 2/m_{ij}$. These results are in complete agreement with the numerical data presented in fig. 11.

The coset identifications for the fixed points visited by the flow can be worked out as explained in section 6 and appendix A, and provide several examples where the fixed point is a true asymmetric coset model. The first occurs in the regime $m_{14} \lll 2r^{-1} \lll m_{25}$, and is determined by the solutions to $\Gamma_{51}(\gamma) = \Gamma_{51}(\mathbb{1})$ and $\Gamma_{52}(\gamma) = \Gamma_{52}(\mathbb{1})$. Taking (6.25) into account, the second condition implies the first, so the effective theory is specified by left and right cosets of the form (6.26) with $i = 5$ and $j = 2$, which in this case are

$$\frac{SU(5)_k}{U(1)^4} \otimes \frac{SO(10)_k}{SU(4) \otimes U(1)^2} \quad \text{and} \quad \frac{SU(5)_k}{SU(4)_k \otimes U(1)} \otimes \frac{SO(10)_k}{U(1)^5}\,. \quad \text{(B.4)}$$

References

[1] C.R. Fernández-Pousa, M.V. Gallas, T.J. Hollowood and J.L. Miramontes, 'The symmetric space and homogeneous sine-Gordon theories', *Nucl. Phys.* **B484** (1997) 609-630, [arXiv:hep-th/9606032].

[2] C.R. Fernández-Pousa, M.V. Gallas, T.J. Hollowood and J.L. Miramontes, 'Solitonic integrable perturbations of parafermionic theories', *Nucl. Phys.* **B499** (1997) 673-689, [arXiv:hep-th/9701109].

[3] J.L. Miramontes and C.R. Fernández-Pousa, 'Integrable quantum field theories with unstable particles', *Phys. Lett.* **472B** (2000) 392-401, [arXiv:hep-th/9910218].

[4] C. Korff, 'Colours associated to non simply-laced Lie algebras and exact S-matrices', *Phys. Lett.* **501B** (2001) 289-296, [arXiv:hep-th/0010287].

[5] O.A. Castro-Alvaredo, A. Fring, C. Korff and J.L. Miramontes, 'Thermodynamic Bethe ansatz of the homogeneous sine-Gordon models', *Nucl. Phys.* **B575** (2000) 535-560, [arXiv:hep-th/9912196].

[6] O.A. Castro-Alvaredo, A. Fring and C. Korff, 'Form factors of the homogeneous sine-Gordon models', *Phys. Lett.* **484B** (2000) 167-176, [arXiv:hep-th/0004089];
O.A. Castro-Alvaredo and A. Fring, 'Identifying the operator content, the Homogeneous Sine-Gordon models', *Nucl. Phys.* **B604** (2001) 367-390, [arXiv:hep-th/0008044].

[7] O.A. Castro-Alvaredo and A. Fring, 'Renormalization group flow with unstable particles', *Phys. Rev.* **D63** (2001) 021701(R), [arXiv:hep-th/0008208].

[8] O.A. Castro-Alvaredo and A. Fring, 'Decoupling the $SU(N)_2$-homogeneous sine-Gordon Model', *Phys. Rev.* **D64** (2001) 085007, [arXiv:hep-th/0010262].

[9] C.R. Fernández-Pousa and J.L. Miramontes, 'Semi-classical spectrum of the homogeneous sine-Gordon theories', *Nucl. Phys.* **B518** (1998) 745-769, [arXiv:hep-th/9706203].

[10] P. Dorey and J.L. Miramontes, 'Aspects of the homogeneous sine-Gordon models', talk by JLM at the 'Workshop on Integrable Theories, Solitons and Duality', Sao Paulo (Brazil), July 2002;
available at `http://www.ift.unesp.br/users/laf/workshop/videos.htm`.

[11] P. Dorey and J.L. Miramontes, 'Aspects of the homogeneous sine-Gordon models', in proceedings of the 'Workshop on Integrable Theories, Solitons and Duality', PRHEP-unesp2002/006, [arXiv:hep-th/0211174].

[12] A.B. Zamolodchikov, 'Integrable field theory from conformal field theory', Advanced Studies in Pure Mathematics **19** (1989) 641-674.

[13] R. Tateo, 'The Sine-Gordon Model as $SO(N)_1 \times SO(N)_1/SO(N)_2$ perturbed coset theory and generalizations', *Int. J. Mod. Phys.* **A10** (1995) 1357-1376, [arXiv:hep-th/9405197].

[14] V.A. Fateev, 'The Sigma Model (dual) representation for a two-parameter family of integrable quantum field theories', *Nucl. Phys.* **B473** (1996) 509-538;
P. Baseilhac and V.A. Fateev, 'Expectation values of local fields for a two-parameter family of integrable models and related perturbed conformal field theories', *Nucl. Phys.* **B532** (1998) 567-587, [arXiv:hep-th/9906010];
V.A. Fateev and M. Lashkevich, 'Form factors of exponential fields for two-parametric family of integrable models', [arXiv:hep-th/0402082].

[15] H. Saleur and P. Simonetti, 'Multiparameter integrable QFT's with N bosons', *Nucl. Phys.* **B535** (1998) 596-620, [arXiv:hep-th/9804080].

[16] D. Gepner, 'New conformal field theories associated with Lie algebras and their partition functions', *Nucl. Phys.* **B290** (1987) 10-24; 'Field identification in coset conformal field theories', *Phys. Lett.* **222B** (1989) 207-212.

[17] V.G. Knizhnik and A.B. Zamolodchikov, 'Current Algebra And Wess-Zumino Model In Two Dimensions', *Nucl. Phys.* **B247** (1984) 83-103.

[18] R.J. Eden, P.V. Landshoff, D.I. Olive and J.C. Polkinghorne, *The analytic S-matrix*, Cambridge Univ. Press (1966);
R.G. Newton, *Scattering theory of waves and particles*, McGraw-Hill (1966)

[19] K. Hagiwara *et al.*, 'The Review of Particle Physics', *Phys. Rev.* **D66** (2002) 010001.

[20] Ref. [19], pg. 251, '37.5.3.1. Resonances';
available at `http://pdg.lbl.gov/2002/kinemarpp.pdf`, pg. 10.

[21] Ref. [19], pg. 289, 'The Z boson';
available at `http://pdg.lbl.gov/2002/zmini_s044203.pdf`.

[22] D.E. Groom *et al.*, 'Review of Particle Physics', *Eur. Phys. J.* **C15** (2000) 1, pg. 696, 'Against Breit-Wigner parameters – a pole-emic';
available at `http://pdg.lbl.gov/2001/ndelmini_b861.pdf`.

[23] A.R. Bohm and N.L. Harshman, 'On the Mass and Width of the Z-boson and other relativistic quasistable particles', *Nucl. Phys.* **B581** (2000) 91-115, [arXiv:hep-ph/0001206];
P.A. Grassi, B.A. Kniehl and A. Sirlin, 'Width and Partial widths of Unstable Particles', *Phys. Rev. Lett.* **86** (2001) 389-392, [arXiv:hep-th/0005149].

[24] Al.B. Zamolodchikov, 'Thermodynamic Bethe ansatz in relativistic models: scaling 3-state Potts and Lee-Yang models', *Nucl. Phys.* **B342** (1990) 695-720.

[25] Al.B. Zamolodchikov, 'Thermodynamic Bethe ansatz for RSOS scattering theories', *Nucl. Phys.* **B358** (1991) 497-523; 'From tricritical Ising to critical Ising by Thermodynamic Bethe ansatz', *Nucl. Phys.* **B358** (1991) 524-546; 'TBA equations for integrable perturbed $SU(2)_k \times SU(2)_l/SU(2)_{k+l}$ coset models', *Nucl. Phys.* **B366** (1991) 122-132;
M.J. Martins, 'The Thermodynamic Bethe ansatz for deformed $WA_N^{(1)}$ conformal field theories', *Phys. Lett.* **277B** (1992) 301-305, [arXiv:hep-th/9201032].

[26] F. Ravanini, 'Thermodynamic Bethe ansatz for $\mathcal{G}_k \otimes \mathcal{G}_l/\mathcal{G}_{k+l}$ coset models perturbed by their $\phi_{1,1,Adj}$ operator, *Phys. Lett.* **282B** (1992) 73-79, [arXiv:hep-th/9202020].

[27] F. Ravanini, R. Tateo and A. Valleriani, 'Dynkin TBAs', *Int. J. Mod. Phys.* **A8** (1993) 1707-1728, [arXiv:hep-th/9207040].

[28] P. Dorey and F. Ravanini, 'Staircase models from affine Toda field theory', *Int. J. Mod. Phys.* **A8** (1993) 873-893, [arXiv:hep-th/9206052].

[29] P. Dorey and F. Ravanini, 'Generalising the staircase models', *Nucl. Phys.* **B406** (1993) 708-726, [arXiv:hep-th/9211115].

[30] H.W. Braden, E. Corrigan, P.E. Dorey and R. Sasaki, 'Affine Toda field theory and exact S-matrices', *Nucl. Phys.* **B338** (1990) 689-746.

[31] Al.B. Zamolodchikov, 'Resonance Factorized Scattering and Roaming Trajectories', preprint ENS-LPS-335 (1991).

[32] M.J. Martins, 'Renormalization-Group Trajectories from Resonance Factorized S Matrices', *Phys. Rev. Lett.* **69** (1992) 2461-2464, [arXiv:hep-th/9205024]; 'Exact resonance ADE S-matrices and their renormalization group trajectories', *Nucl. Phys.* **B394** (1993) 339-355, [arXiv:hep-th/9208011].

[33] A.N. Kirillov, 'Identities for the Rogers dilogarithmic function connected with simple Lie algebras', *J. Sov. Math.* **47** (1989), 2450-2458;
A. Kuniba and T. Nakanishi, 'Spectra in conformal field theories from the Rogers dilogarithm', *Mod. Phys. Lett.* **A7** (1992) 3487-3494, [arXiv:hep-th/9206034];
V.V. Bazhanov and N. Reshetikhin, 'Restricted solid-on-solid models connected with simply laced algebras and conformal field theory', *J. Phys. A: Math. Gen.* **23** (1990) 1477-1492.

[34] D. Altschuler, 'Quantum equivalence of coset space models', *Nucl. Phys.* **B313** (1989) 293-307.

[35] K. Gawedzki and A. Kupianen, 'Coset construction from functional integrals', *Nucl. Phys.* **B320** (1989) 625-668

[36] D. Karabali, Q.H. Park, H.J. Schnitzer and Z. Yang, 'A GKO Construction based on a path integral formulation of gauged Wess-Zumino-Witten actions', *Phys. Lett.* **216B** (1989) 307;
D. Karabali and H. J. Schnitzer, 'BRST quantization of the gauged WZW action and coset conformal field theories', *Nucl. Phys.* **B329** (1990) 649;
K. Gawedzki and A. Kupianen, 'G/H conformal field theory from gauged WZW model', *Phys. Lett.* **215B** (1988) 119-123;
E. Witten, 'On Holomorphic Factorization of WZW Coset Models', *Commun. Math. Phys.* **144** (1992) 189-212.

[37] E. Witten, 'Non-abelian bosonization in two dimensions', *Commun. Math. Phys.* **92** (1984) 455-472.

[38] E. Guadagnini, M. Martellini and M. Mintchev, 'Scale invariant sigma models on homogeneous spaces', *Phys. Lett.* **194B** (1987) 69;
E. Guadagnini, 'Current algebra in sigma models on homogeneous spaces', *Nucl. Phys.* **B290** (1987) 417.

[39] T. Quella and V. Schomerus, 'Asymmetric cosets', *JHEP* **0302** (2003) 030, [arXiv:hep-th/0212119]; 'Asymmetrically Gauged WZNW Models', *Fortsch. Phys.* **51** (2003) 843-849.

[40] I. Bars and K. Sfetsos, 'Generalized duality and singular strings in higher dimensions', *Mod. Phys. Lett.* **A7** (1992) 1091-1104, [arXiv:hep-th/9110054].

[41] T. Gannon, 'Partition Functions for Heterotic WZW Conformal Field Theories', *Nucl. Phys.* **B402** (1993) 729-753, [arXiv:hep-th/9209042].

[42] M.A. Walton and J.G. Zhou, 'D-branes in asymmetrically gauged WZW models and axial-vector duality', *Nucl. Phys.* **B648** (2003) 523-541, [arXiv:hep-th/0205161].

[43] G. Sarkissian, 'On D-branes in the Nappi-Witten and GMM models', *JHEP* **0301** (2003) 059, [arXiv:hep-th/0211163].

[44] C.V. Johnson and H.G. Svendsen, 'An exact string theory model of closed time-like curves and cosmological singularities', [arXiv:hep-th/0405141].

[45] D. Israel, C. Kounnas, D. Orlando and P.M. Petropoulos, 'Electric/Magnetic Deformations of S^3 and AdS_3, and Geometric Cosets', [arXiv:hep-th/0405213].

[46] O.A. Castro-Alvaredo, J. Dreissig and A. Fring, 'Integrable scattering theories with unstable particles', [arXiv:hep-th/0211168].

[47] A.B. Zamolodchikov, 'Irreversibility of the flux of the Renormalization Group in a 2-D field theory', *Sov. Phys. JETP Lett.* **43** (1986) 730-732 [Pisma Zh. Eksp. Teor. Fiz. **43** (1986) 565].

[48] J.L. Cardy, 'The central charge and universal combinations of amplitudes in two-dimensional theories away from criticality', *Phys. Rev. Lett.* **60** (1988) 2709.

[49] J. Cardy and G. Mussardo, 'Universal properties of self-avoiding walks from two-dimensional field theory', *Nucl. Phys.* **B410** (1993) 451-493, [arXiv:hep-th/9306028].

[50] F.A. Smirnov, 'A comment on A. Zamolodchikov's paper concerning selfavoiding polymers', *Phys. Lett.* **275B** (1992) 109-111.

[51] J.L. Cardy, 'Critical Exponents Of The Chiral Potts Model From Conformal Field Theory', *Nucl. Phys.* **B389** (1993) 577-586, [arXiv:hep-th/9210002].

[52] V.V. Bazhanov, S.L. Lukyanov and A.B. Zamolodchikov, 'Quantum field theories in finite volume: Excited state energies', *Nucl. Phys.* **B489** (1997) 487-531, [arXiv:hep-th/9607099].

[53] P. Dorey and R. Tateo, 'Excited states by analytic continuation of TBA equations', *Nucl. Phys.* **B482** (1996) 639-659, [arXiv:hep-th/9607167].